

1996

# Numerical simulation of flow through pipes with multiple constrictions and with moving walls.

Vijayakanthan. Damodaran  
*University of Windsor*

Follow this and additional works at: <http://scholar.uwindsor.ca/etd>

---

## Recommended Citation

Damodaran, Vijayakanthan., "Numerical simulation of flow through pipes with multiple constrictions and with moving walls." (1996). *Electronic Theses and Dissertations*. Paper 2887.

This online database contains the full-text of PhD dissertations and Masters' theses of University of Windsor students from 1954 forward. These documents are made available for personal study and research purposes only, in accordance with the Canadian Copyright Act and the Creative Commons license—CC BY-NC-ND (Attribution, Non-Commercial, No Derivative Works). Under this license, works must always be attributed to the copyright holder (original author), cannot be used for any commercial purposes, and may not be altered. Any other use would require the permission of the copyright holder. Students may inquire about withdrawing their dissertation and/or thesis from this database. For additional inquiries, please contact the repository administrator via email ([scholarship@uwindsor.ca](mailto:scholarship@uwindsor.ca)) or by telephone at 519-253-3000ext. 3208.



National Library  
of Canada

Acquisitions and  
Bibliographic Services Branch

395 Wellington Street  
Ottawa, Ontario  
K1A 0N4

Bibliothèque nationale  
du Canada

Direction des acquisitions et  
des services bibliographiques

395, rue Wellington  
Ottawa (Ontario)  
K1A 0N4

Tout les autres renseignements

chez les autres universités

## NOTICE

The quality of this microform is heavily dependent upon the quality of the original thesis submitted for microfilming. Every effort has been made to ensure the highest quality of reproduction possible.

If pages are missing, contact the university which granted the degree.

Some pages may have indistinct print especially if the original pages were typed with a poor typewriter ribbon or if the university sent us an inferior photocopy.

Reproduction in full or in part of this microform is governed by the Canadian Copyright Act, R.S.C. 1970, c. C-30, and subsequent amendments.

## AVIS

La qualité de cette microforme dépend grandement de la qualité de la thèse soumise au microfilmage. Nous avons tout fait pour assurer une qualité supérieure de reproduction.

S'il manque des pages, veuillez communiquer avec l'université qui a conféré le grade.

La qualité d'impression de certaines pages peut laisser à désirer, surtout si les pages originales ont été dactylographiées à l'aide d'un ruban usé ou si l'université nous a fait parvenir une photocopie de qualité inférieure.

La reproduction, même partielle, de cette microforme est soumise à la Loi canadienne sur le droit d'auteur, SRC 1970, c. C-30, et ses amendements subséquents.

**NUMERICAL SIMULATION OF FLOW THROUGH PIPES WITH  
MULTIPLE CONSTRICTIONS AND WITH MOVING WALLS**

by

Vijayakanthan Damodaran

A Dissertation

Submitted to the Faculty of Graduate Studies and Research  
through the Department of Mechanical and Materials Engineering  
in Partial Fulfilment of the Requirements for  
the Degree of Doctor of Philosophy at the  
University of Windsor

Windsor, Ontario, Canada



National Library  
of Canada

Bibliothèque nationale  
du Canada

Acquisitions and  
Bibliographic Services Branch

Direction des acquisitions et  
des services bibliographiques

395 Wellington Street  
Ottawa, Ontario  
K1A 0N4

395, rue Wellington  
Ottawa (Ontario)  
K1A 0N4

Your title / Votre référence

Your title / Votre référence

The author has granted an irrevocable non-exclusive licence allowing the National Library of Canada to reproduce, loan, distribute or sell copies of his/her thesis by any means and in any form or format, making this thesis available to interested persons.

L'auteur a accordé une licence irrévocable et non exclusive permettant à la Bibliothèque nationale du Canada de reproduire, prêter, distribuer ou vendre des copies de sa thèse de quelque manière et sous quelque forme que ce soit pour mettre des exemplaires de cette thèse à la disposition des personnes intéressées.

The author retains ownership of the copyright in his/her thesis. Neither the thesis nor substantial extracts from it may be printed or otherwise reproduced without his/her permission.

L'auteur conserve la propriété du droit d'auteur qui protège sa thèse. Ni la thèse ni des extraits substantiels de celle-ci ne doivent être imprimés ou autrement reproduits sans son autorisation.

ISBN 0-612-10986-0

Canada

Name JITPIK ANTHAN DAMBA PRDN

Dissertation Abstracts International and Masters Abstracts International are arranged by broad, general subject categories. Please select the one subject which most nearly describes the content of your dissertation or thesis. Enter the corresponding four-digit code in the spaces provided.

MECHANICAL ENGINEERING

SUBJECT TERM

0548

SUBJECT CODE

UMI

Subject Categories

**THE HUMANITIES AND SOCIAL SCIENCES**

**COMMUNICATIONS AND THE ARTS**

Architecture ..... 0729  
 Art History ..... 0377  
 Cinema ..... 0900  
 Dance ..... 0378  
 Fine Arts ..... 0357  
 Information Science ..... 0723  
 Journalism ..... 0391  
 Library Science ..... 0399  
 Mass Communications ..... 0708  
 Music ..... 0413  
 Speech Communication ..... 0459  
 Theater ..... 0465

**EDUCATION**

General ..... 0515  
 Administration ..... 0514  
 Adult and Continuing ..... 0516  
 Agricultural ..... 0517  
 Art ..... 0273  
 Bilingual and Multicultural ..... 0282  
 Business ..... 0688  
 Community College ..... 0275  
 Curriculum and Instruction ..... 0727  
 Early Childhood ..... 0518  
 Elementary ..... 0524  
 Finance ..... 0277  
 Guidance and Counseling ..... 0519  
 Health ..... 0680  
 Higher ..... 0745  
 History of ..... 0520  
 Home Economics ..... 0278  
 Industrial ..... 0521  
 Language and Literature ..... 0279  
 Mathematics ..... 0280  
 Music ..... 0522  
 Philosophy of ..... 0998  
 Physical ..... 0523

Psychology ..... 0525  
 Reading ..... 0535  
 Religious ..... 0527  
 Sciences ..... 0714  
 Secondary ..... 0533  
 Social Sciences ..... 0534  
 Sociology of ..... 0340  
 Special ..... 0529  
 Teacher Training ..... 0530  
 Technology ..... 0710  
 Tests and Measurements ..... 0288  
 Vocational ..... 0747

**LANGUAGE, LITERATURE AND LINGUISTICS**

Language  
 General ..... 0679  
 Ancient ..... 0289  
 Linguistics ..... 0290  
 Modern ..... 0291

Literature  
 General ..... 0401  
 Classical ..... 0294  
 Comparative ..... 0295  
 Medieval ..... 0297  
 Modern ..... 0298  
 African ..... 0316  
 American ..... 0591  
 Asian ..... 0305  
 Canadian (English) ..... 0352  
 Canadian (French) ..... 0355  
 English ..... 0593  
 Germanic ..... 0311  
 Latin American ..... 0312  
 Middle Eastern ..... 0315  
 Romance ..... 0313  
 Slavic and East European ..... 0314

**PHILOSOPHY, RELIGION AND THEOLOGY**

Philosophy ..... 0422  
 Religion  
 General ..... 0318  
 Biblical Studies ..... 0321  
 Clergy ..... 0319  
 History of ..... 0320  
 Philosophy of ..... 0322  
 Theology ..... 0469

**SOCIAL SCIENCES**

American Studies ..... 0323  
 Anthropology  
 Archaeology ..... 0324  
 Cultural ..... 0326  
 Physical ..... 0327

Business Administration  
 General ..... 0310  
 Accounting ..... 0272  
 Banking ..... 0770  
 Management ..... 0454  
 Marketing ..... 0338  
 Canadian Studies ..... 0385

Economics  
 General ..... 0501  
 Agricultural ..... 0503  
 Commerce-Business ..... 0505  
 Finance ..... 0508  
 History ..... 0509  
 Labor ..... 0510  
 Theory ..... 0511

Folklore ..... 0358  
 Geography ..... 0366  
 Gerontology ..... 0351  
 History  
 General ..... 0578

Ancient ..... 0579  
 Medieval ..... 0581  
 Modern ..... 0582  
 Black ..... 0328  
 African ..... 0331  
 Asia, Australia and Oceania ..... 0332  
 Canadian ..... 0334  
 European ..... 0335  
 Latin American ..... 0336  
 Middle Eastern ..... 0333  
 United States ..... 0337  
 History of Science ..... 0585  
 Law ..... 0398  
 Political Science  
 General ..... 0615  
 International Law and Relations ..... 0616  
 Public Administration ..... 0617  
 Recreation ..... 0814  
 Social Work ..... 0452

Sociology  
 General ..... 0626  
 Criminology and Penology ..... 0627  
 Demography ..... 0938  
 Ethnic and Racial Studies ..... 0631  
 Individual and Family Studies ..... 0628  
 Industrial and Labor Relations ..... 0629  
 Public and Social Welfare ..... 0630  
 Social Structure and Development ..... 0700  
 Theory and Methods ..... 0344  
 Transportation ..... 0709  
 Urban and Regional Planning ..... 0999  
 Women's Studies ..... 0453

**THE SCIENCES AND ENGINEERING**

**BIOLOGICAL SCIENCES**

Agriculture  
 General ..... 0473  
 Agronomy ..... 0285  
 Animal Culture and Nutrition ..... 0475  
 Animal Pathology ..... 0476  
 Food Science and Technology ..... 0359  
 Forestry and Wildlife ..... 0478  
 Plant Culture ..... 0479  
 Plant Pathology ..... 0480  
 Plant Physiology ..... 0817  
 Range Management ..... 0777  
 Wood Technology ..... 0746

Biology  
 General ..... 0306  
 Anatomy ..... 0287  
 Biostatistics ..... 0308  
 Botany ..... 0309  
 Cell ..... 0379  
 Ecology ..... 0329  
 Entomology ..... 0353  
 Genetics ..... 0369  
 Limnology ..... 0793  
 Microbiology ..... 0410  
 Molecular ..... 0307  
 Neuroscience ..... 0317  
 Oceanography ..... 0416  
 Physiology ..... 0433  
 Radiation ..... 0821  
 Veterinary Science ..... 0778  
 Zoology ..... 0472

Biophysics  
 General ..... 0786  
 Medical ..... 0760

**EARTH SCIENCES**  
 Biogeochemistry ..... 0425  
 Geochemistry ..... 0996

Geodesy ..... 0370  
 Geology ..... 0372  
 Geophysics ..... 0373  
 Hydrology ..... 0388  
 Mineralogy ..... 0411  
 Paleobotany ..... 0345  
 Paleocology ..... 0426  
 Paleontology ..... 0418  
 Paleozoology ..... 0985  
 Palynology ..... 0427  
 Physical Geography ..... 0368  
 Physical Oceanography ..... 0415

**HEALTH AND ENVIRONMENTAL SCIENCES**

Environmental Sciences ..... 0768  
 Health Sciences  
 General ..... 0566  
 Audiology ..... 0300  
 Chemotherapy ..... 0992  
 Dentistry ..... 0567  
 Education ..... 0350  
 Hospital Management ..... 0769  
 Human Development ..... 0758  
 Immunology ..... 0982  
 Medicine and Surgery ..... 0564  
 Mental Health ..... 0347  
 Nursing ..... 0569  
 Nutrition ..... 0570  
 Obstetrics and Gynecology ..... 0380  
 Occupational Health and Therapy ..... 0354  
 Ophthalmology ..... 0381  
 Pathology ..... 0571  
 Pharmacology ..... 0419  
 Pharmacy ..... 0572  
 Physical Therapy ..... 0382  
 Public Health ..... 0573  
 Radiology ..... 0574  
 Recreation ..... 0575

Speech Pathology ..... 0460  
 Toxicology ..... 0383  
 Home Economics ..... 0386

**PHYSICAL SCIENCES**

Pure Sciences  
 Chemistry  
 General ..... 0485  
 Agricultural ..... 0749  
 Analytical ..... 0486  
 Biochemistry ..... 0487  
 Inorganic ..... 0488  
 Nuclear ..... 0738  
 Organic ..... 0490  
 Pharmaceutical ..... 0491  
 Physical ..... 0494  
 Polymer ..... 0495  
 Radiation ..... 0754  
 Mathematics ..... 0405

Physics  
 General ..... 0605  
 Acoustics ..... 0986  
 Astronomy and Astrophysics ..... 0606  
 Atmospheric Science ..... 0608  
 Atomic ..... 0748  
 Electronics and Electricity ..... 0607  
 Elementary Particles and High Energy ..... 0798  
 Fluid and Plasma ..... 0759  
 Molecular ..... 0609  
 Nuclear ..... 0610  
 Optics ..... 0752  
 Radiation ..... 0756  
 Solid State ..... 0611  
 Statistics ..... 0463

Applied Sciences  
 Applied Mechanics ..... 0346  
 Computer Science ..... 0984

Engineering  
 General ..... 0537  
 Aerospace ..... 0538  
 Agricultural ..... 0539  
 Automotive ..... 0540  
 Biomedical ..... 0541  
 Chemical ..... 0542  
 Civil ..... 0543  
 Electronics and Electrical ..... 0544  
 Heat and Thermodynamics ..... 0348  
 Hydraulic ..... 0545  
 Industrial ..... 0546  
 Marine ..... 0547  
 Materials Science ..... 0794  
 Mechanical ..... 0548  
 Metallurgy ..... 0743  
 Mining ..... 0551  
 Nuclear ..... 0552  
 Packaging ..... 0549  
 Petroleum ..... 0765  
 Sanitary and Municipal ..... 0554  
 System Science ..... 0790

Geotechnology ..... 0428  
 Operations Research ..... 0796  
 Plastics Technology ..... 0795  
 Textile Technology ..... 0994

**PSYCHOLOGY**

General ..... 0621  
 Behavioral ..... 0384  
 Clinical ..... 0622  
 Developmental ..... 0620  
 Experimental ..... 0623  
 Industrial ..... 0624  
 Personality ..... 0625  
 Physiological ..... 0989  
 Psychobiology ..... 0349  
 Psychometrics ..... 0632  
 Social ..... 0451

2000

© Vijayakanthan Damodaran 1995

## ABSTRACT

A numerical method has been developed to solve steady laminar flow through a tube with multiple constrictions and pulsatile flow through tubes with moving boundaries. The governing equations were formulated in body fitted curvilinear coordinates so that arbitrary domains and moving boundaries could be handled. A finite volume discretization procedure was used to solve the governing equations. Four practical flow problems were numerically simulated in this work. In the first case, tubes with one, two, three, four and seven constrictions were considered. For the second case, the flow through a tube with multiple constrictions was solved by considering a single module where the flow field was assumed to be periodic. By comparing the results of these two cases, the effects of the number of constrictions on wall shear stress, pressure drop, vorticity, streamlines and velocity distributions as the flow passed through the tube were studied and the development of periodicity characteristics was investigated. The computations were carried out for a range of Reynolds number between 50 and 250. The third case studied had a pulsatile flow at the inlet of a tube having a constriction which changed in shape periodically with time at a prescribed frequency. The fourth case also had a pulsatile flow at the inlet with a portion of the wall that changed shape periodically with time. In this case, however, the variation caused contraction of the pipe at one portion of the cycle and distention

at another portion alternatively. The presence of moving boundaries in the above mentioned cases caused additional unsteadiness to occur in the flow. This unsteady behaviour in the flow was investigated over a range of frequency.



*To*  
*My Parents*  
*and*  
*My Dear Wife Veni*

## **ACKNOWLEDGEMENTS**

I wish to express my sincere gratitude to my supervisors Dr. G.W. Rankin and Dr. C. Zhang for their excellent support, encouragement and guidance throughout the course of this dissertation. My sincere thanks to Dr. K. Sridhar for his helpful suggestions towards my dissertation and his personal help during some of my difficult times. I am deeply indebted to Dr. R. Barron for making me like the subject and his unceasing help throughout this study. I would also like to thank Dr. P.N. Kaloni for his suggestions and encouragement.

Dinakara was always there to help me. His advice and friendship proved invaluable to me. I would like to thank Reji for his single minded devotion towards my welfare and for always standing by me. I am thankful to Rajeev, Narinder and Basu for their willingness to spend time with me and my fellow graduate students Abi, Soma, Atish and Satya for all their help. My thanks are also due to Dr. Lakshmi Sridhar who was genuinely interested in me finishing my dissertation. I deeply appreciate the love and support provided by my wife Veni without which this work would not be possible and the encouragement provided by my parents throughout the duration of this study.

The work was financially supported through Natural Sciences and Engineering Research Council of Canada Grant Numbers GP0001404 and OGP0105727.

## TABLE OF CONTENTS

	Page
ABSTRACT	iv
DEDICATION	vi
ACKNOWLEDGEMENTS	vii
TABLE OF CONTENTS	viii
LIST OF TABLES	x
LIST OF FIGURES	xi
NOMENCLATURE	xiii
Chapter i INTRODUCTION	1
1.1 Motivation	1
1.2 Objectives of the Present Work	5
1.3 Statement of the Problem	6
Chapter II LITERATURE REVIEW	8
2.1 Flow Through Tubes with Constrictions in the Flow Passage	8
2.2 Flow Through Tubes with Moving Boundaries	11
2.3 Other Related Work with Irregular Domains and Moving Boundaries	14
Chapter III PROBLEM FORMULATION	17
3.1 Governing Equations	20
3.2 Transformation of Basic Equations	21
3.3 Assumptions and Boundary Conditions	23
3.4 Grid Generation Methodology	29
Chapter IV NUMERICAL METHODOLOGY	37
4.1 Numerical Method	37
4.2 Pressure Correction Equation	40
4.3 Solution Algorithm	43

Chapter V	RESULTS AND DISCUSSION	46
5.1	Model Validation	46
5.2	Tube with Multiple Constrictions (Case 1)	49
5.2.1	Pressure	49
5.2.2	Velocity	50
5.2.3	Wall shear stress, vorticity and streamlines	51
5.2.4	Periodic nature of the flow	52
5.3	Modular Approach (Case 2)	53
5.4	Pulsatile Flow with Time Dependent Constriction (Case 3)	55
5.4.1	Stream function	55
5.4.2	Wall shear stress and vorticity	57
5.4.3	Pressure	61
5.5	Pulsatile Flow with Moving Boundary (Case 4)	62
5.5.1	Stream function	62
5.5.2	Wall shear stress	65
5.5.3	Pressure	68
Chapter VI	CONCLUSIONS AND RECOMMENDATIONS	112
6.1	Conclusions	112
6.1.1	Flow in a tube with multiple constrictions	112
6.1.2	Pulsatile flow with time dependent constriction	114
6.1.3	Pulsatile flow with moving boundary	115
6.2	Recommendations	115
	REFERENCES	117
	VITA AUCTORIS	122

## LIST OF TABLES

Table	Title	Page
3.1	Geometry of the models studied in Case 1	31

## LIST OF FIGURES

Figure	Title	Page
3.1	Tube with multiple constrictions	32
3.2	Geometry of a module	33
3.3	Geometry of time dependent constriction	34
3.4	Geometry of moving boundary	35
3.5	Computational domain	36
4.1	Staggered grid arrangement	45
5.1	Comparison of numerical and analytical results for pipe flow	69
5.2	Comparison of non-dimensional pressure drop across stenosis	70
5.3	Comparison of non-dimensional velocity distributions	71
5.4	Comparison of friction coefficients for simple pulsatile flow	73
5.5	Non-dimensional pressure drop across the constrictions	74
5.6	Non-dimensional pressure distribution along the wall	75
5.7	Non-dimensional centreline velocity distribution	77
5.8	Non-dimensional wall shear stress distribution	79
5.9	Stream function contours	81
5.10	Vorticity contours	82
5.11	Comparison of non-dimensional centreline velocity across the modules	83
5.12	Comparison of skin friction coefficient across the modules	86

5.13	Non-dimensional pressure drop across the module versus Reynolds number	89
5.14	Comparison of skin friction coefficients (Case 1 versus Case 2)	90
5.15	Comparison of non-dimensional centreline velocity (Case 1 versus Case 2)	90
5.16	Stream function contours	91
5.17	Vorticity contours	91
5.18	Stream function contours for one complete cycle of pulsation (Case 3)	92
5.19	Skin friction coefficient distribution (Case 3)	94
5.20	Skin friction contours for one complete cycle of pulsation (Case 3)	97
5.21	Vorticity contours for one complete cycle of pulsation (Case 3)	98
5.22	Non-dimensional pressure distribution along the wall (Case 3)	100
5.23	Stream function contours for one complete cycle of pulsation (Case 4)	103
5.24	Skin friction coefficient distribution (Case 4)	105
5.25	Skin friction contours for one complete cycle of pulsation (Case 4)	108
5.26	Non-dimensional pressure distribution along the wall (Case 4)	109

## NOMENCLATURE

$A_c$	amplitude of the constriction (vibrating wall)
$A_E, A_W, A_N, A_S, A_P, A_p^\circ$	coefficients in the general finite volume equations
$A_E^p, A_W^p, A_N^p, A_S^p, A_P^p$	coefficients in the pressure correction equation
$B_u, B_v, C_u, C_v$	coefficients in the velocity corrections
$C_f$	skin friction coefficient = $2\tau_w/\rho U^2$
$D$	diffusion
$D_o$	unconstricted diameter of the tube
$F$	convection
$f$	friction factor = $8\tau_w/\rho U^2$
$m_p$	mass source in the pressure correction equation
$P_e$	Peclet number = $F/D$
$p$	pressure
$r, x$	radial and axial coordinates
$R$	radius of the tube = $f(x, t)$
$Re$	Reynolds number = $\rho U D_o / \mu$
$S$	source term
$s$	axial distance from the centre of the $i^{\text{th}}$ constriction = $x - S_{c(i)}$
$S_p$	spread of the constriction (vibrating portion of the wall)
$St$	Strouhal number = $\omega D_o / U$



$S_{c(i)}$	distance to the centre of the $i^{\text{th}}$ constriction (vibrating wall) from the pipe inlet
$S^{\circ}$	average value of the source term over the control volume
$2T$	time period of one complete cycle of pulsation
$t$	time in the physical domain
$\Delta t$	time step
$U$	time mean cross sectional average velocity at the inlet
$u, v$	x and r components of velocities
$u_m$	instantaneous cross sectional average velocity
$z$	axial distance measured from the centre of the constriction
$\alpha$	dimensionless frequency parameter
$\alpha_1, \beta_1, \beta_2, \gamma, A^t, B^t$	coordinate transformation parameters
$\delta$	phase lag of the instantaneous cross-sectional average velocity to the pressure gradient
$\Delta\xi, \Delta\eta$	cell boundary sizes in the $\xi$ and $\eta$ directions
$K$	pressure drop across a module
$\lambda$	length of a module
$\mu$	viscosity
$\nu$	kinematic viscosity
$\xi, \eta$	non-dimensional curvilinear coordinates
$\rho$	density
$\tau$	time in computational domain

$\tau_w$	wall shear stress
$\phi$	general dependent variable
$\omega$	frequency of pulsation
$\sigma_u$	coefficient of amplitude in the instantaneous cross-sectional average velocity

### **Subscripts**

E,W,N,S	grid points (east,west,north,south)
e,w,n,s	control volume faces (east,west,north,south)
P	central grid point under consideration
*	indicates the dimensional form when used with the variables u, v, x, r, p, t

---

# CHAPTER I

# *Introduction*

---

## **1.1 Motivation**

Internal flow through tubes has many applications in industry and in biofluid mechanics.

Tubes with multiple axisymmetric constrictions have applications in enhancing heat transfer in heat exchangers. A succession of annular tube inserts, uniformly spaced along the length of the tube wall, are used to enhance heat transfer in heat exchangers. Another example of a heat exchanger with a periodic geometry in the flow passage is the offset plate-fin heat exchanger (Patankar et. al (1977)). The reflux condenser used in the distillation process is a concentric pipe heat exchanger which has a number of spatially periodic constrictions in the circular flow passage. The presence of a periodic geometry in the flow passage can lead to spatially periodic flow conditions beyond a certain distance from the inlet. In this region the flow and heat transfer characteristics can be modelled using one single module in the flow region with periodic boundary conditions on the flow variables (Sparrow and Prata (1983)). Identifying the distance from the tube inlet to where the flow field becomes spatially periodic is important in the design of such heat

exchangers. The overall heat transfer rate from a tube of this geometry depends upon the extent of this region.

A common human disease is the hardening of the arterial wall known as atherosclerosis. It involves a lesion on the arterial wall characterized by the accumulation of lipids (fatty acids) (Lighthill (1975)). The build up of atherosclerotic plaque causes a reduction of arterial distensibility and gives rise to increasing demands on the human heart. A local build up of plaque in an artery is commonly known as a stenosis. This is a generic medical term indicating the narrowing of any body passage. The exact reason for the initiation of this arterial growth is still not known. However, some investigators have determined that minor injuries in the arterial wall can quickly lead to the development of gross lesions in the vicinity of the damaged area. The initial injury to the artery may be caused by the large shear stresses which occur near the branches of arteries. It has also been suggested that the localized change in pressure and shear stresses may trigger some biological mechanisms whereby the endothelial cells which line the arterial wall, proliferate with a subsequent narrowing of the artery (Young (1968)). Similarly Lighthill (1975) has indicated that high rates of shear causes actual mechanical damage to the endothelial lining of the arterial wall and fosters the onset of atherosclerosis.

Regardless of the exact initiating factors, the presence of a localized stenosis causes disordered blood flow within and downstream of the constricted region. Knowledge of the flow pattern through a partial occlusion may assist in understanding the pathology of atherosclerosis (Deshpande (1976)). Clark et al. (1983) suggested that the additional changes in flow and shear that are initiated by the atherosclerotic process can cause further build up in the artery. Researchers working in this area place an emphasis on obtaining the precise distributions of the velocity, pressure gradient and shear stress in the vicinity of the stenosis. They believe that these quantities play an important role in the genesis and proliferation of the stenosis. van Dreumel and Kuiken (1989) used the geometry of a stenosis obtained from an angiogram and a numerical method to model stenotic flow. It was suggested that the flow structure obtained numerically, when correlated with the patients symptoms, might provide valuable information regarding the patients prognosis. Angiograms taken from patients showing coronary symptoms have also indicated the presence of several stenoses on the same artery (Talukder et al (1977)). Eventhough this is a common clinical symptom, only a limited amount of information is available on the effect of stenoses in series on a given arterial segment.

The presence of a moving boundary occurs in practically all fluid carrying conduits in the human body. The arteries in the human body experience a positive pressure difference between the inside and outside of the artery and are therefore distended

or inflated (Shapiro (1977)). During cardiac ventricular contraction, however, the muscular action causes an increased pressure on the outside of the artery which causes a contraction of the wall. Unsteady flow behaviour in the portion of the tube which undergoes a contraction and distension of the tube wall may help to gain a better understanding of the actual arterial blood flow. The time and space dependent wall shear stress distribution obtained from studying such flows is considered to be important in the early stages of atherosclerosis (Ralph and Pedley (1988)). The airway in the lung is another example of a place in the human body where repetitive shape changes of a vessel wall occur. The wall motion in this case is a small-amplitude, high-frequency wall flutter. The sound heard during wheezing is due to this motion. Distention of the arterial vessels may occur distal to a stenosis and near bifurcations of arteries. The presence of a minor arterial distention may lead to a condition known as an aneurysm (gross distention of the arterial wall). This is thought to be caused in response to fluctuating pressures and wall shear stresses. The pulsatile nature of the blood flow is also known to create minor shape changes in stenoses.

A lack of information in the areas mentioned above indicates the need for a systematic study of the fluid dynamic quantities and periodicity characteristics associated with internal flow through tubes with constrictions. Also, the models used to analyze moving boundary flows in the human body that are presently available need to be improved upon considerably.

The complexity of the flow fields associated with arbitrary shapes and moving boundaries makes it difficult to analyze the flow field either experimentally or theoretically. Analytical methods to solve fluid flow problems are limited in their range of applicability due to the difficulty in handling complex geometries. Numerical solutions with greater accuracy and reliability are steadily becoming the norm in industry. The advent of more powerful computers together with several major developments in the field of computational fluid dynamics has resulted in an ever increasing activity in the area of numerical simulations of fluid flow problems. Numerical approaches with reliable and robust codes which are thoroughly validated are powerful tools. The approach taken to analyze the problem of arbitrary domains and moving boundaries in the present study is numerical.

A control volume formulation is used in discretizing the governing equations. In numerical simulations of moving boundary problems, there is a need to adapt the grid with time as the shape of the boundary changes. The grid adaptation must be performed with each time step and the movement of the grid must be properly accounted for in the governing equations. A boundary fitted curvilinear coordinate transformation is used in the present study to accomplish this.

## **1.2 Objectives of the Present Work**

The purpose of the present investigation is to study steady flow behaviour through tubes with constrictions and pulsatile flow through a tube with moving boundaries.

The main objectives of this study are:

1. to investigate the spatial periodicity effects in the case of the steady flow through tubes with multiple constrictions;
2. to solve the problem for a single isolated module where the flow field is assumed to be spatially periodic;
3. to provide a reasonable model of pulsatile flows with moving boundaries and
4. to investigate the effect of the moving wall and the frequency of pulsation on the unsteadiness present in the flow.

### **1.3 Statement of the Problem**

Four practical problems were numerically simulated in this work in order to achieve the objectives stated in Section 1.2 and to provide better models of various physiological flows. The spatial periodicity effects were determined by solving the problem of flow in a tube with multiple constrictions. The same problem was then solved by considering a single module in the region where the spatial periodicity of the flow is achieved. The effects of moving boundaries on pulsatile flows were studied using two models. The first model had a constriction which changed in shape periodically with time at a prescribed frequency. The second model had a portion of the wall that distended and contracted at a prescribed frequency of pulsation.



This dissertation has the following format. A review of past work in the area of interest is presented in the next chapter. Chapter 3 gives a detailed description of the problem geometry and the formulation of the governing equations in the computational domain. The boundary conditions and the assumptions associated with the problem are also provided. The numerical methodology used in the present study is presented in Chapter 4. The results obtained for the problems studied are given in Chapter 5. Based on the discussion of the results, conclusions are drawn in Chapter 6 along with recommendations for future work.

---

## **CHAPTER II**

## ***Literature Review***

---

The general area of concern in the present study is internal flows in pipes with constrictions and moving boundaries. Abundant literature is available in the area of steady and unsteady pipe flows and stenotic flows. The purpose of this review is to outline only those investigations that have a direct bearing on the present study. Accordingly an overview of the relevant literature on flow through pipes having single and multiple constrictions, flow in regions having identical geometrical modules in the flow domain, time dependent stenotic flows, flows through flexible tubes and some of the other related works with irregular domains and moving boundaries is presented in this chapter.

### **2.1 Flow Through Tubes with Constrictions in the Flow Passage**

Studies of the stenotic flow fields have been conducted by numerous investigators. Young and Tsai (1973) conducted a series of steady flow experiments concerning stenotic flows for various steady flow factors such as pressure drop, separation and turbulence. Young (1979) gave a wide overview of various aspects of the fluid mechanics of arterial stenosis. Ahmed and Giddens (1983) investigated the velocity field in the neighbourhood of axisymmetric constrictions using a laser

Doppler anemometer. Gowda et al. (1988) presented a flow visualization study of flow through constrictions with different geometries. Ohja et al. (1989) investigated pulsatile flows through constricted tubes using photochromic tracer methods. Experimental studies of stenotic flows have been augmented by various numerical and analytical models. Lee and Fung (1970) used a finite difference method to solve the axisymmetric flow of a viscous incompressible fluid through a locally constricted tube. A stream function-vorticity formulation was used to solve the governing equations and the numerical solution failed to converge for Reynolds number greater than twenty-five. Deshpande et al. (1976) obtained numerical solutions for steady flow utilizing a stream function-vorticity formulation in cylindrical coordinates. O'Brien and Ehrlich (1985) developed finite difference approximations to study the effect of a simple pulsatile flow in a tube with constriction. Durst and Loy (1985) summarized the results of experimental and numerical investigations of laminar flow in a pipe with a sudden constriction in the cross sectional area. The experimental investigation was conducted by using laser Doppler anemometry and the numerical investigations were carried out using a finite volume based method with a primitive variable formulation. They encountered no difficulties for Reynolds numbers at which the flow is known to be laminar. Theodorou and Bellet (1986) presented a perturbation method for determining the velocity distribution for laminar flows of a non-Newtonian fluid under mild stenotic conditions. Kasivisvanathan et al. (1991) studied flows of a non-Newtonian fluid

through axisymmetric pipes of varying cross-sections by means of a perturbation method.

Investigations of flows through tubes with more than one constriction have also been conducted by a few researchers. van Dreumel and Kuiken (1989) conducted experimental and numerical investigations for flows in a tube with double constrictions under steady conditions. The experiments were conducted using a laser Doppler anemometer and numerical results were obtained using a commercial code. Lee (1990) investigated the flow field in the neighbourhood of double constrictions in a tube. The governing equations were expressed in stream function-vorticity form and were transformed into body fitted coordinates. A finite difference method was used to discretize the governing equations. Talukder et al. (1977) conducted an experimental study of the fluid dynamics of multiple noncritical stenoses. In vivo and in vitro measurements of the pressure drop were carried out in the experiments along with the flow visualization studies. They concluded that the total effect of a series of noncritical stenoses is approximately equal to the sum of their individual effects and the combined effect of a series of noncritical stenoses can be critical.

Patankar et al. (1977) identified the periodicity characteristics of ducts whose cross sectional area varies periodically in the streamwise direction and confined the flow field analysis to a single isolated module without involvement of the entrance

region problem. A numerical procedure using a finite volume based approach with primitive variable formulation was used to solve the problem. Sparrow and Prata (1983) obtained a numerical solution of the heat transfer problem in the fully developed region in a pipe with periodically varying cross section. They solved the problem for a module in the spatially periodic region in polar coordinates by partially blocking the flow passage in such a manner to approximate the geometry of a converging-diverging duct. The periodicity boundary conditions were used to solve the problem. Prata and Sparrow (1984) obtained a numerical solution for the heat transfer and fluid flow in an annular tube with periodically varying cross section using essentially a similar approach as in the previous paper.

## **2.2 Flow Through Tubes with Moving Boundaries**

An attempt towards a systematic study of the effect of a time dependent stenosis on flow through a tube was first initiated by Young (1968). An analysis concerning the effect of an axially symmetric, time dependent constriction of the tube of nominally constant cross section, for a Newtonian fluid flow, was presented in the study. The approximate analytical solution presented was based on a simplified model in which the convective terms were neglected. Misra and Chakravarthy (1986) presented a theoretical study of the flow in arteries in the presence of a stenosis by assuming the arterial wall is an initially stressed elastic tube. The wall motion was accounted for by considering that the fluid adheres to the inner surface

of the wall, and the velocity of the fluid on the wall is equal to the velocity of the wall.

Analytical solutions of wave propagation through elastic tubes have been developed by a few researchers. These solutions assume axially symmetric two dimensional flow with the convective terms neglected in the governing equations. The wall motion was modelled as a second order response. Atabek and Lew (1966) gave an analysis of the blood flow in arteries as a viscous incompressible fluid contained in an initially stressed elastic tube by casting the dependent variables in terms of a power series and substituting them in the governing equation. Atabek (1968) analyzed the wave propagation for an initially stressed elastic tube with the additional constraint that the wall was tethered. Dragon and Grotberg (1991) investigated the mass transport of a diffusible substance for oscillatory flow in a flexible tube and derived general perturbation solutions for the flow equations. Wang and Tarbell (1992) analyzed the nonlinear flow of a Newtonian fluid in an elastic tube subjected to an oscillatory pressure gradient using a perturbation based method.

Numerous investigators have conducted experiments using collapsible tubes with the objective of understanding the flow of various fluid carrying conduits in the human body. Most of the work was done in this area using a silicone rubber tube suspended between two rigid pipes. Brower and Scholten (1975) presented

experimental evidence of the instabilities in the flow for such a tube. Bertram (1987) found the effects of wall thickness, axial strain and end proximity on the pressure-area relation of collapsible tubes. Bertram et al. (1990) and (1991) mapped the instabilities for the flow through collapsed tubes of differing length. A detailed study of the pressure-area relationships and application of nonlinear dynamic concepts to the analysis of self-excited oscillations in the collapsible tubes was also presented in the paper.

One dimensional mathematical models were also developed by many investigators for collapsible tubes. Cancelli and Pedley (1985) presented a separated flow model for collapsible tube oscillations. The main features of the model are the inclusion of the wall tension and the energy loss of the separated flow downstream of the time dependent constriction in a collapsing tube. Jensen and Pedley (1989) investigated the existence of steady flow in a one-dimensional collapsible tube model and compared the results with experiments. Jensen (1990) investigated the stability of the steady flow present in a collapsed tube when subjected to small time dependent perturbations.

Experimental and numerical studies have been conducted for flows in a 2-D channel with time dependent oscillation in one wall and steady flow at the inlet with the objective of studying physiological flows. Pedley and Stephanoff (1985) conducted flow visualization experiments for flow along a channel with time

dependent indentation in one wall and gave some theoretical reasoning on the development of various types of eddies created by the moving indentation. Ralph and Pedley (1988) presented a numerical solution for such a flow. The solution was obtained in stream function-vorticity form using a finite difference method. Ralph and Pedley (1989) presented solutions for both viscous and inviscid flows in a similar channel. The numerical results for inviscid flows were also compared with the predictions using a small amplitude inviscid theory (Pedley and Stephanoff (1985)).

### **2.3 Other Related Work with Irregular Domains and Moving Boundaries**

A solution of the incompressible steady Navier-Stokes equations in a general curvilinear coordinate system using a finite difference approximation by solving all variables simultaneously was developed by Vradis et al. (1992). The method was utilized to compute flow through channels with different geometries. Hamdan et al. (1993) studied fluid flow through curved porous channels. The flow equations were formulated using a stream function coordinate system and solved numerically using a finite difference method. An and Barron (1995) solved transonic Euler flows in stream function coordinates. This stream function coordinate system avoids the grid generation step by introducing a von Mises transformation, which produces a formulation in streamwise and natural body-fitting coordinates thereby allowing a single set of equations to function both as flow equations and grid generation equations.



Rhie and Chow (1983) presented a finite volume numerical method for the solution of the two-dimensional incompressible, steady Navier-Stokes equations in general curvilinear coordinates. An ordinary grid system (collocated grid) was utilized instead of the usual staggered grid arrangement. A specific scheme was developed to suppress pressure oscillations. The numerical procedure used was a modified version of the Semi-Implicit Method for Pressure-Linked Equations (SIMPLE) developed by Patankar and Spalding (1972). Peric et al. (1988) gave a detailed comparison of finite volume numerical methods with staggered and collocated grids. Majumdar (1988) studied the role of underrelaxation in momentum interpolation for the calculation of flow with collocated grids.

Demirdzic and Peric (1990) developed a finite volume based method for the flow through a channel with a moving indentation using the integral form of the governing equations for arbitrarily moving control volumes. Fully implicit temporal differencing was used to make the method stable for any time step. Rosenfeld and Kwak (1991) presented a time accurate method to solve incompressible Navier-Stokes equations in generalized moving coordinates. A finite volume discretization procedure that satisfies the geometric conservation laws for time-varying computational cells was utilized. The discretized equations were solved by a fractional step procedure. Venkat and Spaulding (1991) presented a numerical model to predict the nonlinear response of external flow over vibrating bodies. A time dependent coordinate transformation was used along with a stream function-

vorticity formulation. Yeung and Vaidhyanathan (1992) investigated the interaction of two-dimensional water waves with a fixed submerged cylinder using a finite difference scheme with boundary fitted coordinates. A mixed Eulerian-Lagrangian formulation was used to satisfy the free surface conditions. Mateescu et al. (1994) presented computational solutions for unsteady annular flows with oscillating boundaries based on time dependent coordinate transformations in stream function-vorticity variables.

To the candidate's knowledge, no numerical simulations have been attempted to study the periodicity effects of flow in tubes with multiple constrictions. Previous numerical work has been limited to a maximum of two constrictions in the flow passage. It was also found that flow characteristics in a module in the spatially periodic region had not been solved in curvilinear coordinates. Papers dealing with numerical work applied to the area of pulsatile flow in the presence of constrictions are relatively few in number and no numerical work has been done which includes changes in shape (moving boundaries) of the constriction. Authors of recent numerical studies have modeled the flow through flexible tubes (arteries and veins) as the flow in a 2-D channel with a steady inlet condition and a time dependent oscillation of one wall. No attempt has been made to study such flows using pulsatile inlet conditions in a tube with a time dependent oscillation of a portion of the wall. The purpose of the present investigation is to study pulsatile flow through a tube with moving boundaries and steady flow with multiple constrictions.

---

## CHAPTER III

## *Problem Formulation*

---

The problems that are formulated in this work are classified into four different cases. The first case deals with tubes with one, two, three, four and seven constrictions located equidistant from each other. Case 2 deals with the situation where there are a number of constrictions in the tube equidistant from each other and the problem is formulated for one module in the system using periodic boundary conditions. Both these cases are at steady state conditions with the constrictions creating a 75% reduction in the flow area at the constriction. In Case 3 there is a pulsatile flow at the inlet of the tube and a time dependent constriction. The constriction was allowed to change in shape with time at a prescribed frequency. In Case 4 the flow behaviour in a tube which has a pulsatile flow inlet condition and a time dependent motion which undergoes both contraction and distension was studied. In the case of pulsating flow, frequencies are usually represented in terms of a non-dimensional frequency parameter,  $\alpha$ , which is sometimes referred to as the Womersley frequency parameter. The phase lag of the instantaneous mass flow rate to that of the pressure gradient increases from zero in steady flow to  $90^\circ$  in a pulsation of infinite frequency. For a low frequency

pulsation, i.e,  $\alpha \leq 1$ , the phase lag is very close to zero and the flow field can be approximated by quasi-steady behaviour (Uchida 1956). This was not considered in the present study. For  $\alpha \geq 10$ , the phase lag is approximately  $90^\circ$ . Flow in a human carotid artery has a frequency parameter of approximately 7.5 and hence only the high frequency range was selected for study. Changes in the shape of the wall of the tube in Cases 3 and 4 were assumed to vary with time at a certain frequency of pulsation. In both of these cases the interaction between the fluid and the wall was decoupled and the influence of wall motion came through a prescribed time dependent motion at the wall. In all of the cases studied, laminar flow conditions were assumed.

#### **Case 1. Tube with multiple constrictions**

This case consists of five flow situations. The flows in a tube with one, two, three, four and seven constrictions were simulated. The geometry of the model with four constrictions, M4, is shown in Figure 3.1. The pertinent geometric characteristics of the models are summarized in Table 3.1. The geometry of the models M1, M2, M3 and M7 are essentially the same as shown in Figure 3.1 except that model M1 has only the first constriction, model M2 has the first and second constrictions, model M3 has the first three constrictions and model M7 has totally seven constrictions. The model with seven similar constrictions, M7, was used to test the development of periodicity.

### **Case 2. Modular approach**

The basic assumption in this approach was that the fluid flowing in a tube with a periodically varying cross section in space attains a spatial periodic regime in the sense that the velocity field repeats itself at corresponding axial stations in successive cycles under laminar flow conditions. Hence the governing equations for the fluid flow were solved for a single isolated module without dealing with the entrance region problem. The geometry of such a module is shown in Figure 3.2.

### **Case 3. Pulsatile flow with time dependent constriction**

The geometry of the model studied for pulsatile flows in a tube with a time dependent constriction is shown in Figure 3.3. The height of the constriction,  $A_c$ , was prescribed to vary between  $0.15D_o$  and  $0.25D_o$ , where  $D_o$  is the unstricted tube diameter. The spread of the constriction,  $S_p$ , was taken to be  $2D_o$ . It was assumed that  $A_c$  will have its lowest value when the instantaneous mass flow rate is maximum and its highest value when the instantaneous mass flow rate is minimum thereby ensuring that the instantaneous mass flow rate and the pipe radius variation are in phase. This assumption is practical as it ensures that the change in the shape of the constriction has a phase lag with respect to the pressure at the wall.

### **Case 4. Pulsatile flow with moving boundary**

Figure 3.4 represents the model studied for this case. The spread of the vibrating

portion of the wall,  $S_p$ , was taken to be  $2D_o$ . The maximum and minimum values of the amplitude of vibration of the wall was between  $\pm 0.05D_o$ . It was assumed that the tube wall will be distended to its maximum extent when the instantaneous mass flow rate is maximum and contracted to its minimum value when the instantaneous mass flow is minimum thereby ensuring that the instantaneous mass flow rate and the pipe radius variation are in phase. This assumption ensures that the change in the shape of the wall has a phase lag with respect to the pressure at the wall.

### **3.1 Governing Equations**

The governing equations are expressed in cylindrical coordinates. Axisymmetric flow conditions are assumed for all the problems considered. The equations representing the flow are expressed in the primitive variable form. The primitive variable form of the governing equations is selected because it is easier to extend the models to three dimensions and to include turbulence effects. A boundary fitted coordinate transformation is necessary due to the presence of arbitrary domains and moving boundaries. Accordingly, a boundary fitted curvilinear coordinate system is selected to enable the problem to be solved in a fixed computational domain. The use of a curvilinear coordinate system also enables the shape of the wall to be changed without any changes to the numerical method.

The non-dimensional quantities are defined as;

$$\begin{aligned}
u &= \frac{u_i}{U}, \quad v = \frac{v_i}{U}, \quad x = \frac{x_i}{D_o}, \quad r = \frac{r_i}{D_o}, \quad p = \frac{p_i}{\rho U^2}, \\
t &= \frac{t_i U}{D_o}, \quad St = \frac{\omega D_o}{U}, \quad \alpha = \frac{D_o}{2} \sqrt{\frac{\omega}{\nu}} \text{ and } Re\theta = \frac{\rho U D_o}{\mu}.
\end{aligned} \tag{3.1}$$

where U is the time mean cross sectional average velocity at the inlet. The non-dimensional frequency parameter,  $\alpha$ , and Strouhal Number, St, are directly related as can be seen from Equation (3.1). The governing equations for axisymmetric, incompressible and laminar flow are the mass conservation equation and the x and r components of the momentum equation which are given below.

### Mass Conservation Equation

$$\frac{\partial u}{\partial x} + \frac{1}{r} \frac{\partial(rv)}{\partial r} = 0. \tag{3.2}$$

### Momentum Equations

$$\left[ \frac{\partial u}{\partial t} + \frac{\partial(uu)}{\partial x} + \frac{1}{r} \frac{\partial(rvu)}{\partial r} \right] = \frac{1}{Re\theta} \left[ \frac{\partial^2 u}{\partial x^2} + \frac{1}{r} \frac{\partial}{\partial r} \left( r \frac{\partial u}{\partial r} \right) \right] - \frac{\partial p}{\partial x}. \tag{3.3}$$

$$\left[ \frac{\partial v}{\partial t} + \frac{\partial(uv)}{\partial x} + \frac{1}{r} \frac{\partial(rvv)}{\partial r} \right] = \frac{1}{Re\theta} \left[ \frac{\partial^2 v}{\partial x^2} + \frac{1}{r} \frac{\partial}{\partial r} \left( r \frac{\partial v}{\partial r} \right) - \frac{v}{r^2} \right] - \frac{\partial p}{\partial r}. \tag{3.4}$$

### 3.2 Transformation of Basic Equations

The physical domain is mapped into a fixed rectangular domain. The new coordinate system is defined as  $\xi = \xi(x,r,t)$  and  $\eta = \eta(x,r,t)$ . The transformed computational domain is shown in Figure 3.5. The partial derivatives of any

function,  $f$ , can be transformed as

$$f_x = \frac{(r_\eta f_\xi - r_\xi f_\eta)}{J} \text{ and } f_r = \frac{(-x_\eta f_\xi + x_\xi f_\eta)}{J}, \quad (3.5)$$

where  $J$  is the Jacobian of the transformation and given by

$$J = x_\xi r_\eta - x_\eta r_\xi = \frac{1}{\xi_x \eta_r - \eta_x \xi_r}. \quad (3.6)$$

The time derivative is represented by the chain rule as

$$f_t = f_\tau + \xi_\tau f_\xi + \eta_\tau f_\eta. \quad (3.7)$$

The terms  $\xi_\tau$  and  $\eta_\tau$  are obtained as

$$\xi_\tau = -\frac{(x_\tau r_\eta - r_\tau x_\eta)}{J} \text{ and } \eta_\tau = -\frac{(x_\xi r_\tau - x_\tau r_\xi)}{J}. \quad (3.8)$$

The governing equations (Equations (3.2),(3.3),(3.4)) can be expressed as

$$\left[ \frac{\partial \phi}{\partial t} + \frac{\partial (u\phi)}{\partial x} + \frac{1}{r} \frac{\partial (rv\phi)}{\partial r} \right] = \frac{1}{Re} \left[ \frac{\partial^2 \phi}{\partial x^2} + \frac{1}{r} \frac{\partial}{\partial r} \left( r \frac{\partial \phi}{\partial r} \right) \right] + S^\phi \quad (3.9)$$

where  $\phi = 1, u$  or  $v$  for the mass conservation and the  $x$  and  $r$  components of the momentum equation respectively.  $S^\phi$  is a source term which is zero for the mass conservation equation.

Employing the procedure of transformation given by Equations (3.5) to (3.8) on Equation (3.9), the governing equations are transformed into the  $(\xi, \eta, \tau)$  coordinate system.  $\tau$  will be represented as  $t$  henceforth as both these quantities are the same. The governing equations in the transformed coordinate system takes the following form.



$$\begin{aligned}
& \phi_r + \frac{1}{J}((r_r x_\eta - x_r r_\eta)\phi_\xi - (r_r x_\xi - x_r r_\xi)\phi_\eta + \\
& \frac{\partial}{\partial \xi}(ur_\eta \phi) - \frac{1}{r} \frac{\partial}{\partial \xi}(rvx_\eta \phi) + \frac{1}{r} \frac{\partial}{\partial \eta}(rvx_\xi \phi) - \frac{\partial}{\partial \eta}(ur_\xi \phi)) = \\
& \frac{1}{ReJ} \left( \frac{\partial}{\partial \xi} \frac{1}{J} (r_\eta r_\eta) \phi_\xi + \frac{1}{r} \frac{\partial}{\partial \xi} \frac{1}{J} (rx_\eta x_\eta) \phi_\xi - \frac{\partial}{\partial \xi} \frac{1}{J} (r_\eta r_\xi) \phi_\eta - \frac{1}{r} \frac{\partial}{\partial \xi} \frac{1}{J} (rx_\eta x_\xi) \phi_\eta + \right. \\
& \left. \frac{\partial}{\partial \eta} \frac{1}{J} (r_\xi r_\xi) \phi_\eta + \frac{1}{r} \frac{\partial}{\partial \eta} \frac{1}{J} (rx_\xi x_\xi) \phi_\eta - \frac{\partial}{\partial \eta} \frac{1}{J} (r_\xi r_\eta) \phi_\xi - \frac{1}{r} \frac{\partial}{\partial \eta} \frac{1}{J} (rx_\xi x_\eta) \phi_\xi \right) + S^\phi
\end{aligned} \tag{3.10}$$

The second and third terms in this equation represent the grid movement, thereby enabling the equation to be solved in a fixed computational plane.

The terms in  $S^\phi$  containing derivatives with respect to the original independent variables are transformed in terms of the new independent variables. Hence for the x and r components of the momentum equation

$$\begin{aligned}
S^v &= -\frac{v}{Re r^2} + \frac{1}{J}(x_\eta p_\xi - x_\xi p_\eta) \text{ and} \\
S^u &= \frac{1}{J}(-r_\eta p_\xi + r_\xi p_\eta) ,
\end{aligned} \tag{3.11}$$

respectively.

### 3.3 Assumptions and Boundary Conditions

For all the cases considered, the fluid was taken to be incompressible and Newtonian with constant properties. Laminar flow conditions were assumed.

### Case 1. Tube with multiple constrictions

The transient terms were neglected as steady state conditions were assumed for this problem. The flow was considered to be axisymmetric.

The boundary conditions on the symmetry line are;

$$\frac{\partial u}{\partial r} = 0 \text{ and } v = 0 \text{ at } r = 0 . \quad (3.12)$$

On the solid bounding walls the no-slip boundary condition is used as follows,

$$u = 0 \text{ and } v = 0 \text{ at } r = R . \quad (3.13)$$

At the inlet, the flow is assumed to be fully developed and laminar, therefore,

$$u = 2(1-4r^2) \text{ and } v = 0 \text{ at } x = 0 , \quad (3.14)$$

and at the exit, the zero gradient boundary conditions are used,

$$\frac{\partial u}{\partial x} = 0 \text{ and } \frac{\partial v}{\partial x} = 0 . \quad (3.15)$$

The equation representing the shape of the wall is expressed as

$$R = 0.5D_o - \sum_{i=1}^n A_c \exp\left(-\frac{1}{2(0.25S_p)^2}(x - S_{c_i})^2\right) . \quad (3.16)$$

where  $n$  is the total number of constrictions. The constrictions are located sufficiently apart from each other such that the shape of one of the constrictions has practically no influence on the other constrictions.

### Case 2. Modular approach

The modular approach was developed under the assumption that the fluid flow in a tube with a periodically varying cross section attains spatial periodicity condition.

Hence the governing equations for the fluid flow could be solved for a single

isolated module without considering the entrance region problem. The periodic conditions of the velocity components is expressed as:

$$\begin{aligned} u(x,r) &= u(x + \lambda, r) \text{ and} \\ v(x,r) &= v(x + \lambda, r) , \end{aligned} \quad (3.17)$$

where  $x$  is any arbitrary location in the spatially periodic region and  $\lambda$  is the length of the module (the distance between two successive constrictions). The cross sectional pressure distributions at  $x$  and  $x + \lambda$  are identical in shape, but the pressure level is lower in the downstream station. It then follows that

$$p(x,r) - p(x + \lambda, r) = p(x + \lambda, r) - p(x + 2\lambda, r) = \dots \quad (3.18)$$

The pressure drop across a module of length  $\lambda$  is defined as:

$$\frac{p(x,r) - p(x+\lambda,r)}{\lambda} = K , \quad (3.19)$$

where  $K$  is a constant. This pressure field at any location  $(x,r)$  could be subdivided into two components as follows:

$$p(x,r) = -Kx + \bar{p}(x,r) , \quad (3.20)$$

where  $\bar{p}(x,r)$  is the periodic component, the value of which is repetitive over successive modules and  $K$  is an assignable parameter, which is related to the average flow rate and Reynolds number. The periodic condition for pressure is expressed as;

$$\bar{p}(x,r) = \bar{p}(x + \lambda, r) . \quad (3.21)$$

The governing equations retain the same form as in Case 1, however, with the following modifications. The reference velocity,  $\mu/(\rho D_o)$ , is used instead of the time mean cross sectional average velocity at the inlet and the non-dimensional

quantities were modified accordingly. The pressure gradient terms that appear in the momentum equations (3.3) and (3.4) are modified using Equations (3.20) and (3.21) as:

$$-\frac{\partial p}{\partial x} = K - \frac{\partial \bar{p}}{\partial x} \text{ and } \frac{\partial p}{\partial r} = \frac{\partial \bar{p}}{\partial r} . \quad (3.22)$$

and the  $S_v$  term in Equation (3.11) has an additional term  $K$ . The boundary conditions at the wall and symmetry line are the same as in Case 1. The periodic conditions, Equations (3.17) and (3.21), are used at the inlet and exit of the module and the value for  $K$  is assigned. The equation representing the shape of the wall is expressed as

$$R = 0.5D_o - A_c \exp\left(-\frac{x^2}{2(0.25S_p)^2}\right) - A_c \exp\left(-\frac{1}{2(0.25S_p)^2}(x - \lambda)^2\right) . \quad (3.23)$$

### Case 3. Pulsatile flow with time dependent constriction

The transient terms were included for this problem as the flow is unsteady. It was assumed that the symmetry about the centreline is maintained and there is no wall movement in the axial direction.

The boundary conditions on the symmetry line are

$$\frac{\partial u}{\partial r} = 0 \text{ and } v = 0 \text{ at } r = 0 . \quad (3.24)$$

On the solid bounding walls the no-slip boundary condition is used as given below.

$$u = 0 \text{ and } v = \frac{\partial R}{\partial t} \text{ at } r = R(x,t) . \quad (3.25)$$

The u component of velocity is zero at the wall because it is assumed that there is no wall movement in the axial direction.

At the inlet, the flow is assumed to have a simple pulsation which is periodic in time. The condition of simple pulsation indicates that only a single harmonic is present. This condition of simple pulsating viscous flow superposed on the steady laminar motion in a pipe has been determined analytically by Uchida (1956). The pressure gradient for a simple periodic pulsation becomes a function of time and can be expressed in terms of a steady and fluctuating component as

$$-\frac{\partial p}{\partial x} = \overline{\left(-\frac{\partial p}{\partial x}\right)} + \left(-\frac{\partial p}{\partial x}\right)' , \quad (3.26)$$

where

$$\overline{\left(-\frac{\partial p}{\partial x}\right)} = x_o \text{ and } \left(-\frac{\partial p}{\partial x}\right)' = x_{cm} \cos(2\pi tSt) . \quad (3.27)$$

$x_o$  represents the time mean component of the pressure gradient, whereas,  $x_{cm}$  represents the amplitude of the fluctuating component of the pressure gradient.

The inlet velocity is assumed to be a fully developed simple pulsatile flow. This is determined by substituting Equations (3.26) and (3.27) into the governing equations for a fully developed time dependent flow. It is expressed in terms of a steady component and an unsteady term as

$$u = u_s + u' . \quad (3.28)$$

The radial component of the velocity is taken as zero at the inlet. The steady and

fluctuating components of axial velocity are expressed respectively as

$$u_s = 2(1-4r^2) \text{ and} \quad (3.29)$$

$$u' = \frac{x_m}{x_o} \left\{ \frac{8B}{(\alpha)^2} \cos(2\pi tSt) + \frac{8(1-A)}{(\alpha)^2} \sin(2\pi tSt) \right\} .$$

A and B are determined from

$$A = \frac{\text{ber}(\alpha)\text{ber}(2\alpha r) + \text{bei}(\alpha)\text{bei}(2\alpha r)}{\text{ber}^2(\alpha) + \text{bei}^2(\alpha)} \text{ and} \quad (3.30)$$

$$B = \frac{\text{bei}(\alpha)\text{ber}(2\alpha r) - \text{ber}(\alpha)\text{bei}(2\alpha r)}{\text{ber}^2(\alpha) + \text{bei}^2(\alpha)} .$$

The functions 'ber' and 'bei' are a certain class of Bessel functions known as Kelvin functions and their generalizations are given by Watson (1966). The instantaneous cross sectional average velocity for the simple periodic velocity produced by Equation (3.28) also changes periodically and can be expressed as

$$u_m = 1 + \frac{x_m}{x_o} \sigma_u \cos(2\pi tSt - \delta) , \quad (3.31)$$

where

$$\sigma_u = \frac{8}{(\alpha)^2} \sqrt{\left(1 - \frac{2C}{\alpha}\right)^2 + \left(\frac{2D}{\alpha}\right)^2} \text{ and} \quad (3.32)$$

$$\delta = \tan^{-1} \left\{ \frac{1 - \frac{2C}{\alpha}}{\frac{2D}{\alpha}} \right\} ,$$

are the coefficients of amplitude and phase lag with respect to the wave of the pressure gradient, respectively. The coefficients C and D in Equation (3.32) are given by Uchida (1956).

At the exit, zero gradient boundary conditions are used as follows:

$$\frac{\partial u}{\partial x} = 0 \text{ and } \frac{\partial v}{\partial x} = 0 . \quad (3.33)$$

The equation for the non-dimensional pipe wall radius which represents the movement of the constriction is given by

$$R = f(x,t) = 0.5 + A_c \exp\left(-\frac{1}{2(0.25S_p)^2}(x - S_p)^2\right) \quad (3.34)$$

$$\text{where } A_c = A_i (1 - B_i \cos(2\pi tSt - \delta)) .$$

#### Case 4. Pulsatile flow with moving boundary

The boundary conditions for this problem are the same as in Case 3. The equation for wall motion is expressed as

$$R = f(x,t) = 0.5 + A_c \exp\left(-\frac{1}{2(0.25S_p^2)}(x - S_p)^2\right) \quad (3.35)$$

$$\text{where } A_c = A_i \cos(2\pi tSt - \delta) .$$

### 3.4 Grid Generation Methodology

Equation (3.10) is the governing equation expressed in general curvilinear coordinates. The grid system that is utilized to solve the governing equations can be generated using algebraic or differential equation methods. For the problems considered here it is convenient to use algebraic grid generation as follows:

$$\begin{aligned}
\tau &= t, \\
\xi &= x \text{ and} \\
\eta &= \frac{r}{f(x,t)}.
\end{aligned}
\tag{3.36}$$

where  $f(x,t)$  is the function which describes the variation of the tube radius. In the present study  $f(x,t)$  is given by Equations (3.16), (3.23), (3.34) or (3.35) for different cases. The metrics of the transformations  $(x_\tau, r_\tau, x_\xi, r_\xi, x_\eta, r_\eta)$  can also easily be found from Equation (3.36). The result is to transform a physical domain with a moving boundary (or arbitrary fixed boundary if  $R = f(x)$ ) into a fixed computational domain like the one shown in Figure 3.5.

In the problems where there is a moving boundary the metrics of the transformation carry information about the moving grid to the governing equations. This effect is taken into account by the second and third terms in Equation (3.10) which represent the grid movement for the problems studied.



Model	Area Reduction	No. of Constrictions	Re	S <sub>c1</sub>	S <sub>c2</sub>	S <sub>c3</sub>	S <sub>c4</sub>	S <sub>c5</sub>	S <sub>c6</sub>	S <sub>c7</sub>
M1	75%	1	50-250	3	-	-	-	-	-	-
M2	75%	2	50-250	3	9	-	-	-	-	-
M3	75%	3	50-250	3	9	15	-	-	-	-
M4	75%	4	50-250	3	9	15	21	-	-	-
M7	75%	7	50-250	3	9	15	21	27	33	39

**Table 3.1. Geometry of the models studied in Case 1**

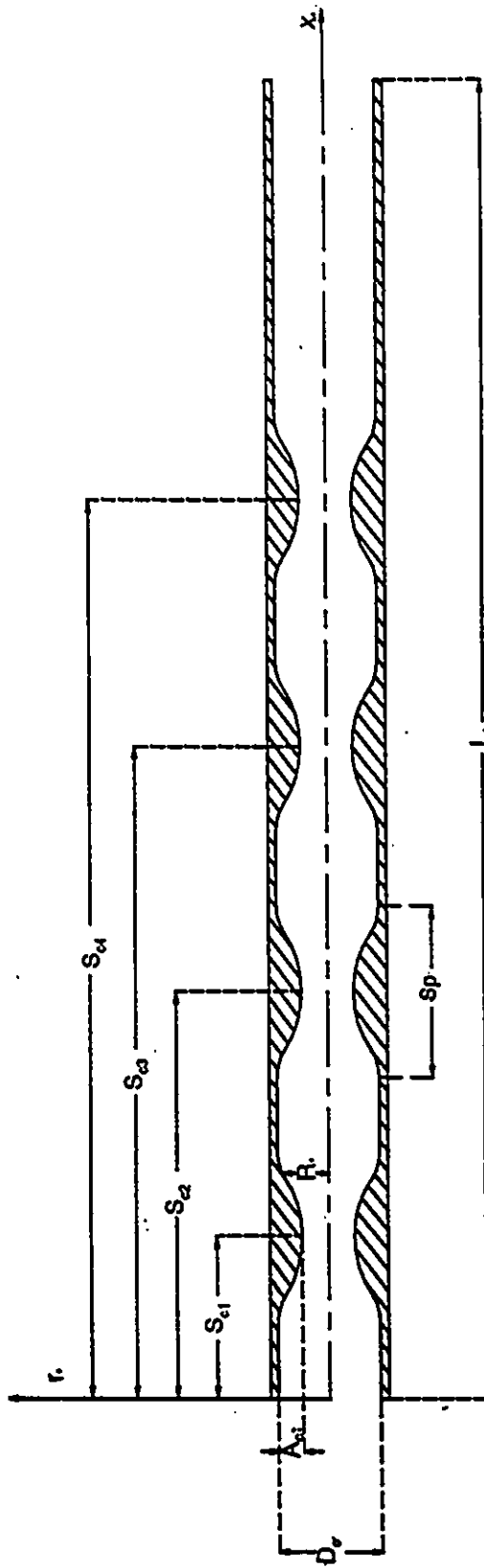
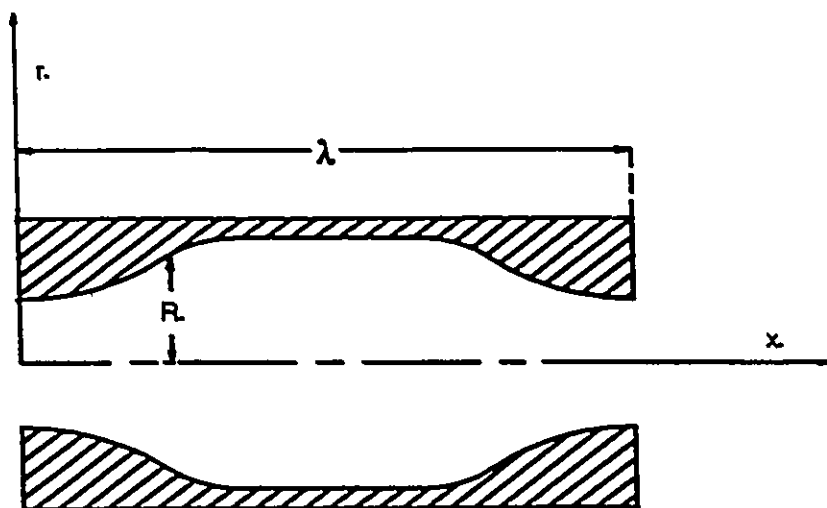
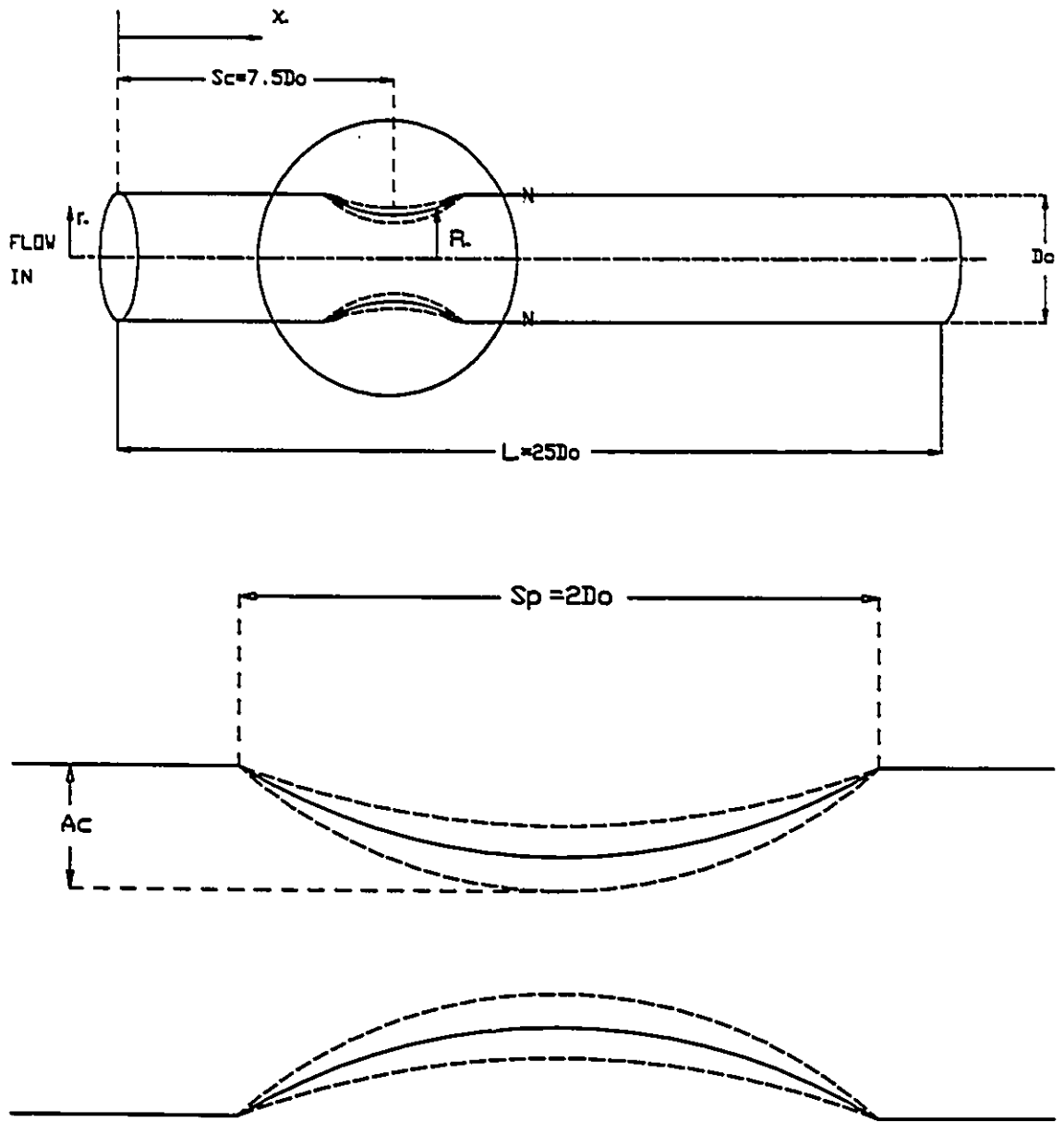


Figure 3.1 Tube with multiple constrictions



**Figure 3.2 Geometry of a module**



**Figure 3.3 Geometry of time dependent constriction**

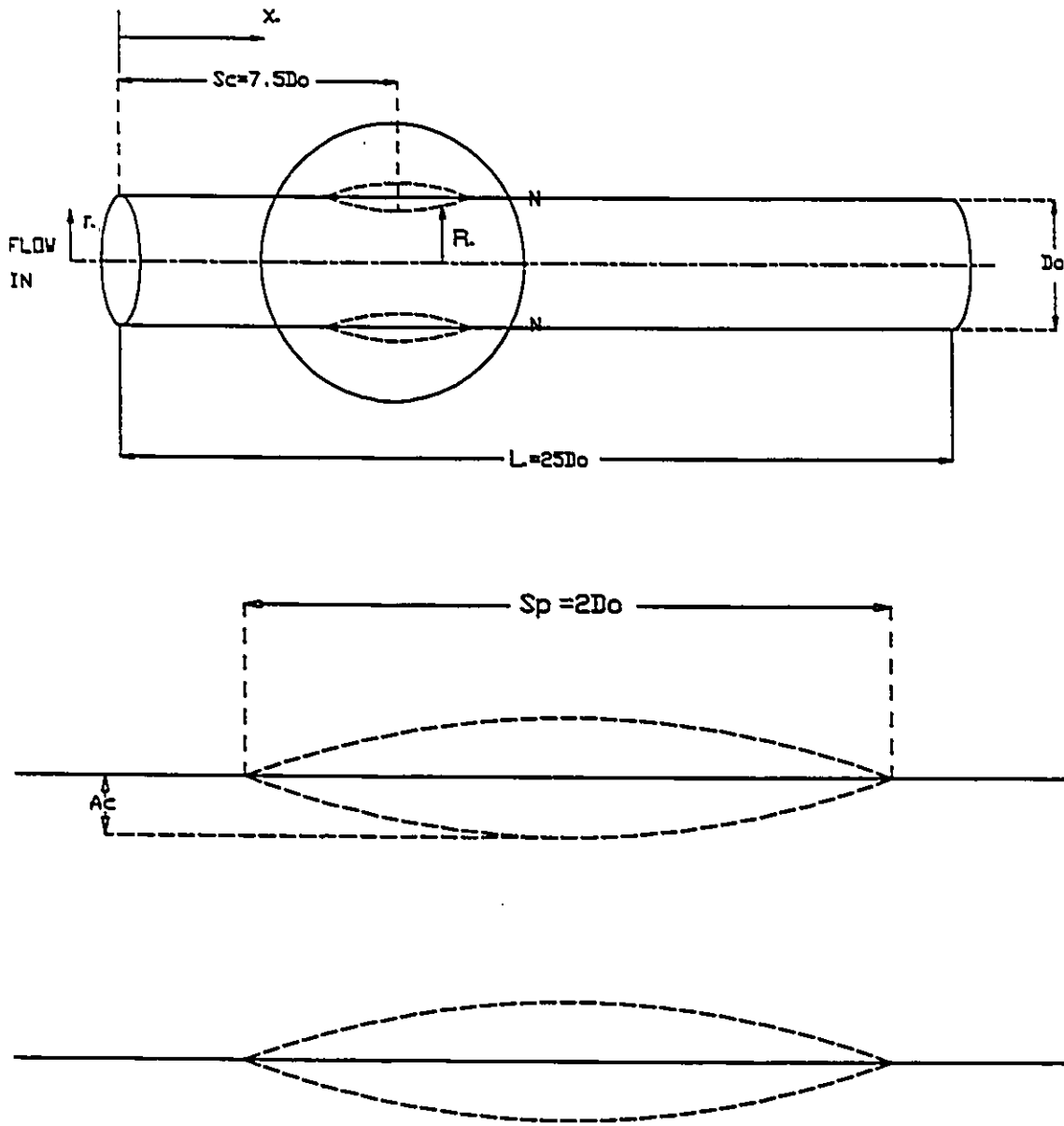


**Figure 3.4 Geometry of moving boundary**

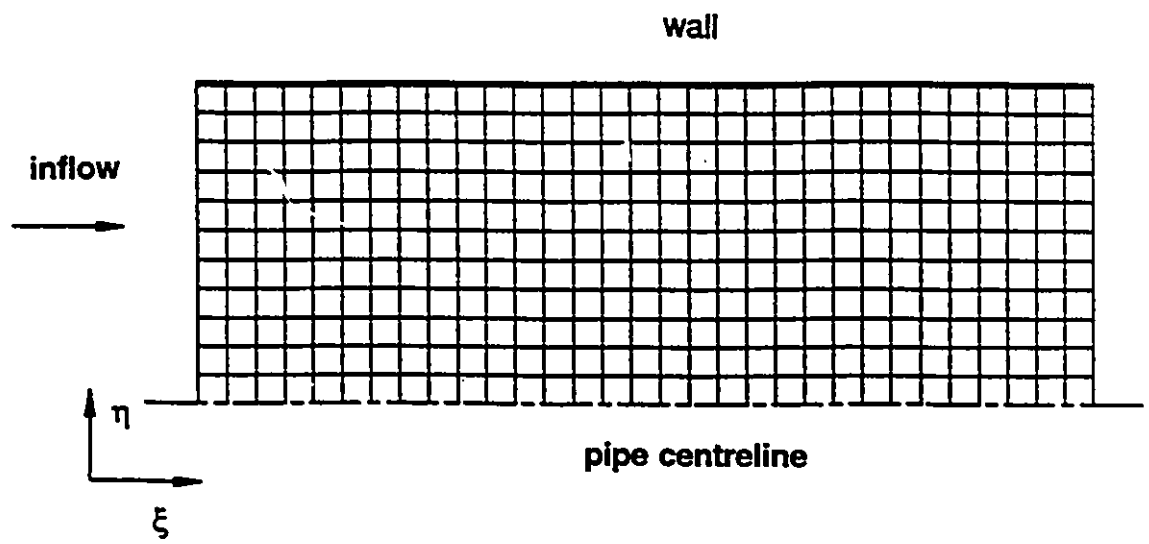


**Figure 3.5 Computational domain**

Numerical prediction of the fluid flow involves the discretization of a set of transformed partial differential equations over the domain of interest to yield a set of algebraic equations. These algebraic equations are solved sequentially by an iterative method. The conversion of the differential equations into approximate algebraic equations is carried out by integrating the differential equations over a small control volume. The numerical scheme used in the present method is similar to the SIMPLE method developed by Patankar and Spalding(1972). Rhie and Chow (1983) adopted a curvilinear coordinate system to remove the geometric limitations of the SIMPLE method for a steady flow problem. The present method is a modified version of their method as it involves transforming the governing equations from polar coordinates to boundary fitted curvilinear coordinates and extends the numerical scheme to handle unsteady problems.

#### **4.1 Numerical Method**

The staggered grid arrangement used for the solution is shown in Figure 4.1. Integrating Equation (3.10) over the control volume, the approximation of the integral conservation equation can be written as

$$\begin{aligned}
& J\Delta\xi\Delta\eta\left(\frac{\phi_p - \phi_p^o}{\Delta t}\right) + (G_{11}\phi\Delta\eta)_w^o + \\
(G_{22}\phi\Delta\xi)_s^n &= \left\{\frac{1}{J R\theta}(\alpha_1\phi_\xi - \beta_1\phi_\eta)\Delta\eta\right\}_w^o + \\
& \left\{\frac{1}{J R\theta}(\gamma\phi_\eta - \beta_2\phi_\xi)\Delta\xi\right\}_s^n + S^\phi J\Delta\xi\Delta\eta,
\end{aligned} \tag{4.1}$$

where  $G_{11} = G_1 + J\dot{\xi}_t$ ,  $G_{22} = G_2 + J\dot{\eta}_t$  and

$$G_1 = ur_{\eta_p} - \frac{r}{r_p}vx_{\eta_p}, \quad G_2 = \frac{r}{r_p}vx_{\xi_p} - ur_{\xi_p}. \tag{4.2}$$

$G_1$  and  $G_2$  are directly related to the contravariant components of velocity. The terms  $\xi_t$  and  $\eta_t$  given in Equation (3.8) correspond to grid movement in the physical plane and

$$\alpha_1 = r_{\eta_p}r_\eta + \frac{r}{r_p}x_{\eta_p}x_\eta, \quad \beta_1 = r_{\eta_p}r_\xi + \frac{r}{r_p}x_{\eta_p}x_\xi, \tag{4.3}$$

$$\beta_2 = r_{\xi_p}r_\eta + \frac{r}{r_p}x_{\xi_p}x_\eta \text{ and } \gamma = r_{\xi_p}r_\xi + \frac{r}{r_p}x_{\xi_p}x_\xi.$$

A relation between the dependent variable  $\phi$  at point P and its neighbouring points, E,W,N,S is then obtained as follows;

$$\begin{aligned}
A_P\phi_P &= A_E\phi_E + A_W\phi_W + A_N\phi_N + A_S\phi_S + S^\phi J\Delta\xi\Delta\eta \\
& - \left[ \left( \frac{1}{R\theta J} \beta_1 \phi_\eta \Delta\eta \right)_w^o + \left( \frac{1}{R\theta J} \beta_2 \phi_\xi \Delta\xi \right)_s^n \right].
\end{aligned} \tag{4.4}$$



The coefficients, A, involve the effects of convection, diffusion and area. The last two terms in the equation are ~~originated~~<sup>obtained</sup> from the cross products of the diffusion terms and can be included in the source terms for numerical computation. Representing the source term as  $\bar{S}$ , it can be linearized as  $\bar{S} = S_c - S_p \phi_p$ . While performing the calculations, the terms corresponding to  $S_p$  are combined with  $A_p$ .

The coefficients are calculated according to the power law scheme (Patankar and Spalding (1972)) which is known to provide an accurate representation of the exact solution when applied to a one-dimensional problem and performs reasonably well in problems of higher dimensions.

The coefficients are expressed as

$$\begin{aligned}
 nA_E &= D_e \max(0, 1 - 0.1 |P_e|^5) + \max(-F_e, 0) , \\
 A_W &= D_w \max(0, 1 - 0.1 |P_w|^5) + \max(F_w, 0) , \\
 A_N &= D_n \max(0, 1 - 0.1 |P_n|^5) + \max(-F_n, 0) , \\
 A_S &= D_s \max(0, 1 - 0.1 |P_s|^5) + \max(F_s, 0) , \tag{4.5}
 \end{aligned}$$

$$A_p^o = \frac{J \Delta \xi \Delta \eta}{\Delta t} ,$$

$$A_p = A_E + A_W + A_N + A_S + A_p^o + S_p J \Delta \xi \Delta \eta \text{ and } P = \frac{F}{D} ,$$

where

$$\begin{aligned}
D_n &= \frac{1}{Re J} \gamma_n \frac{\Delta \xi}{\Delta \eta} \text{ and } F_n = (G_2)_n \Delta \xi , \\
D_s &= \frac{1}{Re J} \gamma_s \frac{\Delta \xi}{\Delta \eta} \text{ and } F_s = (G_2)_s \Delta \xi , \\
D_o &= \frac{1}{Re J} \alpha_{1o} \frac{\Delta \eta}{\Delta \xi} \text{ and } F_o = (G_1)_o \Delta \eta , \\
D_w &= \frac{1}{Re J} \alpha_{1w} \frac{\Delta \eta}{\Delta \xi} \text{ and } F_w = (G_1)_w \Delta \eta .
\end{aligned}
\tag{4.6}$$

The quantities such as  $(G_1)_o$  and  $D_o$  are obtained by linear interpolation in the physical plane and the pressure correction terms are derived in a manner similar to the SIMPLE method.

#### 4.2 Pressure Correction Equation

It can be seen that the momentum equations can be solved only when the pressure field is known. The velocity field will not satisfy the continuity equation and instead produces a net mass source if the pressure field is guessed. Representing the imperfect velocity field as  $u^*$  and  $v^*$ , based on the guessed pressure field  $p^*$ , it can be seen that an imperfect (starred) velocity field will result from the solution of the momentum equation.

To remove this mass source, it is assumed that at each iteration level the velocity field is corrected by the following relations. The terms with primes represent the correction terms

$$\begin{aligned}
u &= u^* + (B^u p'_\xi + C^u p'_\eta) \text{ and} \\
v &= v^* + (B^v p'_\xi + C^v p'_\eta) .
\end{aligned}
\tag{4.7}$$

where

$$\begin{aligned}
B^u &= \frac{-r_\eta \Delta \eta \Delta \xi}{A_p} , \quad C^u = \frac{r_\xi \Delta \eta \Delta \xi}{A_p} , \\
B^v &= \frac{x_\eta \Delta \eta \Delta \xi}{A_p} , \quad C^v = \frac{-x_\xi \Delta \eta \Delta \xi}{A_p} ,
\end{aligned}
\tag{4.8}$$

and  $p'$  is the pressure correction which is related to  $p$  according to

$$p = p^* + p' . \tag{4.9}$$

The correction equations for  $G_1$  and  $G_2$  are obtained by using the velocity and pressure corrections and Equation (3.2) as

$$\begin{aligned}
G_1 &= G_1^* + (B^u r_{\eta_p} - \frac{r}{r_p} B^v x_{\eta_p}) p'_\xi + (C^u r_{\eta_p} - \frac{r}{r_p} C^v x_{\eta_p}) p'_\eta \text{ and} \\
G_2 &= G_2^* + (\frac{r}{r_p} B^v x_{\xi_p} - B^u r_{\xi_p}) p'_\xi + (\frac{r}{r_p} C^v x_{\xi_p} - C^u r_{\xi_p}) p'_\eta .
\end{aligned}
\tag{4.10}$$

The terms corresponding to  $p'_\eta$  in the equation for  $G_1$  and  $p'_\xi$  in the equation for  $G_2$  are omitted as a matter of computational convenience and hence

$$G_1 = G_1^* + \bar{B}p'_\xi \text{ and } G_2 = G_2^* + \bar{C}p'_\eta$$

where  $\bar{B} = B^u r_{\eta p} - \frac{r}{r_p} B^v x_{\eta p}$  and  $\bar{C} = \frac{r}{r_p} C^v x_{\xi p} - C^u r_{\xi p}$ .

(4.11)

The pressure correction equation can be obtained by substituting Equation (4.11) into the mass conservation equation (Equation (3.2)). The omission of various terms in determining the velocity corrections will not affect the final converged solution. In the final converged solution the correction terms vanish, thereby satisfying the governing equations.

The pressure correction equation takes the form;

$$(G_1^* \Delta \eta)_e - (G_1^* \Delta \eta)_w + (G_2^* \Delta \xi)_n - (G_2^* \Delta \xi)_s + (\bar{B}p'_\xi \Delta \eta)_e - (\bar{B}p'_\xi \Delta \eta)_w + (\bar{C}p'_\eta \Delta \xi)_n - (\bar{C}p'_\eta \Delta \xi)_s = 0.$$
(4.12)

A relationship for the variable p at point P and its neighbouring points E,W,N,S can be obtained is given as

$$A_p p_p' = A_E p_E' + A_W p_W' + A_N p_N' + A_S p_S' + m_p$$
(4.13)

where

$$A_N^p = \bar{C} \frac{\Delta \xi}{\Delta \eta} \Big|_n, \quad A_S^p = \bar{C} \frac{\Delta \xi}{\Delta \eta} \Big|_s,$$

$$A_E^p = \bar{B} \frac{\Delta \eta}{\Delta \xi} \Big|_e, \quad A_W^p = \bar{B} \frac{\Delta \eta}{\Delta \xi} \Big|_w, \quad (4.14)$$

$$A_p^p = A_E^p + A_W^p + A_N^p + A_S^p,$$

$$\text{and } m_p = (G_1 \cdot \Delta \eta)_e - (G_1 \cdot \Delta \eta)_w + (G_2 \cdot \Delta \xi)_n - (G_2 \cdot \Delta \xi)_s.$$

### 4.3 Solution Algorithm

The solution algorithm for the calculation of unsteady flows in curvilinear coordinates and moving boundaries can be summarized as follows.

1. The initial grid and the values of the dependent variables (at time  $t_0$ ) were provided.
2. The time step was advanced by  $\Delta t$ . The new location of the boundary was assumed to be known (as a function of time in this problem). The grid system in the computational domain does not change, whereas, in the physical domain the old grid automatically has moved to fit the new boundaries because the governing equations are represented in boundary fitted curvilinear coordinates. The number of control volumes was thereby kept constant.
3. The coefficients of the momentum equations were assembled and the new values of velocity components were obtained by employing the currently available pressure and velocities. One pass of the solver was often

sufficient. An Alternating Direction Implicit (ADI) solver was used for this problem.

4. The pressure correction equation was solved using the new values of the velocity components and the solver was applied until the residuals became negligible.
5. The velocity components and the pressure were corrected by using the pressure correction values.
6. The procedure was repeated from step 3 until the difference of velocity between two iterations became negligible.
7. The time was advanced by another increment  $\Delta t$  and the procedure was repeated from step 2 repeated until the prescribed number of time steps was completed.

Grid dependency tests were carried out using grid sizes of 150x15, 200x20, 250x25 and 300x30 for Cases 1, 2 and 3 and a grid size of 300x30 was selected for these cases. For Case 2 grid dependency tests were carried out using grid sizes of 20x15, 30x20, 35x25 and 40x30 and a grid size of 40x30 was selected.

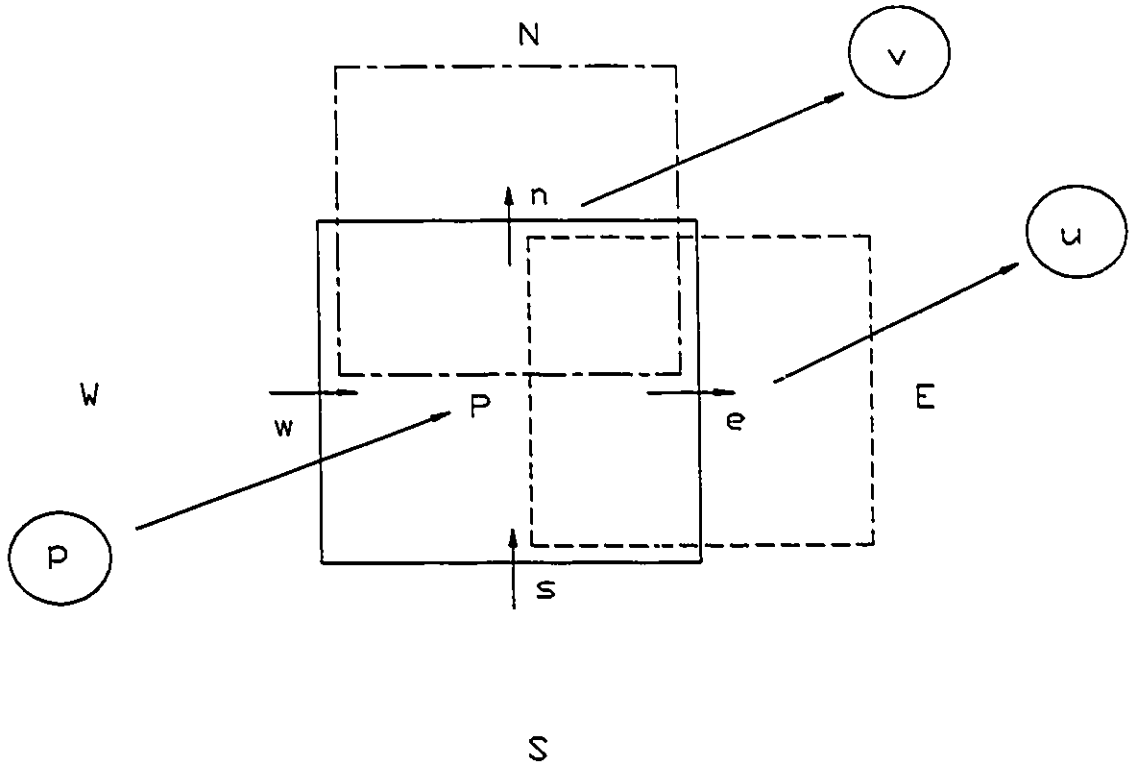


**Figure 4.1 Staggered grid arrangement**

Numerical solutions for steady laminar flow through a tube with constrictions and pulsatile flow through tubes with moving boundaries are presented here. The first part of the chapter is concerned with validating the present numerical procedure with other available results. Following that, the results obtained for the four cases studied, namely tube with multiple constrictions, modular approach, pulsatile flow with time dependent constriction and pulsatile flow with moving boundary, are presented in detail.

### **5.1 Model Validation**

The model was compared with several known results, such as pipe flow, flow with a single constriction and flow with simple periodic pulsation before applying it to the problem of interest. In order to compare the model with steady pipe flow, the amplitude of the vibrating wall in the present numerical model was made negligible and the unsteady terms were neglected. Figure 5.1 shows a comparison of the predicted friction factors with the analytical values for the steady pipe flow. The predictions are considered to be quite accurate.



The model was also compared with the experimental results of Young and Tsai (1973). The experiments were conducted at steady state conditions and the measured pressure drops across a single constriction for various models of stenosis were compared. The fluid used in the experiments was water. Two test cases were selected for comparison, one with 89% constriction and a spread of the constriction,  $S_p$ , four times the tube diameter and the other with 89% constriction and the spread of the constriction twice the tube diameter. The tube diameter was 18.9mm (0.744 inches) and the pressure taps were located 152.4mm (6 inches) on either side of the constriction. The numerical results showed reasonable agreement with the experimental results as shown in Figure 5.2.

The velocity measurements in a tube with a single constriction in steady state conditions were conducted by Ahmed and Giddens (1983) using a laser Doppler anemometer. The tube internal diameter was 50.8mm (2 inches) and the spread of the constriction was twice the tube internal diameter. The fluid used had a kinematic viscosity of  $1.2 \times 10^{-5} \text{ m}^2/\text{sec}$  (0.12 stokes). The measurements were taken in tubes having constrictions of 25% and 75% area reduction. The results of these experiments were compared with the results obtained using the present model for a Reynolds number of 500 at values of  $z$  equal to 0.0, 1.0, 2.5 and 4.0 where  $z$  is the distance measured from the centre of the constriction along the axis in the direction of the flow. The results are shown in Figure 5.3. It can be seen that

the predictions are quite reasonable. For the 75% constriction, the experimental flow field was suspected of becoming turbulent. The probable cause of the discrepancy in the comparison of results at 75% constriction may be due to the onset of turbulence.

Uchida (1956) gives the skin friction factor for the simple periodic pulsation as

$$C_f = \frac{16}{Re} \left\{ 1 + \frac{x_{cn}}{x_o} \sigma_\tau \cos(2\pi tSt - \delta_\tau) \right\} \quad (5.1)$$

where

$$\sigma_\tau = \sqrt{\left(\frac{2C}{\alpha}\right)^2 + \left(\frac{2D}{\alpha}\right)^2} \text{ and} \quad (5.2)$$

$$\delta_\tau = \tan^{-1} \frac{D}{C} .$$

$\sigma_\tau$  and  $\delta_\tau$  represent the coefficients of the amplitude of shearing stress at the wall and the phase lag of the skin friction waveform to that of pressure gradient respectively. In the present model, the amplitude of the vibrating wall was made to go to zero in order to compare the model with simple periodic pulsatile flow. The skin friction factors were compared with the exact solution for a Reynolds number of 200 in the range of  $\alpha$  between 5 and 10. The results of the comparison are shown in Figure 5.4 and were found to be reasonably accurate.

These test simulations show that the present model can handle arbitrary domains and unsteady flow problems with reasonable accuracy.

## 5.2 Tube with Multiple Constrictions (Case 1)

The characteristics of the flow were investigated for Reynolds numbers of 50 to 250 for models having one, two, three, four and seven constrictions in the tube (Models M1, M2, M3, M4 and M7 in Case 1). The spread of the constriction,  $S_p$ , was taken to be twice the tube diameter. The size of the constriction was assumed to be such that it represents 75% reduction in the flow area. This corresponds to an  $A_c$  value of  $0.25D_o$ . Other pertinent geometric characteristics of the models studied were shown previously in Table 3.1. The maximum value of 250 was selected for the Reynolds number to ensure that the flow remains laminar.

### 5.2.1 Pressure

The pressure flow relationship is one means of obtaining information about the severity of a coronary stenosis. For a given Reynolds number the presence of a constriction increases the resistance that the flow experiences. The pressure drops across the constrictions for the various models are shown in Figure 5.5. It can be seen that the pressure drop increases as the number of constrictions increases. The non-dimensional pressure drop for each of the models, in a manner similar to Poiseuille flow, decreases as the Reynolds number increases.

The non-dimensional pressure distribution along the tube wall in the axial direction is also of interest and is shown in Figure 5.6 for various numbers of constrictions and Reynolds numbers. There is a rapid fall in the pressure as the occlusion is

approached, with pressure recovery taking place over a greater length. As the number of constrictions increase the curves tend to show a similar pressure drop and recovery across every constriction even as they are shifted correspondingly downwards. This shift is due to the mass flow in the positive  $x$  direction. The curves are, however, not similar enough to claim periodicity has been achieved. A large number of constrictions is required, which will be considered later.

### **5.2.2 Velocity**

The variation of centreline velocity in the axial direction, for the range of Reynolds numbers considered, is shown in Figure 5.7 for one, two, three and four constrictions. For all of the models, the maximum centreline velocity occurs slightly downstream of the constriction due the formation of a recirculation zone near the wall as a result of flow separation. This effectively reduces the cross sectional area of the flow. The centreline velocity is seen to take a larger distance to recover to its initial value as the Reynolds number increases. As the number of constrictions increases, the fluid does not have an opportunity to recover to its initial value of the velocity before it encounters another constriction. Only for low Reynolds numbers does the fluid have time to recover. For lower Reynolds numbers, the velocity field is such that it is independent of the other constrictions.

### 5.2.3 Wall shear stress, vorticity and streamlines

The wall shear stress is an important parameter in atherosclerosis. The non-dimensional wall shear stress can be represented in terms of skin friction coefficient,  $C_f$ . The peak value of the skin friction coefficient decreases with an increase in Reynolds number. The peak values of the dimensional wall shear stress, however, increase with an increase in Reynolds number. The decrease of the skin friction coefficient with the increase in Reynolds number can be explained by noting that the wall shear stress is normalized by  $0.5\rho U^2$  to obtain the skin friction coefficient. In order to indicate the increase in the peak value of wall shear stress with the increase in Reynolds number, yet retain a non-dimensional representation of the wall shear stress, a new non-dimensional quantity was defined. The skin friction coefficient was multiplied by the square of the Reynolds number. This quantity,  $C_f Re^2$ , is now used. Figure 5.8 shows the nature of the non-dimensional wall shear stress variation in the axial direction. The wall shear stress increases rapidly as the flow approaches the constriction and reaches a peak value near the maximum constricted area. Downstream of the constriction, the wall shear stress decreases rapidly and reverses sign which indicates a separation in the flow near the wall of the tube. An increase in Reynolds number causes the magnitude of the negative wall shear stress values to increase downstream of the constriction. This is due to an increase in the size of the recirculation region. The maximum value of wall shear stress generated by the first constriction is always greater than the maximum value of wall shear stress generated by the second

constriction. This is because the recirculation eddy formed downstream of the first constriction has a diminishing effect on the vortices generated by the main stream near the second constriction area. However, an increase in the number of constrictions causes a tendency for the periodic nature of the flow to develop and hence the wall shear stress to behave similarly for the other constrictions. In the case of more than two constrictions, the peak value of wall shear stress is slightly higher in the vicinity of the last constriction. This may be attributed to the presence of no other constrictions downstream.

Sample streamlines and contours of vorticity are shown for a Reynolds number of 200 for all the models in Figure 5.9 and Figure 5.10 respectively. There is a recirculation eddy downstream of each constriction. The recirculating eddies divide the flow into two regimes, one of which is the recirculating region, and the other is the main flow field carrying the bulk of the flow near the centre of the tube.

#### **5.2.4 Periodic nature of the flow**

The development of the periodic nature of the flow was studied by simulating the flow passing through a tube with seven constrictions (Model M7). The results were compared for a range of Reynolds numbers between 50 to 250. As the Reynolds number is increased the flow is expected to reach its spatially periodic state after a larger number of such constrictions. The results are presented by superimposing plots of centreline velocity profile and wall shear stress profiles in each module.

The space between the constriction is referred to as a module. For example Module 1 is between constriction 1 and 2, Module 2 is between constrictions 2 and 3 and so on. This results in 6 modules for seven constrictions. As expected, the last module did not exhibit periodic flow behaviour due to the non-periodic shape of the wall downstream. Therefore, the results of Module 6 were omitted. The superimposed profiles are shown in Figure 5.11 and Figure 5.12 for the centerline velocity and wall shear stress respectively. The development of the periodic nature of the flow can be clearly seen from the results. The flow pattern repeats itself after the second module for lower Reynolds numbers and after the third module for higher Reynolds numbers. An approximate expression for the length for development of spatial periodicity for laminar flow can be obtained for a problem having a similar geometry and inlet conditions as studied in this work. i.e.,

$$n_m = \frac{l_o}{D_o} \geq 1 + \left\lceil \left[ \frac{Re}{100} + 1 \right] \right\rceil \quad (5.3)$$

where the function  $\lceil \cdot \rceil$  is the greatest integer function,  $n_m$  refers to the number of modules and  $l_o$  is the entrance length.

### 5.3 Modular Approach (Case 2)

The previous results indicate the development of periodic characteristics of the flow in the streamwise direction after a number of similar constrictions. The flow field under such conditions can be solved by isolating the problem in a single module corresponding to the fully developed region in the duct. A sample problem is

solved corresponding to a Reynolds number of 200. For this problem, the periodic boundary condition must be applied at the inlet and outlet of the module. The pressure drop across the module,  $K$ , is an assignable parameter which corresponds to a particular value of the Reynolds number. The value of the Reynolds number corresponding to the unstricted tube diameter could only be found after the model is solved by performing a numerical integration of the following form at any axial location in the module, where  $D_o$  is the unstricted tube diameter.

$$Re_m = \frac{4}{v\pi D_o} \int_0^{0.5D_o} u(r)2\pi r dr \quad (5.4)$$

where  $u(r)$  is the velocity at  $r$ , for this particular axial location. The simulation was carried out for various values of  $K$  and the corresponding Reynolds number was obtained using Equation (5.4). These results are shown in Figure 5.13. The model was validated by comparing the results of the centreline velocity profile and wall shear stress with module 4 (between the third and fourth constriction) in the tube having seven constrictions for a Reynolds number of 200. Module 4 was selected for comparison as the flow field has become periodic at this location. The results of the comparison are shown in Figures 5.14 and 5.15 which indicate that the model performs reasonably well. Sample plots of stream function and vorticity and their comparisons with Module 4 are also shown for a Reynolds number of 200 in Figure 5.16 and Figure 5.17. The results are similar to those discussed in Case 1.



### **5.4 Pulsatile Flow with Time Dependent Constriction (Case 3)**

The shape of the constriction was specified to change periodically with a particular frequency. The frequencies considered correspond to non-dimensional frequency of pulsation,  $\alpha$ , values of 10, 7.5 and 5. The height of the constriction,  $A_c$ , was prescribed to vary between  $0.15D_o$  and  $0.25D_o$ . The results were obtained for a Reynolds number of 200. The results of the stream function are presented only for an  $\alpha$  value corresponding to 10 due to the complex nature of the flow at this frequency. For  $\alpha$  values of 7.5 and 5, only the wall shear stress and pressure variations are presented.

#### **5.4.1 Stream function**

The unsteady nature of the flow can be understood better by looking at the stream function contours. The stream function contours for one complete cycle of pulsation at  $\alpha = 10$  are shown in Figure 5.18. One complete cycle of pulsation corresponds to a time span of  $2T$ . The value of  $A_c$  corresponding to  $0.15D_o$  is the smallest position of the constriction and occurs at  $t = T/2$ .

The analysis is started at time step  $t = 3T/4$ . At this point in time the constriction has just begun its inward motion. A recirculation eddy is formed immediately downstream of the constriction. This eddy is referred to as the primary eddy. The nature of the rotation of this eddy is counterclockwise. There is another eddy of similar nature further downstream. This eddy was formed at an earlier time at the

same position as the primary eddy and has been carried further downstream by the flow. The downstream eddy is weaker than the primary eddy as the viscous effects of the flow have dissipated the eddy. There is evidence that much weaker eddies are present further downstream. The nature of the core flow at this point is wavy. This waviness in the flow was created during the outward motion of the constriction, the nature of which will become clearer later in this discussion. At  $t = T$  the constriction moves further inward. The primary recirculation eddy has increased in strength. The constriction is at its mean value and has maximum inward velocity at this point, thereby, causing the fluid to be pushed inward (i.e. towards the line of symmetry) with a greater velocity. At  $t = 5T/4$  the constriction moves further inwards causing the primary eddy to increase further in strength. Up to this point in the cycle, the inward motion of the constriction has been pushing the fluid into the mean flow as is evident from the streamlines. The constriction begins to move outward at  $t = 3T/2$ . The velocity of the constriction is zero at this point and the amount of the constriction is a maximum. The fluid immediately in the vicinity of the constriction adheres to the wall of the constriction due to the no-slip condition. There is some evidence of the outward motion of the fluid at this point (core flow is beginning to get wavy). At  $t = 7T/4$  the size of the constriction becomes smaller as it moves outward. There is a clear evidence of the outward motion of the fluid here and the primary eddy is pushed downstream. At  $t = 0$  (or  $t = 2T$ ) the constriction is at its mean position and has maximum velocity. The primary eddy (counterclockwise rotation) is now formed upstream of the

constriction. A weak eddy of opposite sense (clockwise rotation) is also formed immediately downstream of the constriction in the mean flow region due to the outward motion. This eddy is referred to as the secondary eddy. The primary recirculation eddy moves further downstream. At  $t = T/4$  the constriction has further decreased in size, the recirculation eddy at the upstream of the constriction has been displaced downstream. At  $t = T/2$  the size of the constriction is at its smallest value and has zero velocity. The secondary eddy has dissipated but its effect is still present in the form of a waviness in the core flow. The effects of both the primary and secondary eddies are seen further downstream of the constriction even though their strength has been dissipated. The small recirculation eddy formed upstream of the constriction has moved downstream of the constriction and becomes the primary eddy at time step  $t = 3T/4$ . From this discussion it is clear that the movement of the constriction and the pulsatile nature of the flow causes unsteadiness in the flow field creating waviness in the core flow. The eddies created by the constriction are carried away downstream and are eventually dissipated.

#### **5.4.2 Wall shear stress and vorticity**

The wall shear stress is represented as a non-dimensional parameter in terms of skin friction coefficient. The profiles of the skin friction coefficient are shown, for  $\alpha = 10, 7.5$  and  $5$  in Figure 5.19 indicate an oscillating wall shear stress profile. The waviness in the profile is maximum in the vicinity of the constriction and exists

further downstream until the eddies created by the constriction and its motion are dissipated. The negative values of wall shear stress also give an idea about flow separation and the extent of the associated recirculation zones. A change in the wall shear stress value from positive to negative indicates flow separation and negative to positive indicates reattachment. We can trace the development of the primary recirculation eddy from the wall shear stress profiles (Figure 5.19) and the stream function contours (Figure 5.18) for  $\alpha = 10$ . Starting our discussion from  $t = 3T/4$  we can see that the wall shear stress value increases rapidly as the flow approaches the constriction and reaches its peak value near the maximum constricted area at  $x = 7.5$ . The increase in shear stress is due to greater fluid average velocity at this point due to the presence of the constriction and its inward motion. There is then a sudden drop in wall shear stress, changing from positive to negative sign which indicates a flow reversal. Comparing wall shear stress profiles with stream function contours we can see the existence of the recirculation eddy downstream of the constriction. The profiles of the shear stress then take a positive sense as there is greater bulk of fluid flowing near the wall caused by the waviness of the core flow. This waviness is caused by the secondary eddy which has dissipated. The value of the wall shear stress gradually becomes negative again. If we look at the stream function contours at this point we can see the existence of another weak eddy which was the primary eddy in the previous cycle and has now become weak and is being carried downstream by the flow. The evidence of this dissipation is indicated by the lower value of the wall shear stress

compared to the previous one. The profile becomes positive and then negative again, however, the values are very low indicating that the eddies created by the constriction in the previous cycles have dissipated. A similar analysis can be performed by comparing shear stress profiles at other time steps with the stream function contours.

The maximum value of the wall shear stress occurs when the constriction is near its maximum size on its inward motion ( $t = 5T/4$ ). The wall shear stress profiles take on negative values. The minimum value of the skin friction coefficient for this time step is also lower compared to the other time step profiles which first show a positive value and then a negative value. This is because the primary eddy is maximum in size at this time step. The minimum value of the wall shear stress occurs when the constriction is near its minimum size on its outward motion ( $t = T/4$ ). The maximum value which occurs after the minimum value of the shear stress for  $t = T/4$  is higher compared to the other time steps due the presence of the secondary eddy in the core flow causing more fluid to be pushed against the wall. A similar analysis can also be performed for the other dimensionless frequencies which follow essentially the same pattern.

The values of the shear stress corresponding to  $\alpha=7.5$  and 5 are also shown in Figure 5.19. A similar wavy nature of the profile is observed. As the frequency decreases we can see that the maximum and minimum values of wall shear stress

correspondingly decrease. However, for the range of frequencies studied, the wall shear stress profiles are similar at different frequencies at the same time step. The lower maximum and minimum values of the shear stress profiles at  $\alpha = 7.5$  and  $\alpha = 5$  indicate that the recirculation eddies are smaller compared to  $\alpha = 10$ . The lower shear stress values are most likely due to the fact that a decreased oscillation frequency with a constant oscillation amplitude of the constriction causes a decrease in both the wall velocity and acceleration amplitudes. The shear stress profiles at lower frequencies of oscillation show less waviness downstream of the constriction indicating that the eddies are dissipated earlier by the viscous forces.

Figure 5.20 shows the contours of the negative skin friction factor along the wall for one complete time cycle of  $t = 0$  to  $t = 2T$  for  $\alpha = 10, 7.5$  and  $5$  respectively. The abscissa represents the location along the wall and the ordinate represents time. The bounding contour has a value of zero, i.e, only contours of  $C_f \leq 0$  are shown. The flow separation at the wall and its movement with time can be visualized easily from these contours. The figures indicate that there are two major separation regions. From these contours it is very clear that the size and extent of the flow separation region decreases as the frequency decreases. At low frequencies the separation regions do not travel extensively in the axial direction. At high frequencies, the separation region caused by the primary eddy in the vicinity of the constriction remains relatively stationary whereas the separation region caused by the weaker eddies show considerable downstream

movement.

The vorticity contours for  $\alpha=10$  are shown in Figure 5.21. The motion of the eddies downstream is evident from the vortex shedding nature of the profiles and is consistent with the movement of the separation regions. A comparison of the streamline and vorticity contours shows the presence of the recirculating eddy wherever there is a concentration of vorticity.

### **5.4.3 Pressure**

The profiles for non-dimensional pressure along the wall are shown for  $\alpha = 10, 7.5$  and  $5$  in Figure 5.22 respectively. The lowest pressure corresponds to the maximum instantaneous cross sectional average velocity and highest pressure corresponds to a lowest instantaneous cross sectional average velocity due to the phase difference between the instantaneous flow rate and the pressure. As the flow approaches the constriction, there is a rapid fall in the pressure with the pressure recovery after the constriction taking place over a greater length. Whenever the size of the constriction is large the pressure downstream of the constriction does not have time to recover. Another factor that is noticeable is that the amount of pressure drop and recovery is greater at higher instantaneous cross sectional average velocity as compared to the values at lower instantaneous cross sectional average velocity. The amount of pressure drop and recovery decreases as the frequency decreases.

## **5.5 Pulsatile Flow with Moving Boundary (Case 4)**

The wall of the tube was forced to vibrate at a non-dimensional frequency of pulsation,  $\alpha$ , values of 10, 7.5 and 5 respectively and at an amplitude of  $\pm 0.05D_o$ . The results were computed for a Reynolds number of 100. A detailed analysis of the stream function, wall shear stress and pressure variation is presented for an  $\alpha$  value corresponding to 10 due to the complex nature of flow at this frequency. For  $\alpha$  values of 7.5 and 5, only the wall shear stress and pressure variations are presented.

### **5.5.1 Stream function**

The flow development and the unsteady nature of the flow can best be understood by considering the stream function contours for  $\alpha$  equal to 10 as shown in Figure 5.23 which contains eight diagrams. Each one contains the stream function contours on the  $r$ - $x$  plane for different times within the cycle of oscillation. One complete cycle has a period of  $2T$ . The flow behaviour is best explained when analysis is started at time  $t=T$ . At this instance the wall is at its mean position and has maximum inward velocity. This is evident from the nature of the streamlines in the vicinity of the vibrating portion of the wall. There are no major areas of flow separation. The core flow is beginning to get wavy. At  $t=5T/4$ , the size of the contraction increases. The fluid is pushed inward towards the centreline due to the inward motion of the flexible portion of the wall and there is a small recirculation eddy which is formed downstream of the contraction. The nature of this eddy is



counterclockwise and this eddy will be referred to as the primary eddy. The existence of dissipated eddies on the wall further downstream of the contraction is also seen from the streamline contours. At  $t=3T/2$ , the flexible portion of the wall moves further inwards and the contraction is at its maximum size which corresponds to a wall velocity of zero. The primary eddy has further increased in strength due to the increase in size of the contraction. The waviness of the core flow is very evident at this time step. This waviness of the core flow was created during the outward motion of the vibrating wall, the nature of which will become clear later in this discussion. At  $t=7T/4$  the size of the contraction has decreased as the flexible portion of the tube wall has started its outward motion. During the outward motion of the tube, the fluid adheres to the wall of the tube thereby causing waviness in the core flow. The primary eddy has shifted further downstream. The strength of the primary eddy has started to decrease. Also, another flow separation region is noticed to occur further downstream at a value of  $x$  approximately equal to 13. Flow separation regions are associated with recirculating eddies at the wall, hence this eddy is referred to as the secondary eddy. The nature of this eddy is counterclockwise. At  $t = 0$ , which also corresponds to  $t = 2T$ , the tube wall has maximum outward velocity and is at the mean position of oscillation. The outward motion causes a weak clockwise recirculating eddy to form in the core flow near the flexible portion of the wall causing the waviness of the flow to increase further. The primary eddy is pushed further downstream and its strength continues to decrease and the effects of the secondary eddy remain.

At  $t=T/4$  the tube wall moves further outwards thereby becoming distended. The clockwise eddy has dissipated. In the vicinity of the distended portion of the wall there is evidence of the outward nature of the flow due to the wall motion. There is also another counterclockwise eddy being formed due to the flow separation at the edge of the distended portion of the wall. This eddy is referred to as the tertiary eddy. The primary eddy is pushed further downstream due to the flow and the secondary eddy has disappeared. At  $t = T/2$ , the tube wall becomes distended to its maximum extent and has zero velocity. The tertiary eddy has further increased in strength and the primary eddy has dissipated. The waviness of the core flow has also reduced. At  $t=3T/4$ , the tube wall is on its inward motion as can be seen from the nature of the streamlines. The strength of the tertiary eddy has decreased as the size of the distended portion of the wall decreased. The core flow also remains relatively smooth. From this discussion it is clear that the motion of the tube wall and the pulsatile nature of the flow causes unsteadiness in the flow. During the inward motion there are relatively few flow phenomenon other than the creation of recirculation eddies of a counterclockwise sense. During the outward motion, the waviness of the core flow increases, and there are eddies of both types (clockwise and counterclockwise) are present and the core flow is more wavy.

### 5.5.2 Wall shear stress

The wall shear stress profiles shown in Figure 5.24 indicate an oscillating wall shear stress profile. The oscillation is maximum in the vicinity of the flexible portion of the tube wall and dissipates further downstream. The creation of the recirculation eddies can be traced by comparing the wall shear stress profiles shown in Figure 5.24 and stream function contours shown in Figure 5.23 for  $\alpha=10$ . As in the case of stream function contours, we begin the discussion at  $t=T$ . It can be seen that downstream of the flexible portion of the wall the shear stress profile shows an oscillatory behaviour. The value of the shear stress is greater than zero indicating no flow reversal. The waviness gradually reduces further downstream due to the viscous force in the flow and the straightening of the wall. At  $t=5T/4$ , the size of the contraction has increased causing an increase in the peak positive value near the contraction. The fluid has a greater instantaneous cross sectional average velocity in this region which causes a greater velocity gradient near the wall. The peak positive value is followed by a sudden drop in the shear stress to a negative value as the distance from the inlet increases. This indicates a flow reversal near the wall. Comparing the streamline contours at this time we can see the presence of a recirculating eddy (primary eddy) just downstream of the contraction. The shear stress takes a greater positive value at  $t = 3T/2$  as there is a greater amount of the fluid pushed against the wall of the tube causing a large velocity gradient in the vicinity of the contraction. Downstream of the contraction the shear stress takes a negative value as the flow separates in this region. This

again indicates the presence of a recirculating eddy mentioned at the previous time caused by flow reversal near the wall. The region of negative shear stress that was present at  $t = 3T/2$  has moved downstream slightly at  $t = 7T/4$ . This region is followed by a positive region and again becomes negative further downstream at the location of the secondary eddy mentioned previously in the discussion of the stream function. The shear stress values at  $t = 0$  or ( $t = 2T$ ), show that the negative value of the shear stress present at  $t = 7T/4$  moves further downstream. These downstream movements are also consistent with the motion of the primary eddy. At  $t = T/4$ , the shear stress profile has shifted slightly downstream and two locations where minimum values occur are shown. These indicate the presence of two recirculation eddies. A comparison with stream function contours at this time indicates the creation of the tertiary eddy corresponding to the first minimum. The magnitude of the second minimum, which is due to the primary eddy, is further downstream and is lower than the first one. This indicates that the primary eddy has become weaker in nature. At  $t = T/2$  the wall is distended to its maximum extent. The tertiary eddy at this time has maximum strength. Similarly the primary eddy has maximum strength when the contraction of the wall is at its maximum extent at time  $t = 3T/2$ . Comparing the values of the shear stress at these two locations it could be concluded that the tertiary eddy is strongest and the secondary eddy is the weakest.

A similar analysis can be done by comparing the shear stress profiles at other times with stream function contours. At all times, there is a waviness in the profile indicating that the fluid is pushed towards the wall at one instance and away from the wall at another. The fluid gets pushed towards the wall either due to the contraction created by the inward motion of the wall which causes the streamlines to converge locally or due to the presence of the dissipating co-rotating eddy in the core flow creating a positive value of the shear stress. Negative values of the shear stress are created by flow reversals which correspond to the counterclockwise recirculating eddies.

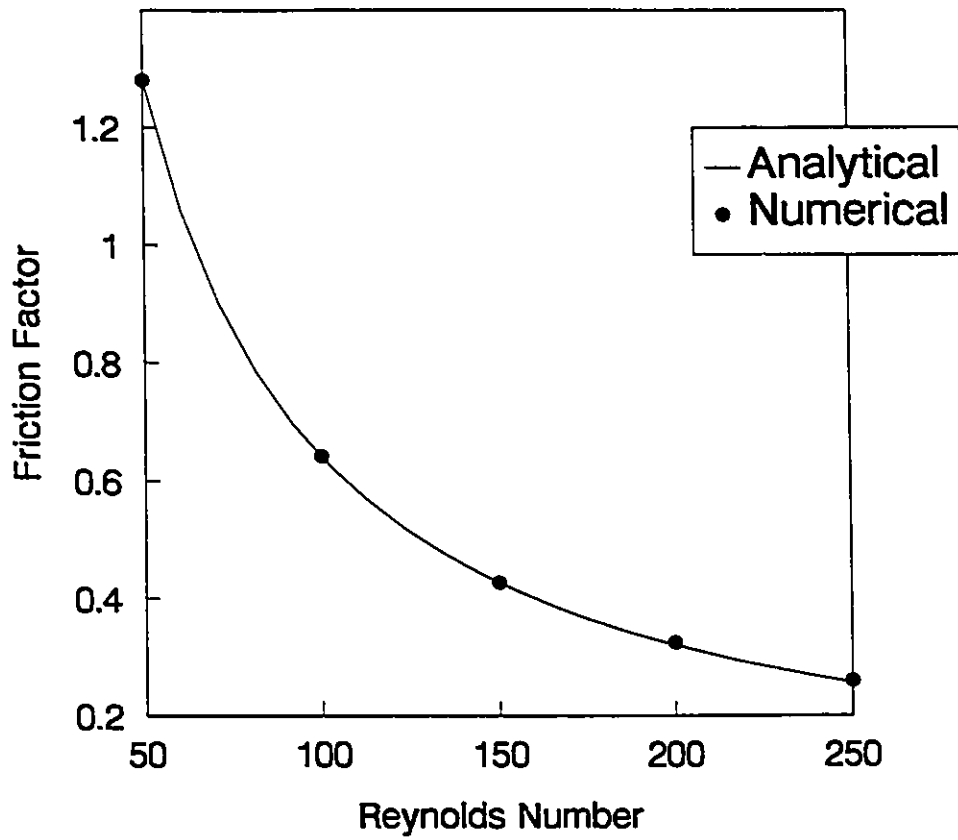
The values of the wall shear stress corresponding to  $\alpha = 7.5$  and 5 are shown in Figure 5.24. A similar wavy nature of the profile is observed. As the frequency decreases, however, the amplitude and the extent of the waviness in the wall shear profiles decrease. This is most likely due to the fact that a decreased oscillation frequency with a constant wall oscillation amplitude causes a decrease in both wall velocity and acceleration amplitudes. This causes the diffusive forces to play a greater role in the dissipation of the eddies.

Figure 5.25 shows the contours of the skin friction coefficients along the wall for one complete time cycle of  $t = 0$  to  $t = 2T$  for  $\alpha = 10, 7.5$  and 5 respectively. Only negative values and zero are shown. The abscissa represents the location along the wall and the ordinate represents time. The bounding contour corresponds to

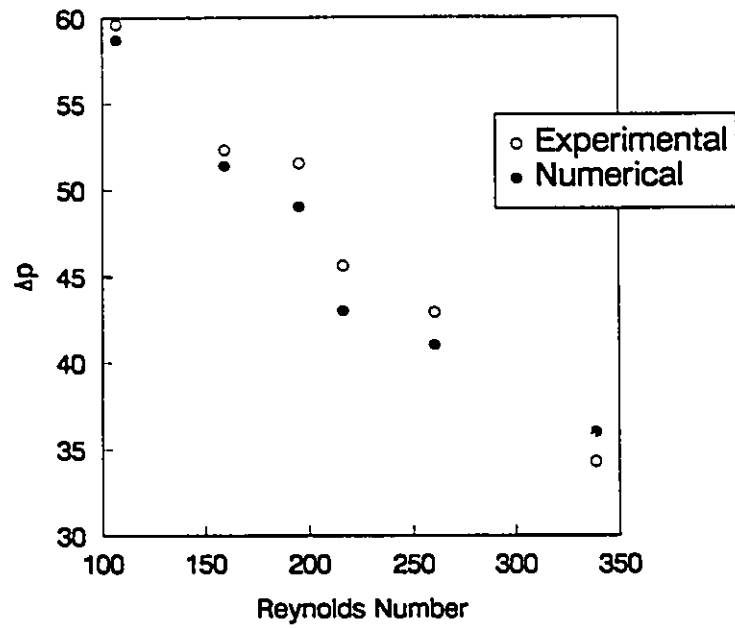
a wall shear stress value of zero. The flow separation at the wall and its movement downstream with time can easily be visualized from these contours. The presence of multiple separation regions at higher frequencies could be seen from these contours. At lower frequencies there is only one main separation region.

### **5.5.3 Pressure**

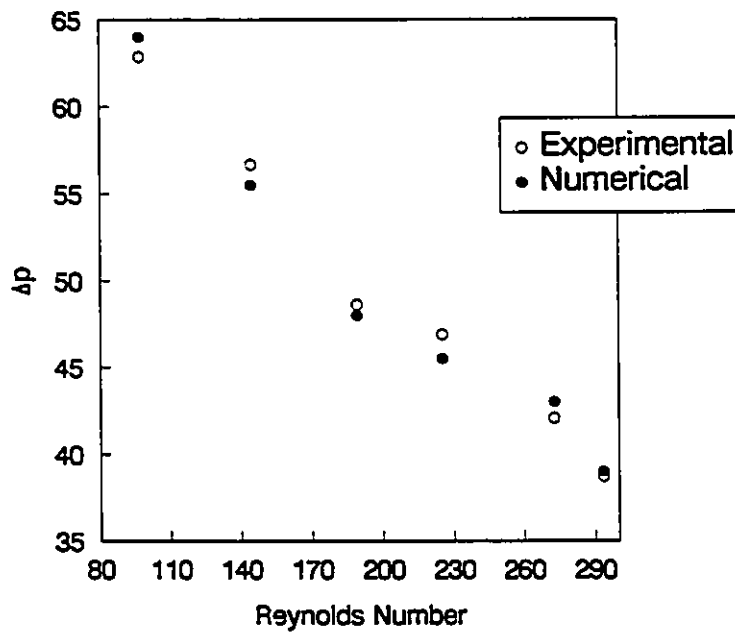
The non-dimensional pressure along the wall is shown in Figure 5.26 for  $\alpha$  values of 10, 7.5 and 5. There is a pressure drop as the flow approaches the contraction if the flexible portion of the wall is on its inward motion. If the vibrating portion of the wall is on its outward motion there is an increase in pressure as the flow approaches the distended region. When the contraction is on its inward motion there is a pressure rise after the contraction. When it is on its outward motion the pressure decreases in this region (after the distended region). As in the previous case, the amount of pressure changes with time decreases as the frequency decreases.



**Figure 5.1 Comparison of numerical and analytical results for pipe flow**



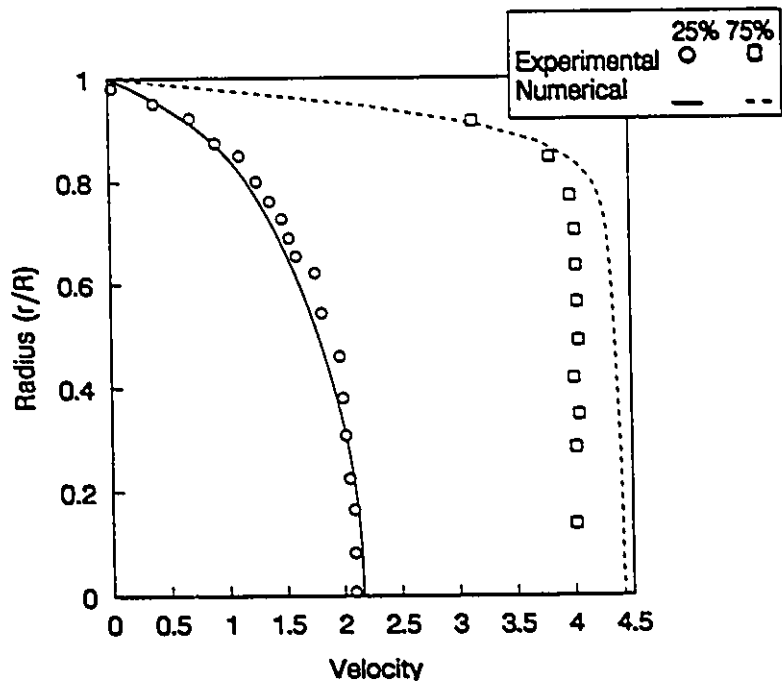
(a)  $S_p = 4D_o$



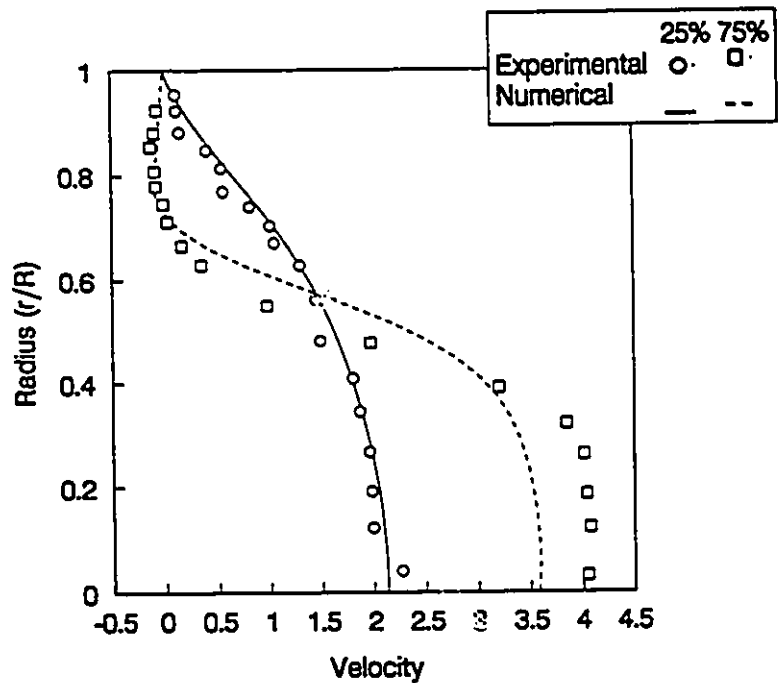
(b)  $S_p = 2D_o$

Figure 5.2 Comparison of non-dimensional pressure drop across stenosis



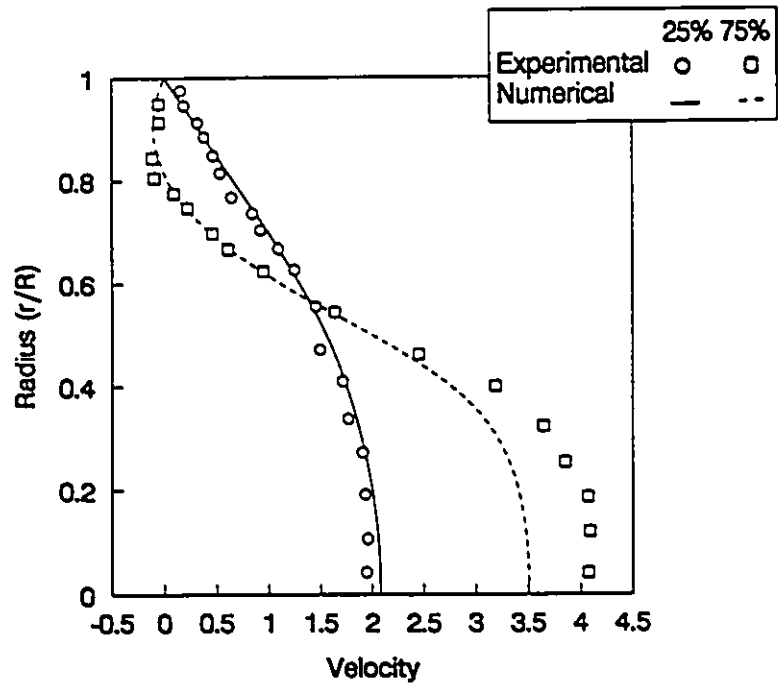


(a)  $z = 0$

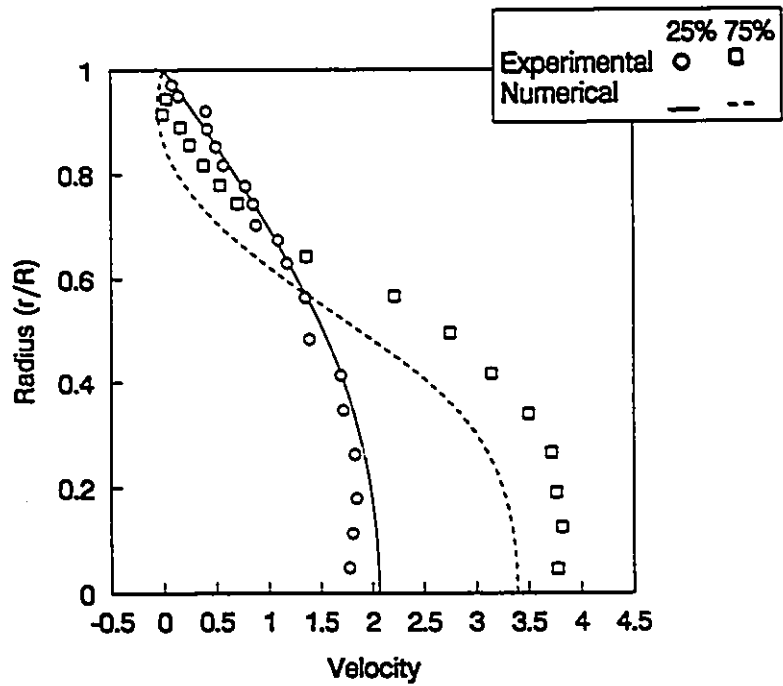


(b)  $z = 1$

Figure 5.3 Comparison of non-dimensional velocity distributions



(c)  $z = 2.5$



(d)  $z = 4$

Figure 5.3 Comparison of non-dimensional velocity distributions (cont'd)

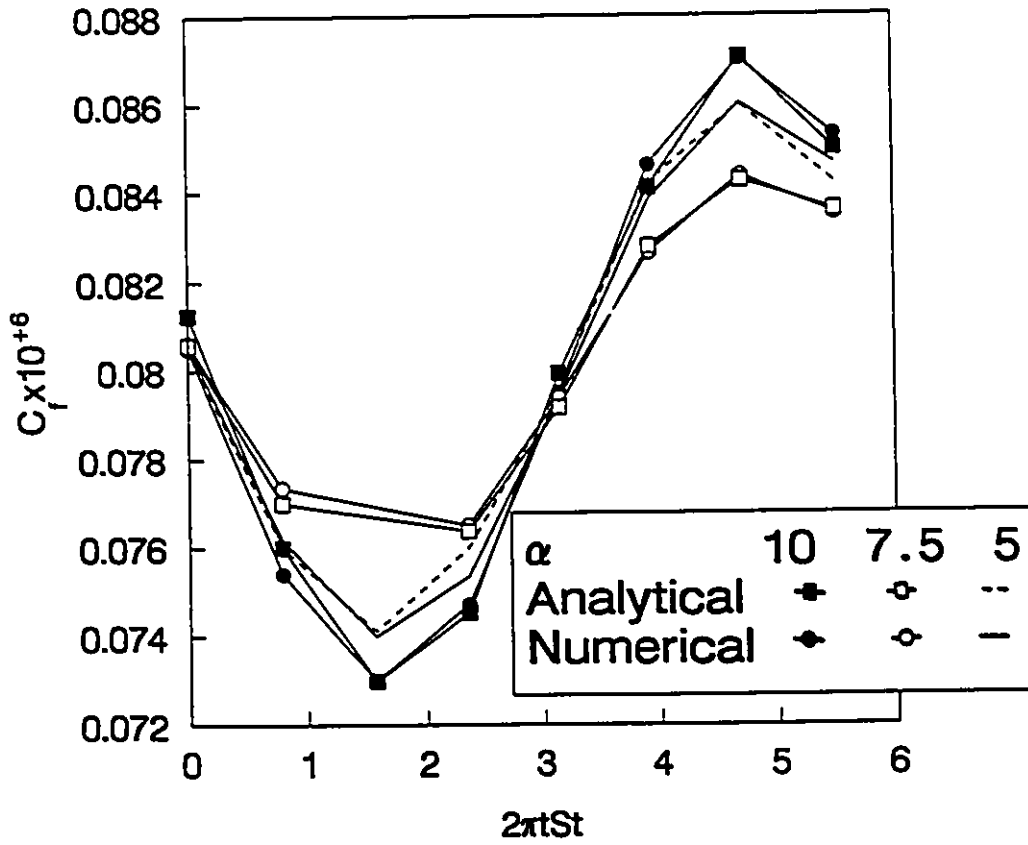


Figure 5.4 Comparison of friction coefficients for simple pulsatile flow

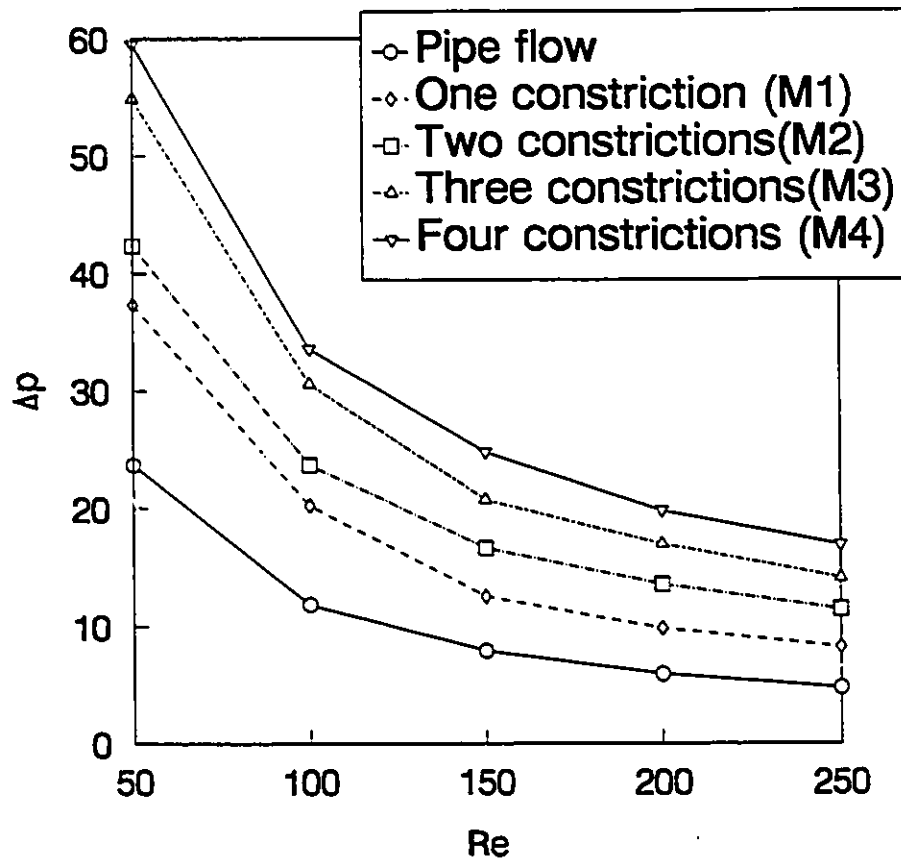
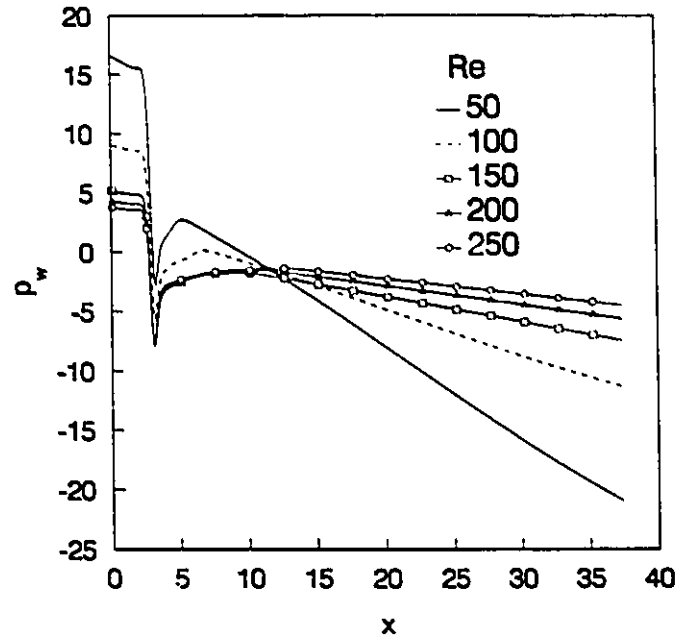
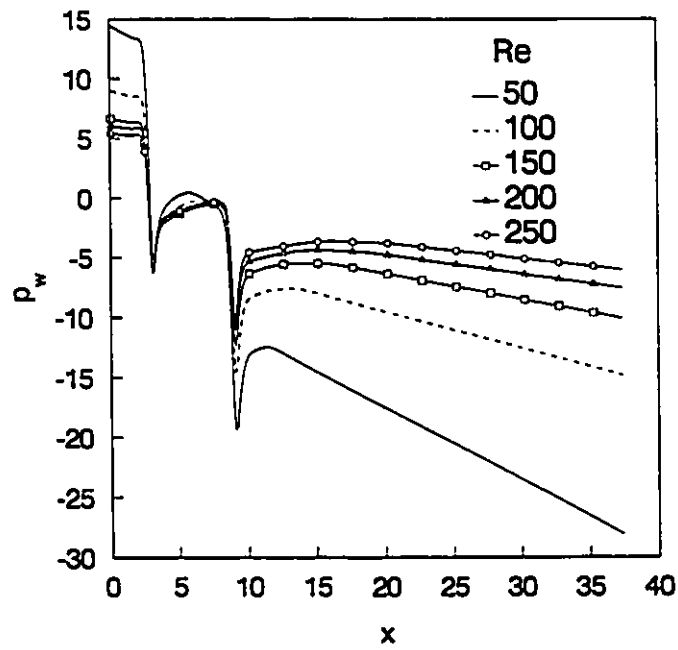


Figure 5.5 Non-dimensional pressure drop across the constrictions

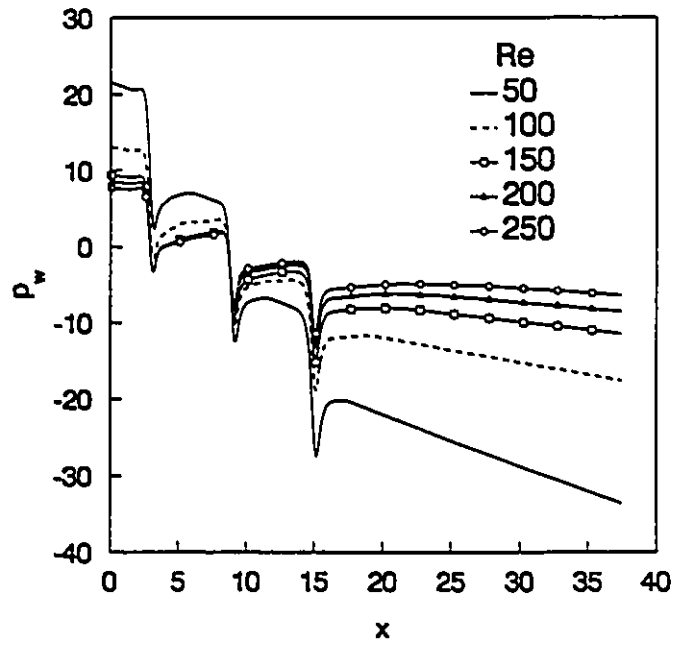


(a) one constriction

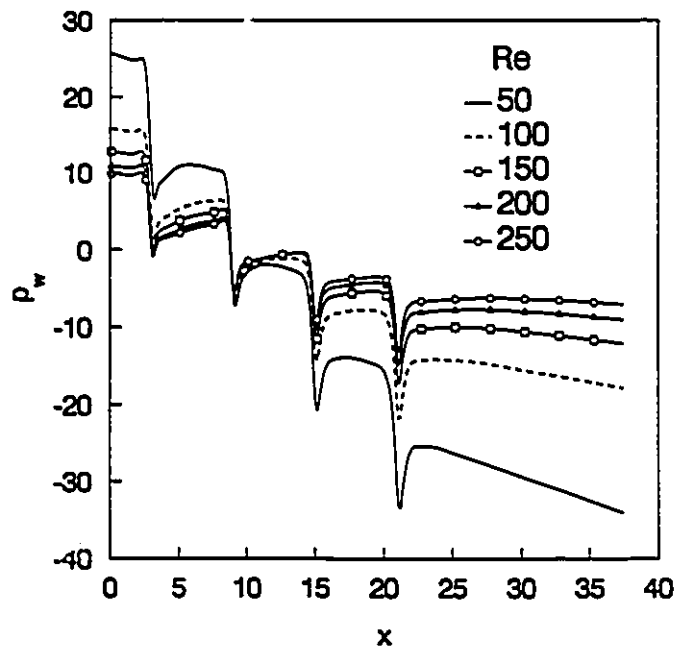


(b) two constrictions

Figure 5.6 Non-dimensional pressure distribution along the wall

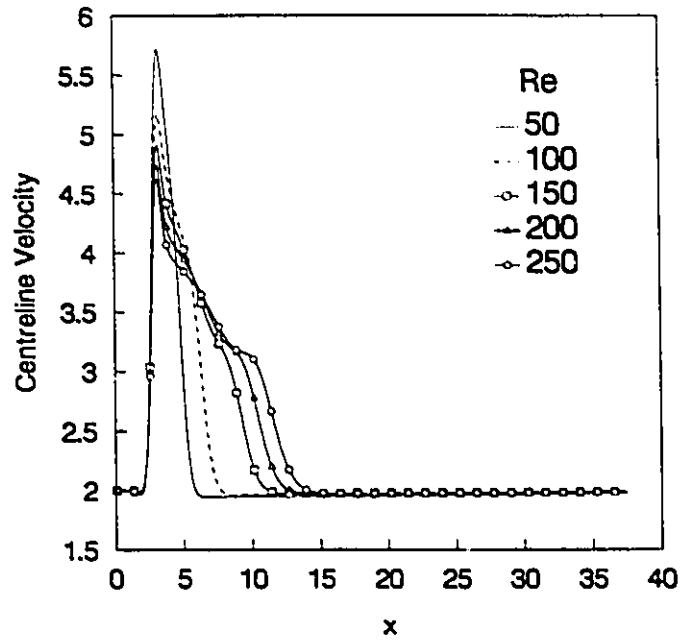


(c) three constrictions

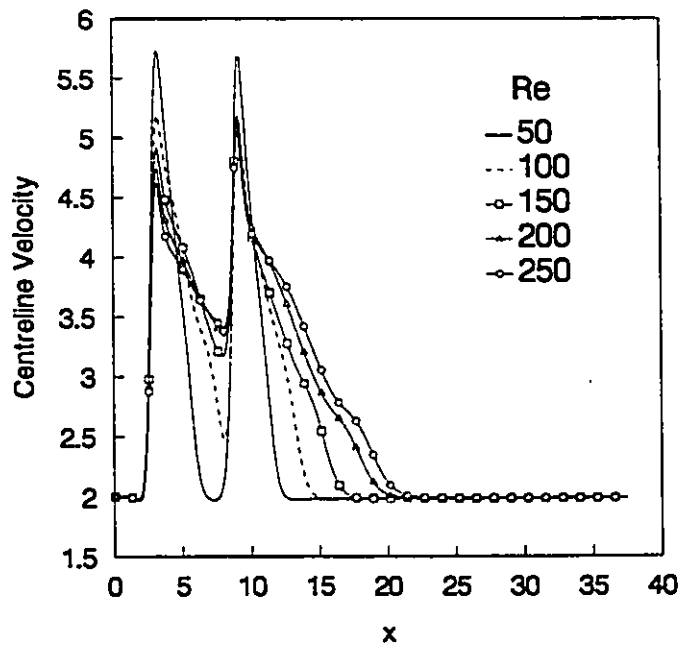


(d) four constrictions

Figure 5.6 Non-dimensional pressure distribution along the wall (cont'd)

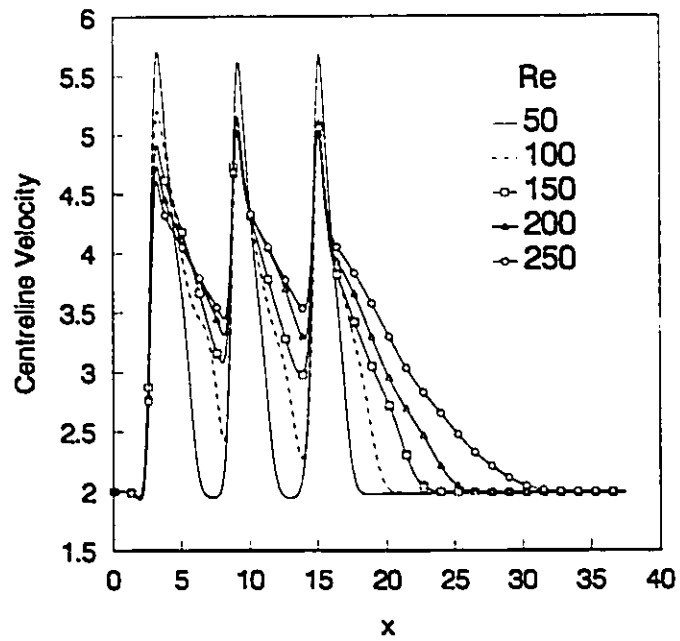


(a) one constriction

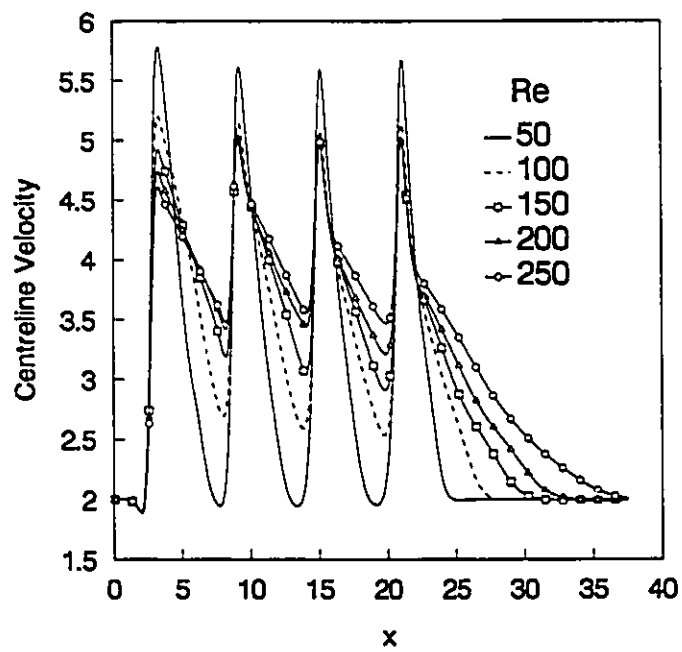


(b) two constrictions

Figure 5.7 Non-dimensional centreline velocity distribution



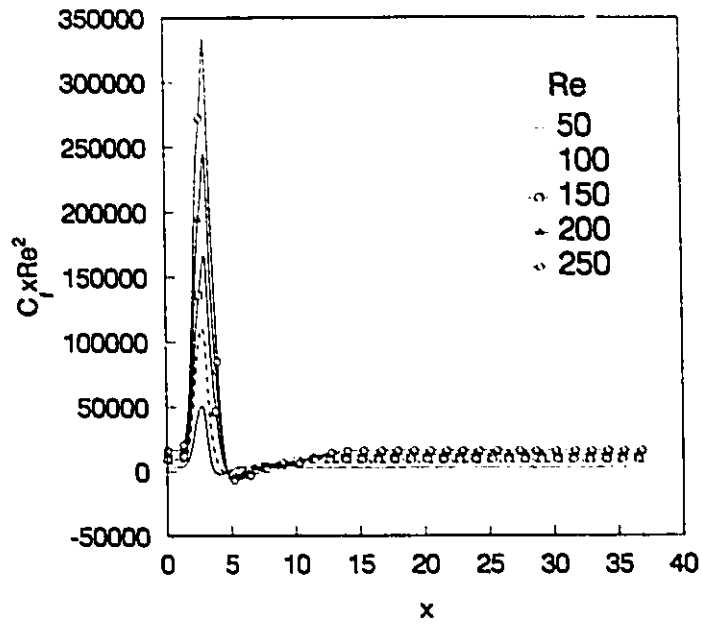
(c) three constrictions



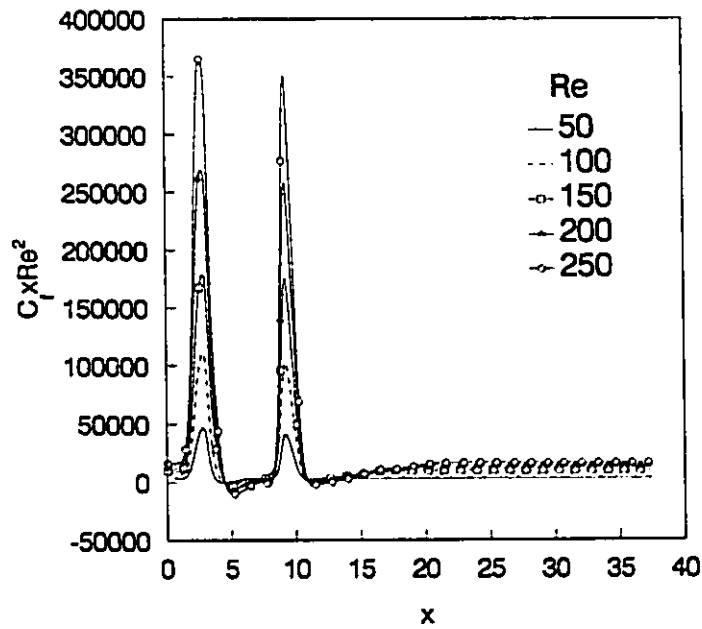
(d) four constrictions

Figure 5.7 Non-dimensional centreline velocity distribution (cont'd)



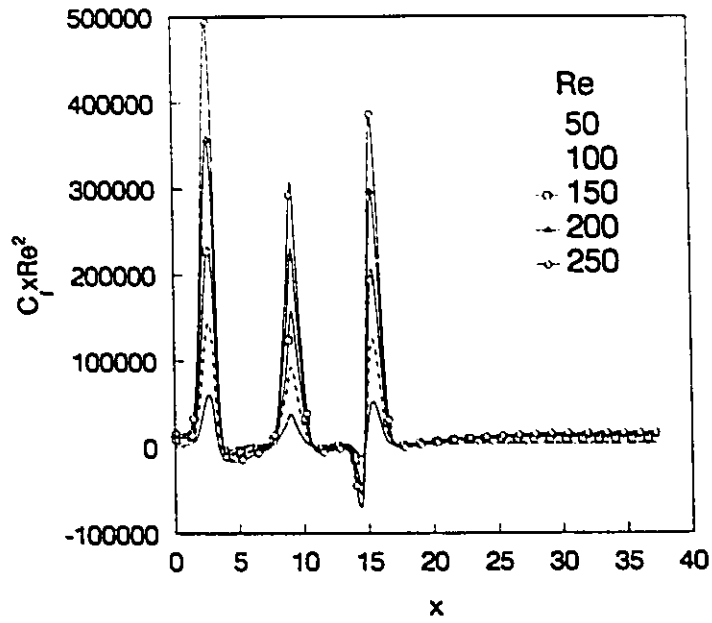


(a) one constriction

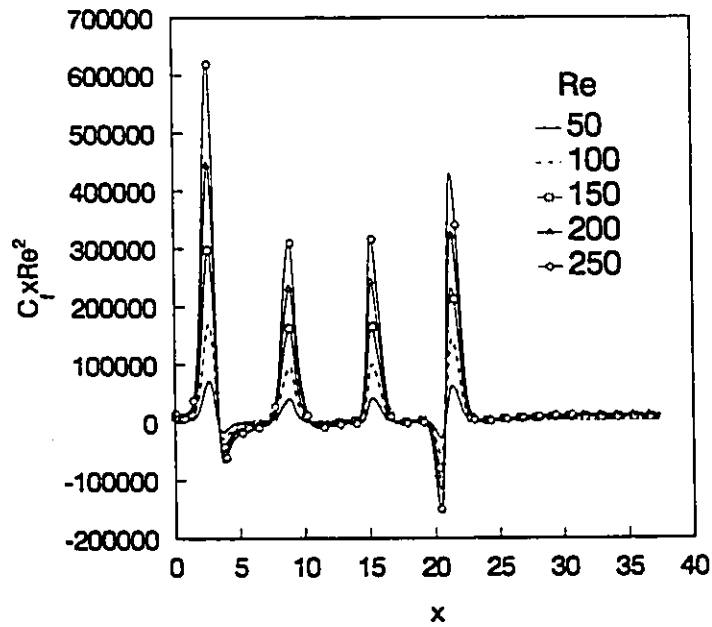


(b) two constrictions

Figure 5.8 Non-dimensional wall shear stress distribution

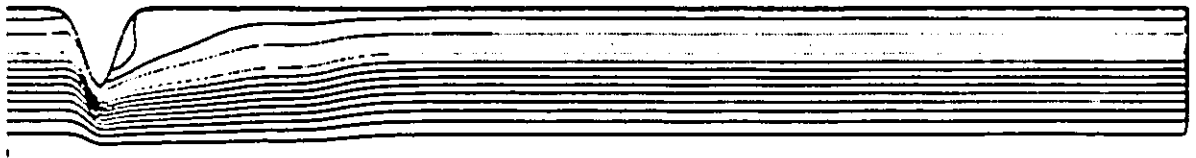


(c) three constrictions

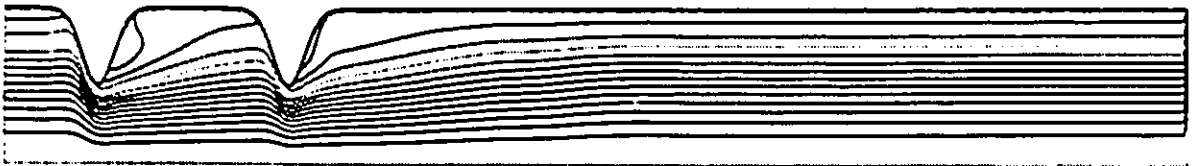


(d) four constrictions

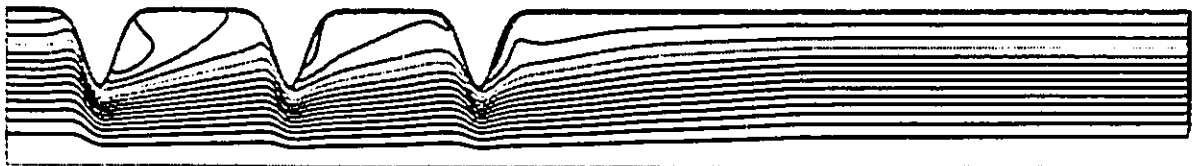
Figure 5.8 Non-dimensional wall shear stress distribution (cont'd)



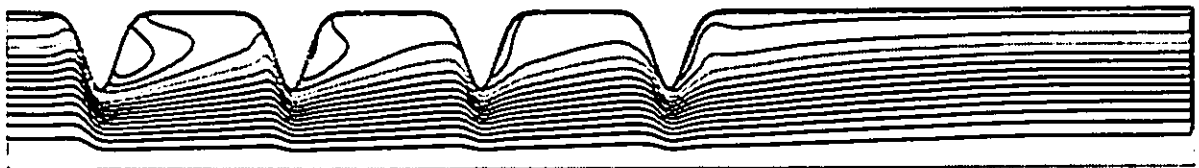
**(a) one constriction**



**(b) two constrictions**

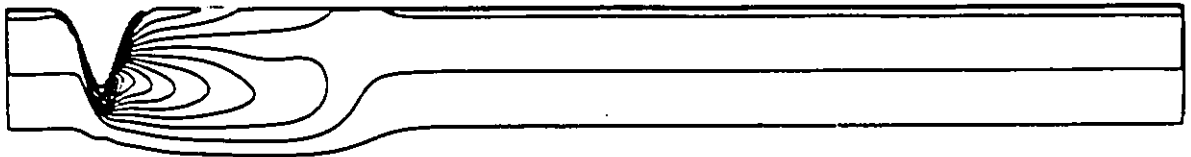


**(c) three constrictions**

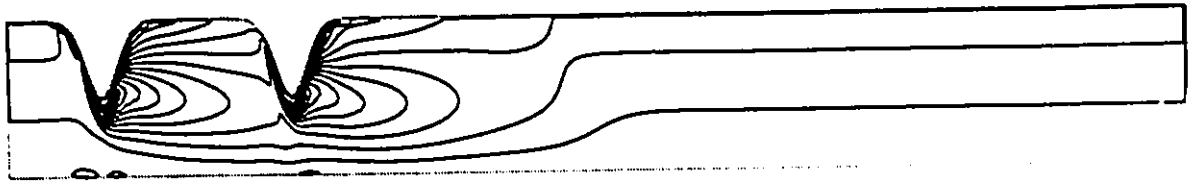


**(d) four constrictions**

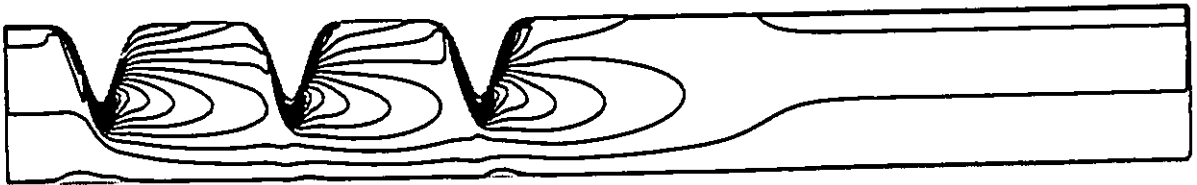
**Figure 5.9 Stream function contours**



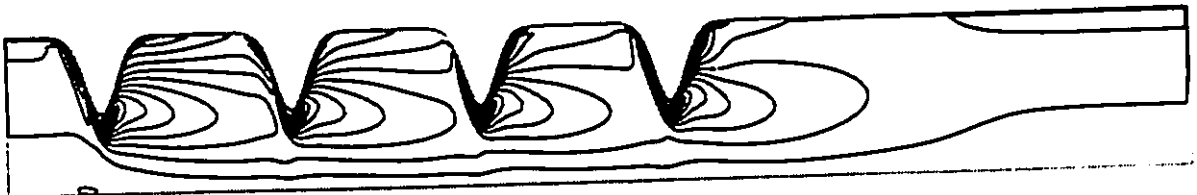
(a) one constriction



(b) two constrictions

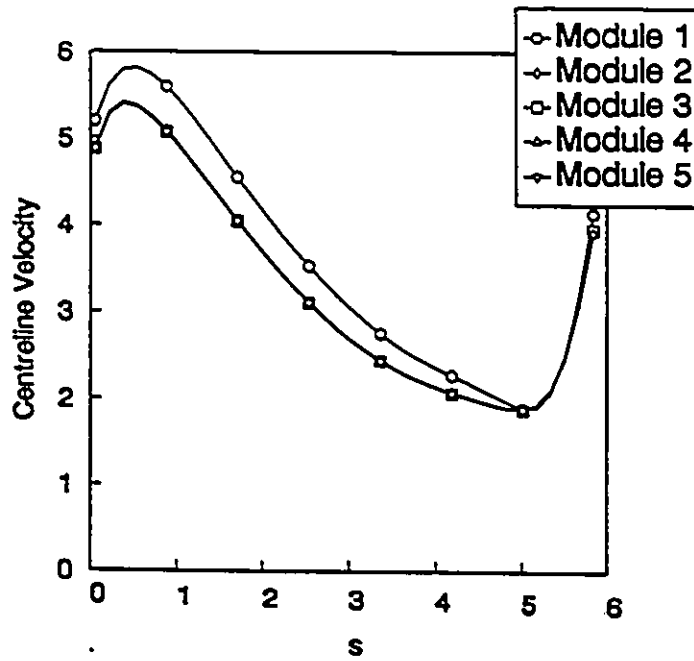


(c) three constrictions

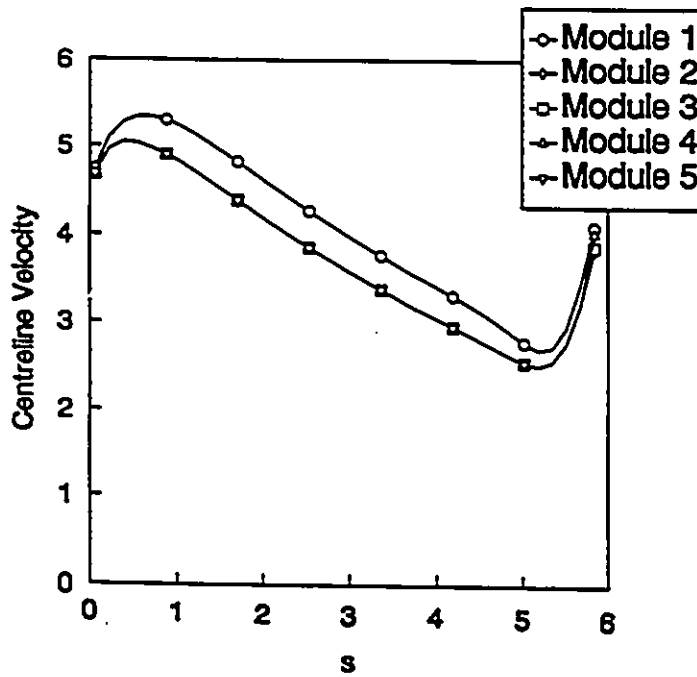


(d) four constrictions

Figure 5.10 Vorticity contours



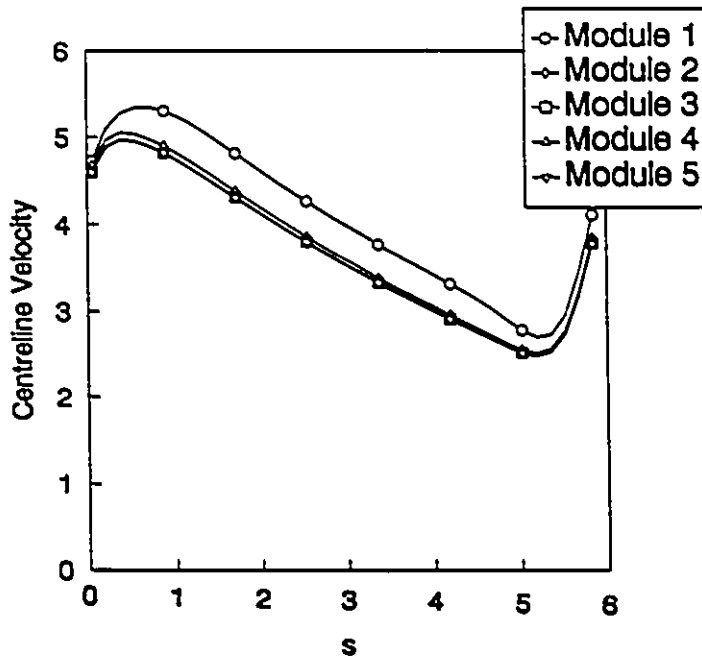
(a)  $Re = 50$



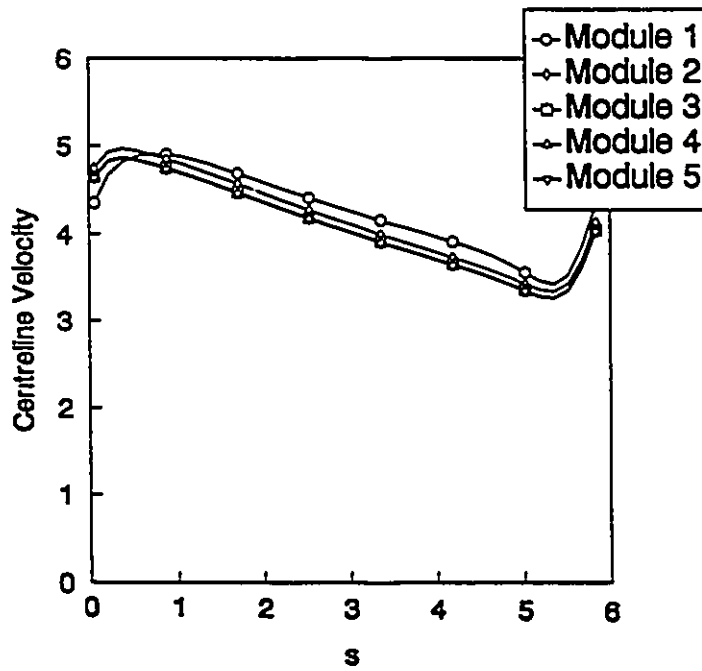
(b)  $Re = 100$

Figure 5.11

Comparison of non-dimensional centreline velocity across the modules

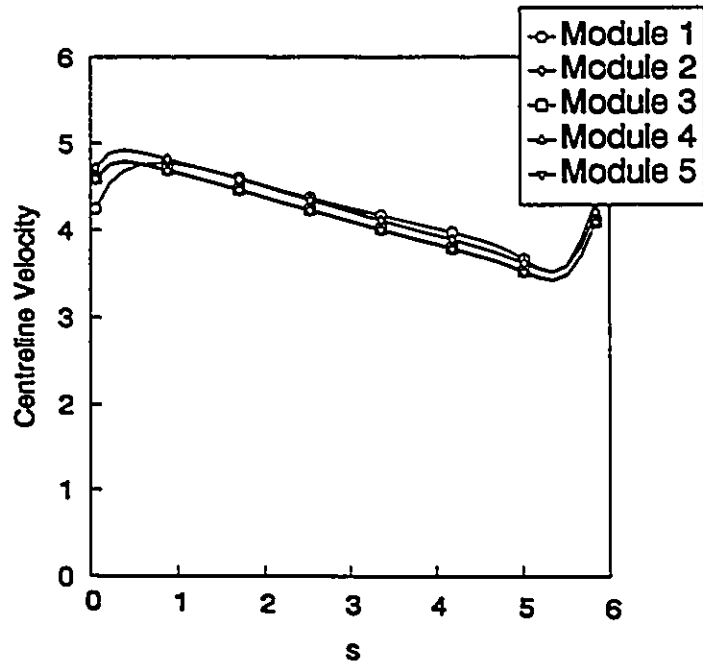


(c) Re = 150



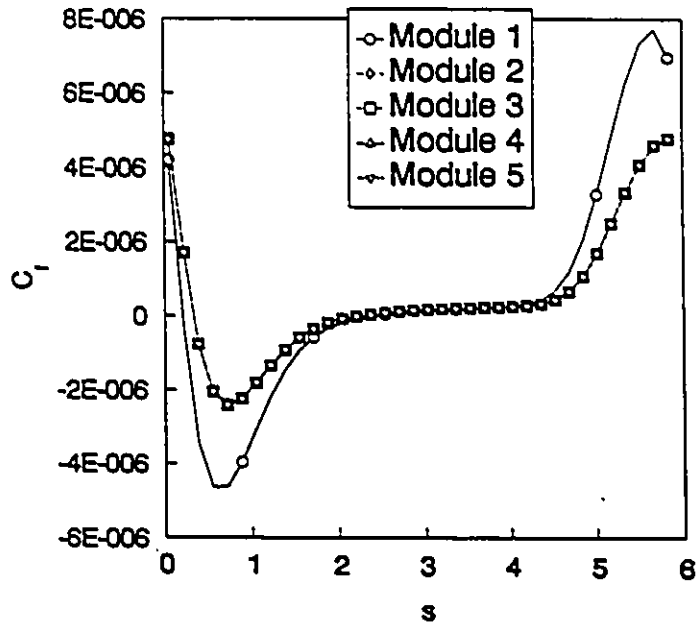
(d) Re = 200

Figure 5.11 Comparison of non-dimensional centreline velocity across the modules (cont'd)

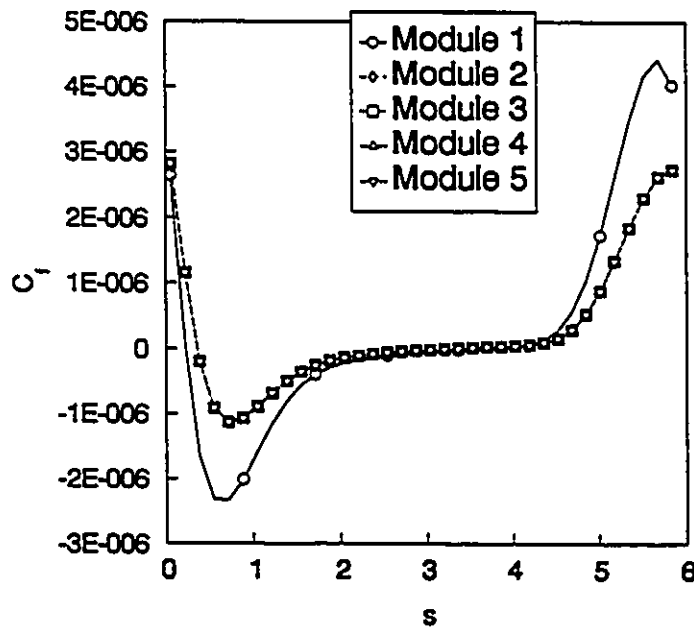


(e)  $Re = 250$

**Figure 5.11** Comparison of non-dimensional centreline velocity across the modules (cont'd)



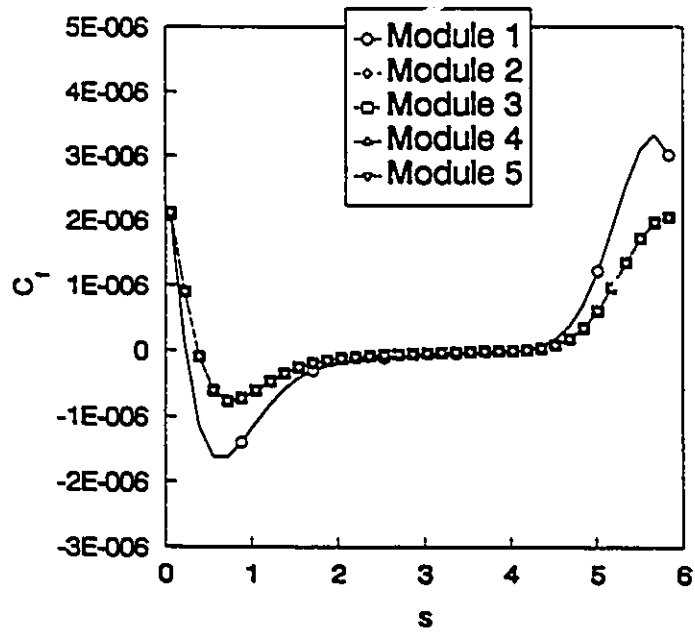
(a)  $Re = 50$



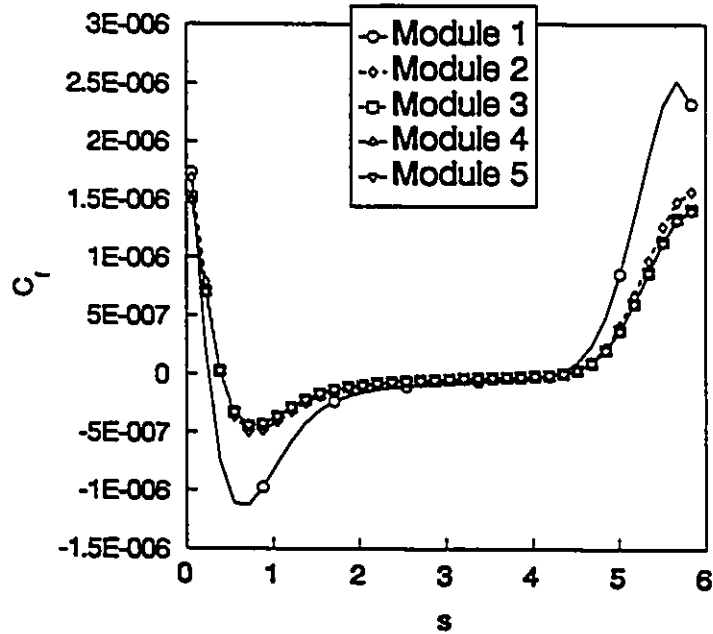
(b)  $Re = 100$

Figure 5.12 Comparison of skin friction coefficient across the modules



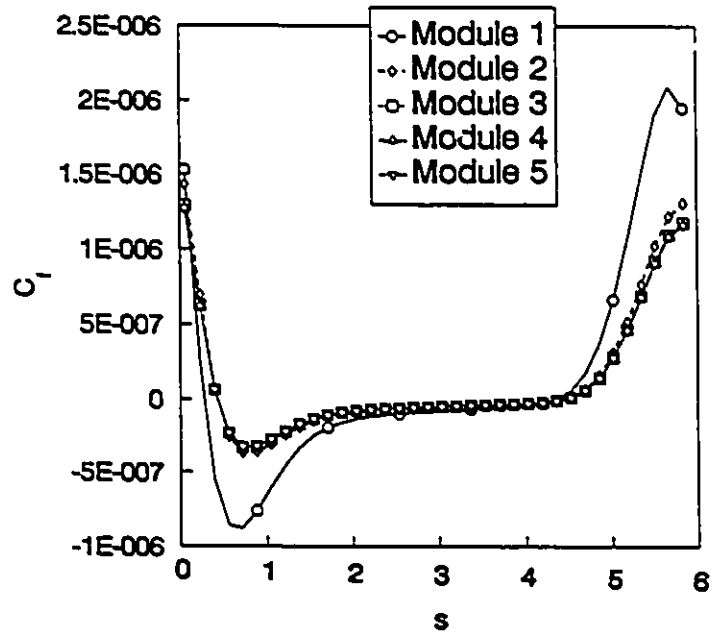


(c)  $Re = 150$



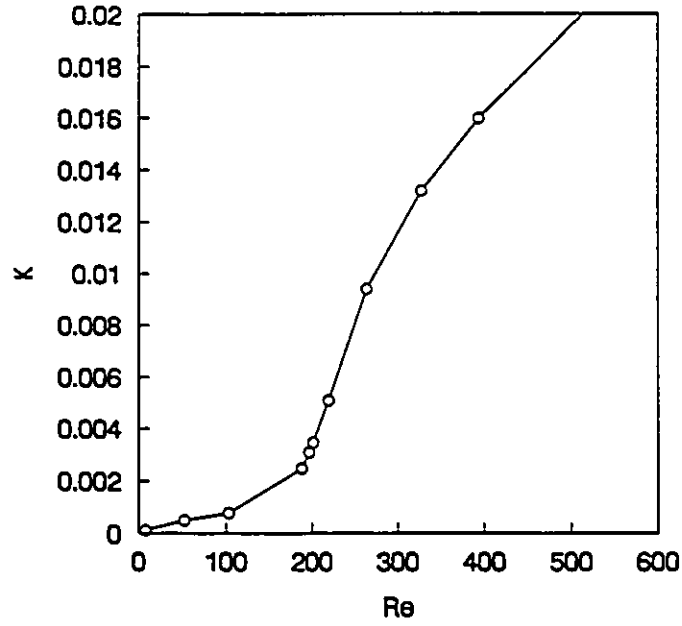
(d)  $Re = 200$

Figure 5.12 Comparison of skin friction coefficient across the modules (cont'd)



(e)  $Re = 250$

Figure 5.12 Comparison of skin friction coefficient across the modules (cont'd)



**Figure 5.13 Non-dimensional pressure drop across the module versus Reynolds number**

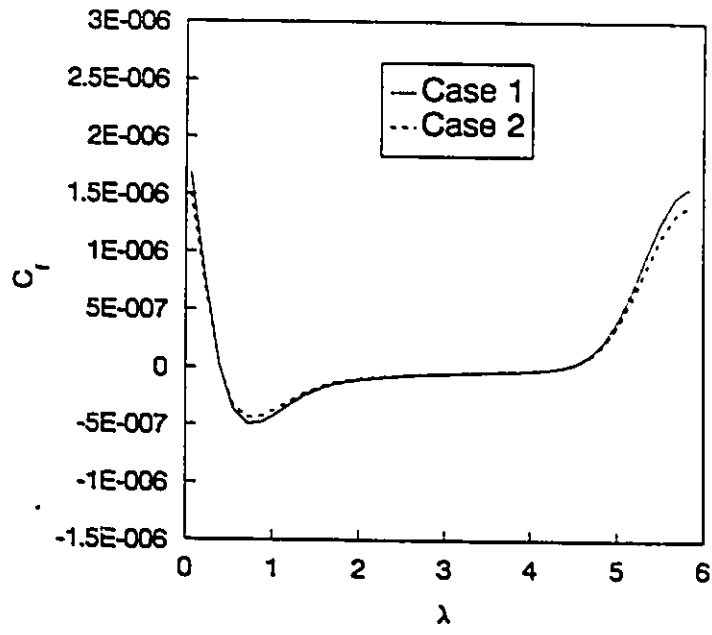


**Figure 5.14 Comparison of skin friction coefficients (Case 1 versus Case 2)**

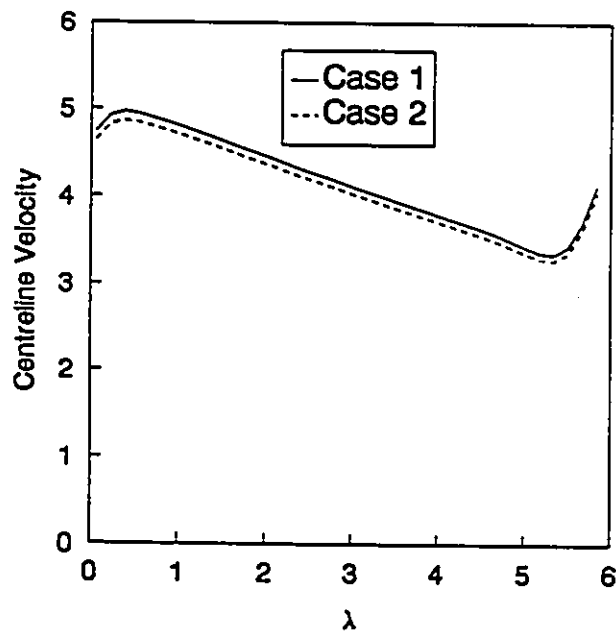
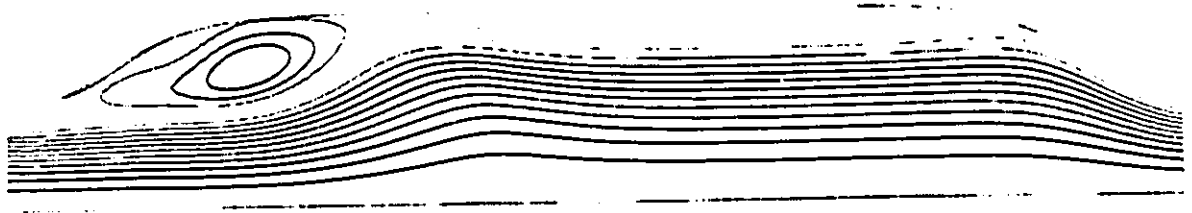
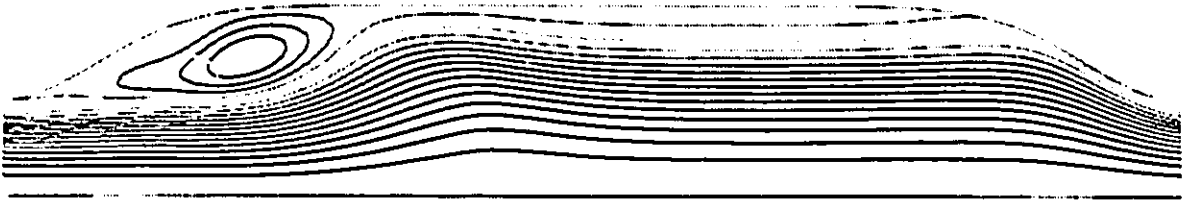


**Figure 5.15 Comparison of non-dimensional centreline velocity (Case 1 versus Case 2)**

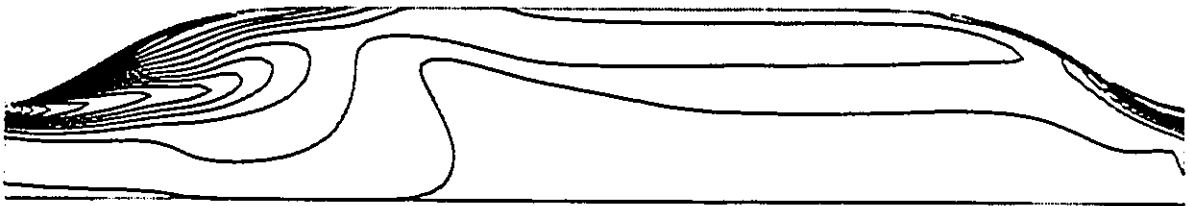


(a) Case 1

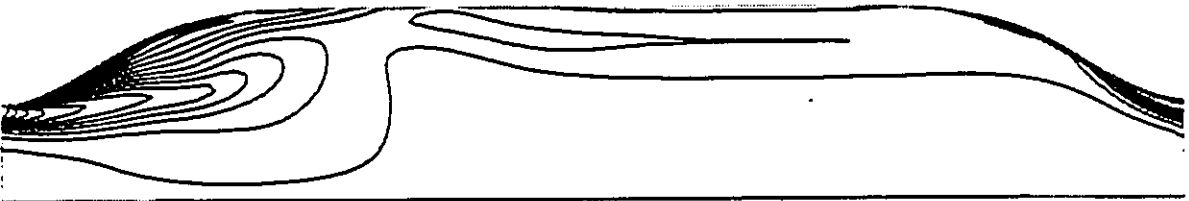


(b) Case 2

Figure 5.16 Stream function contours



(a) Case 1



(b) Case 2

Figure 5.17 Vorticity contours

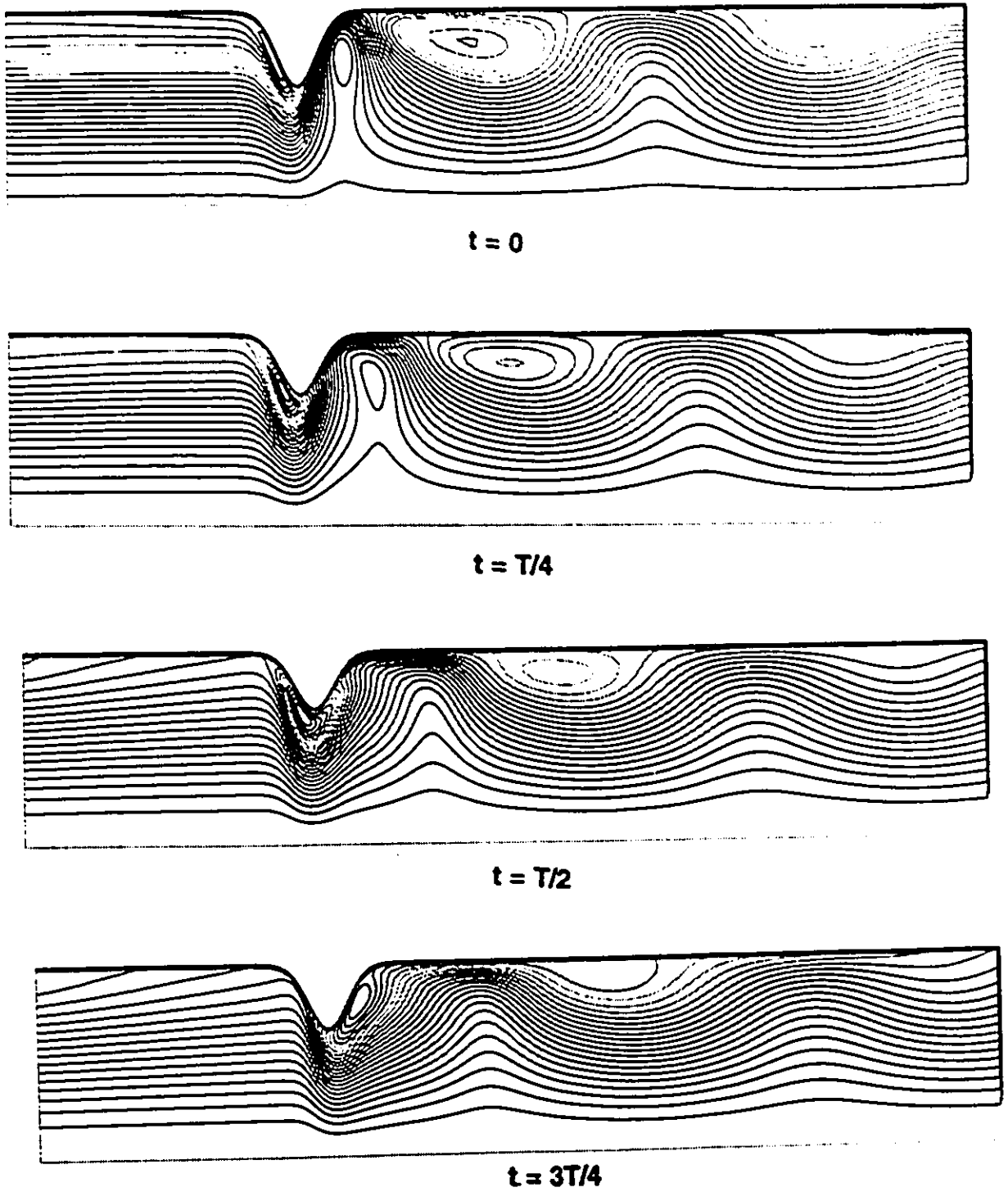
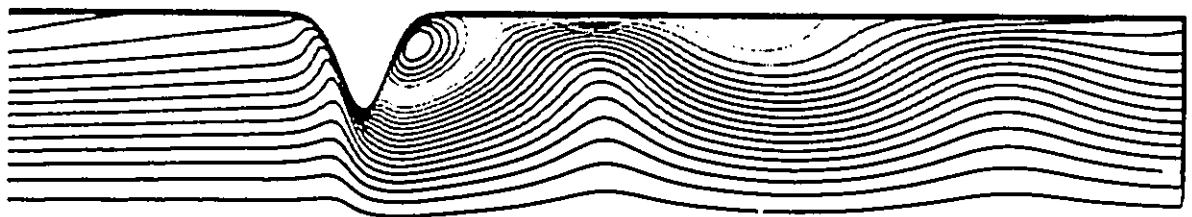
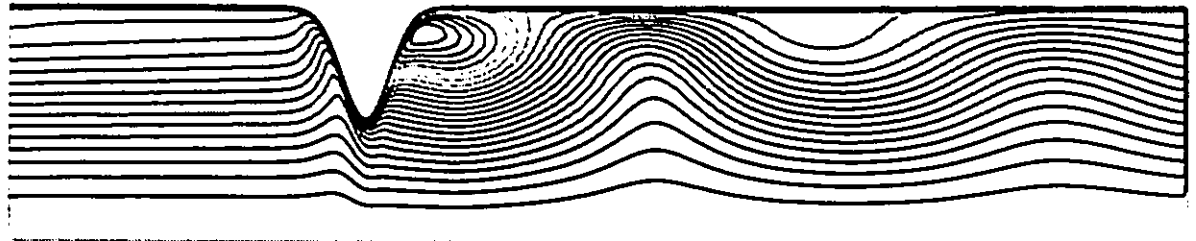


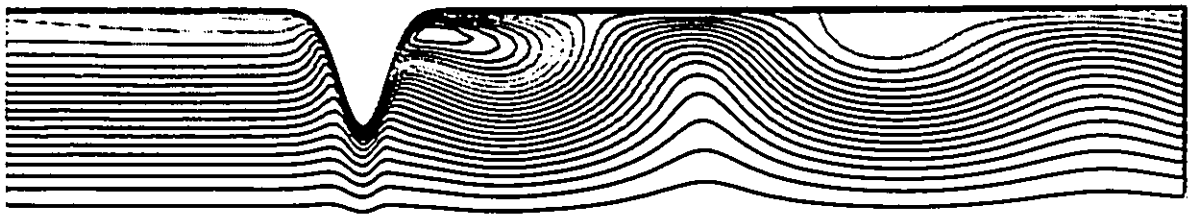
**Figure 5.18 Stream function contours for one complete cycle of pulsation (Case 3)**



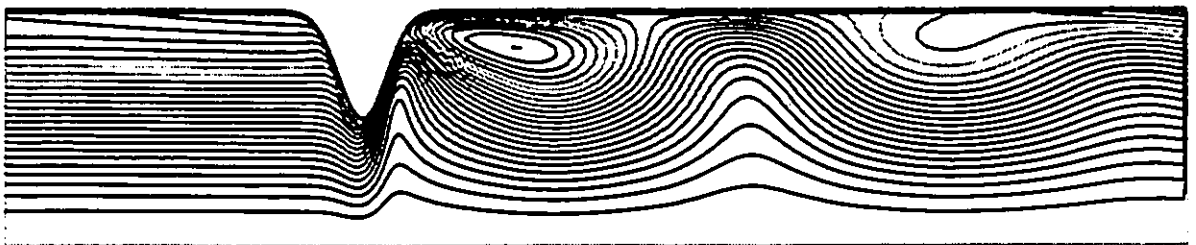
$t = T$



$t = 5T/4$

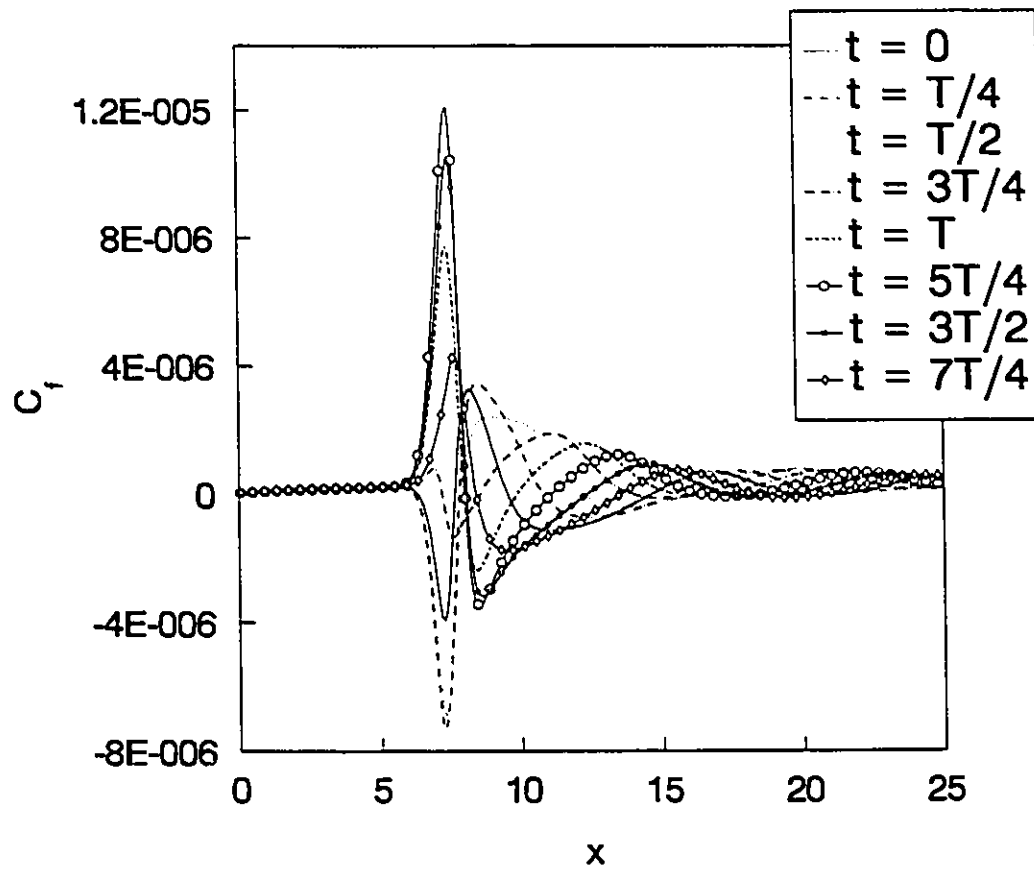


$t = 3T/2$



$t = 7T/4$

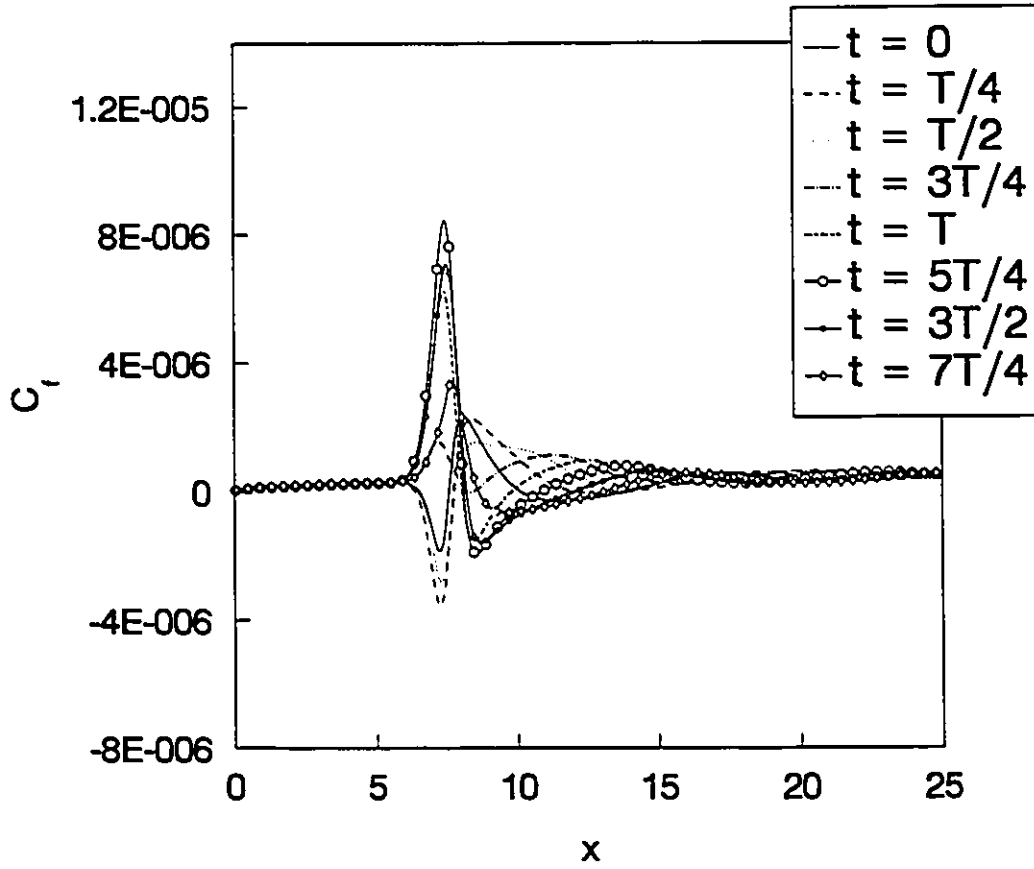
**Figure 5.18** Stream function contours for one complete cycle of pulsation  
(Case 3) (cont'd)



(a)  $\alpha = 10$

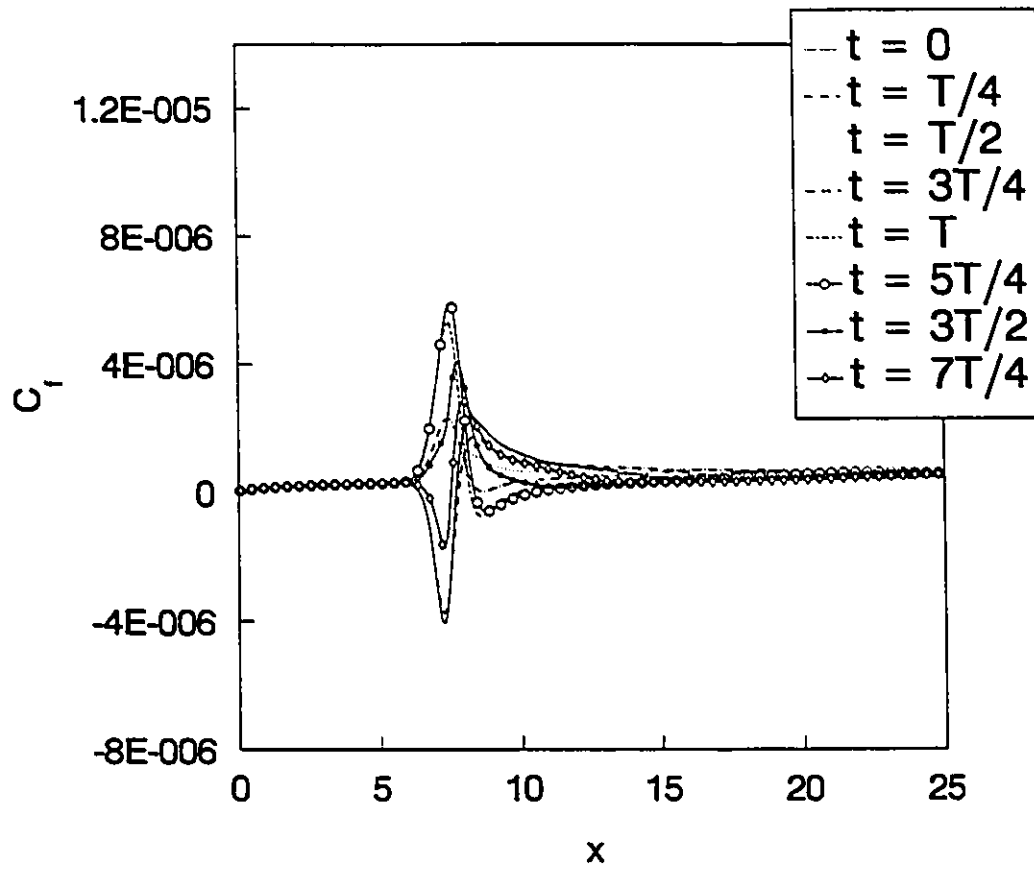
Figure 5.19 Skin friction coefficient distribution (Case 3)





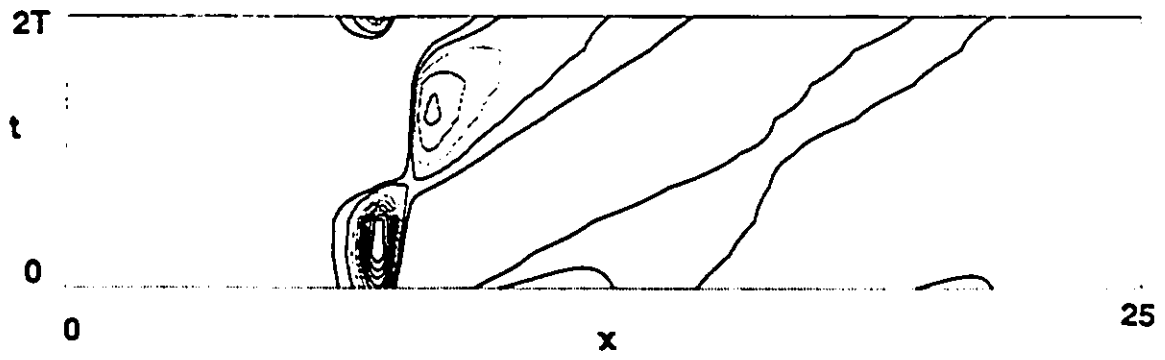
(b)  $\alpha = 7.5$

Figure 5.19 Skin friction coefficient distribution (Case 3)  
(cont'd)

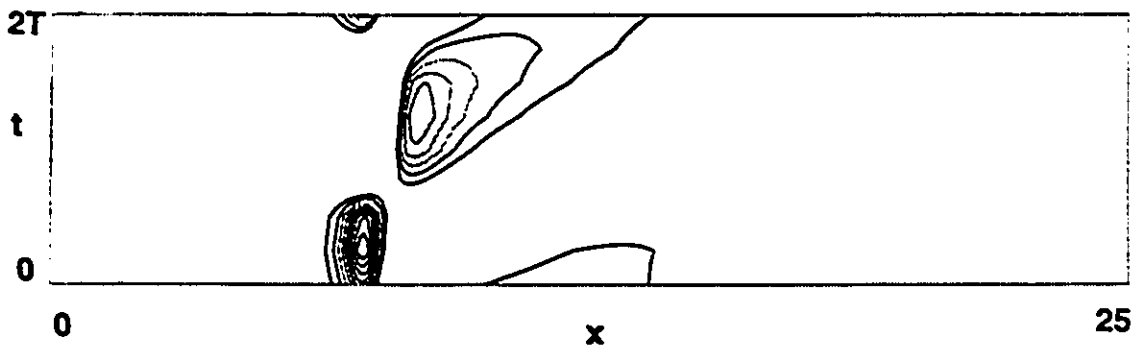


(c)  $\alpha = 5$

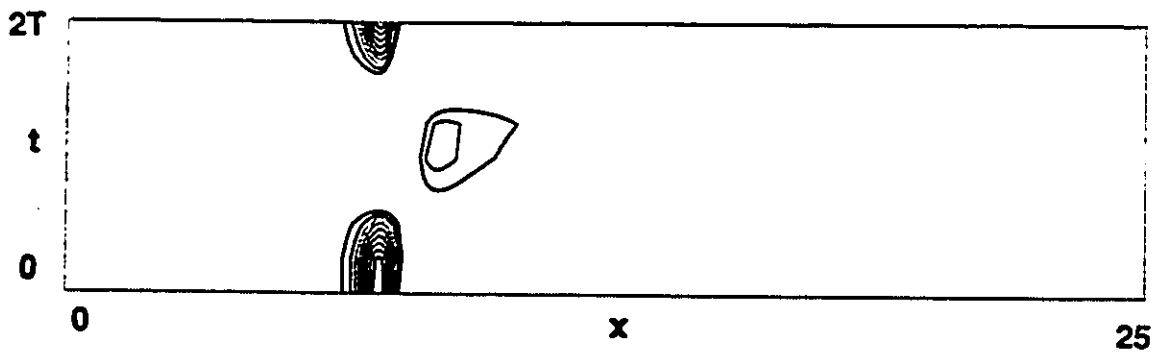
Figure 5.19 Skin friction coefficient distribution (Case 3)  
(cont'd)



(a) ( $\alpha = 10$ )

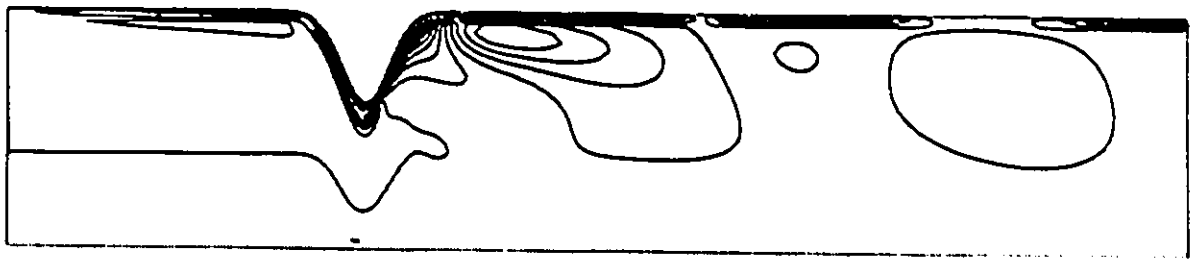


(b) ( $\alpha = 7.5$ )



(c) ( $\alpha = 5$ )

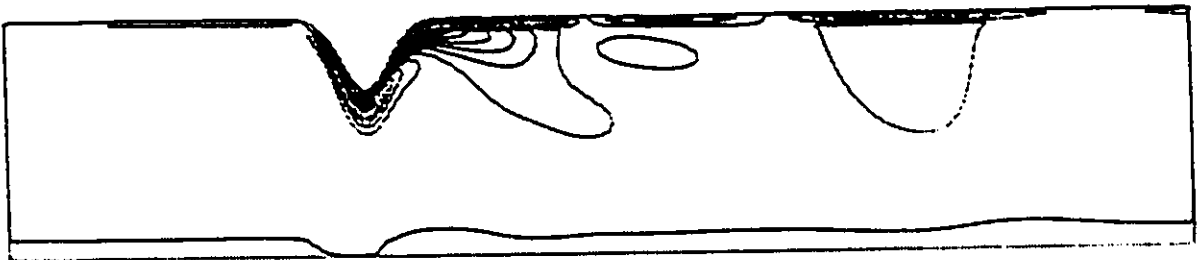
Figure 5.20 Skin friction contours for one complete cycle of pulsation (Case 3)



$t = 0$



$t = T/4$

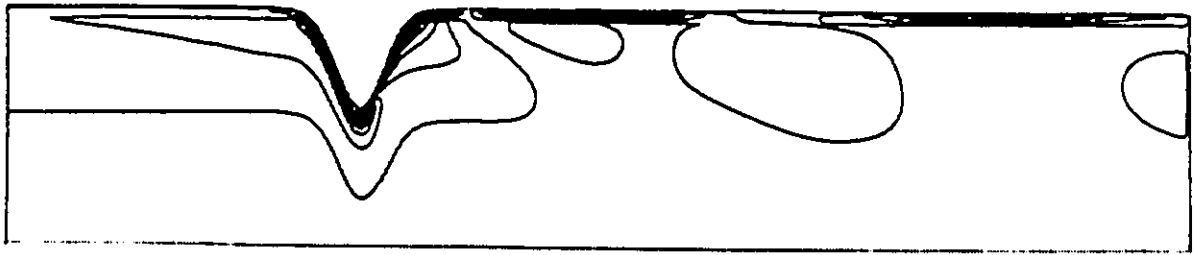


$t = T/2$

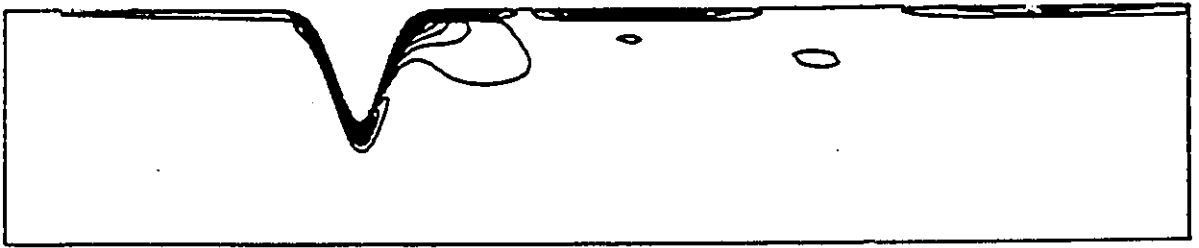


$t = 3T/4$

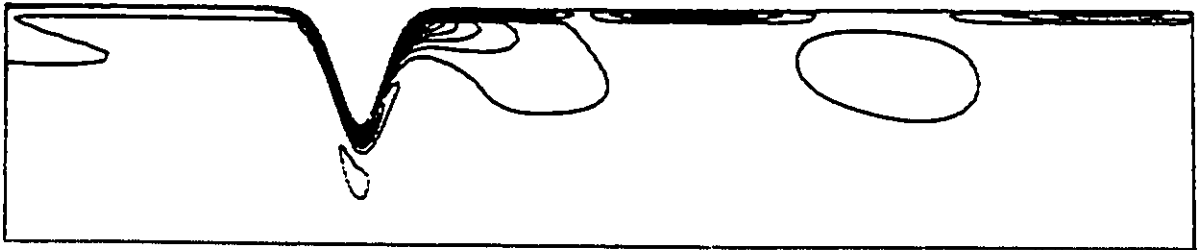
**Figure 5.21 Vorticity contours for one complete cycle of pulsation (Case 3)**



$t = T$



$t = 5T/4$

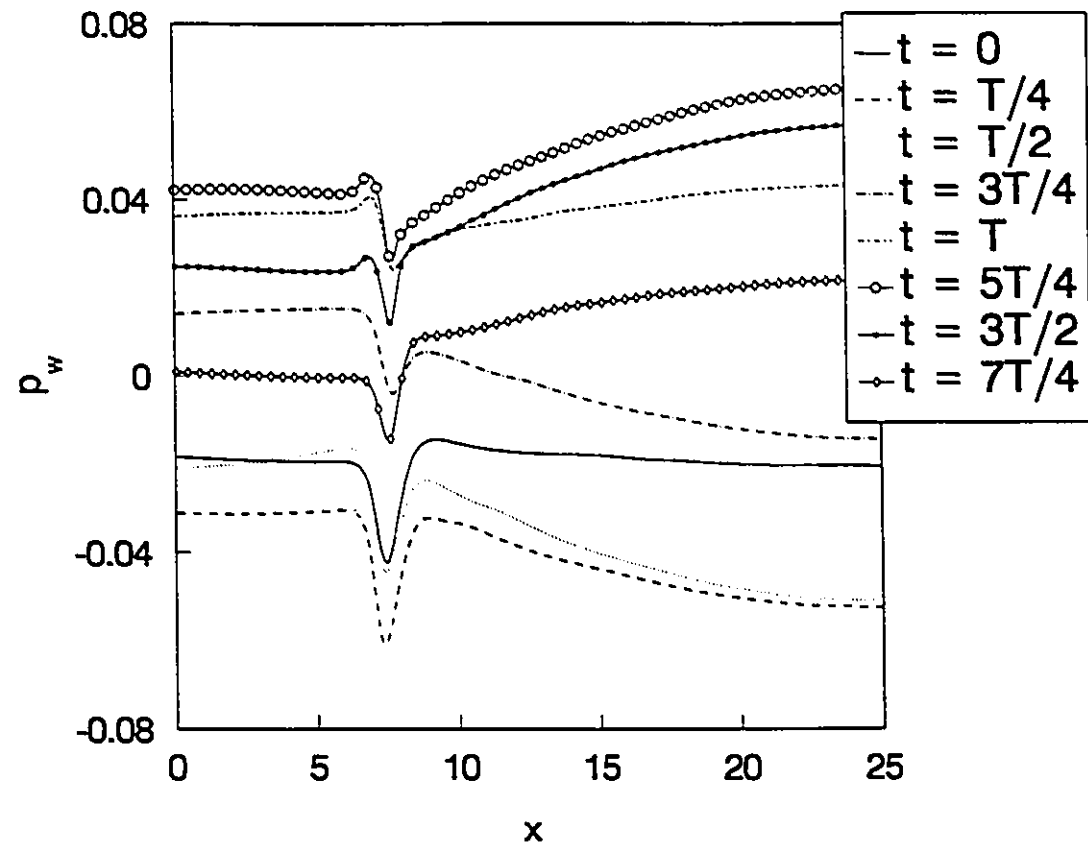


$t = 3T/2$



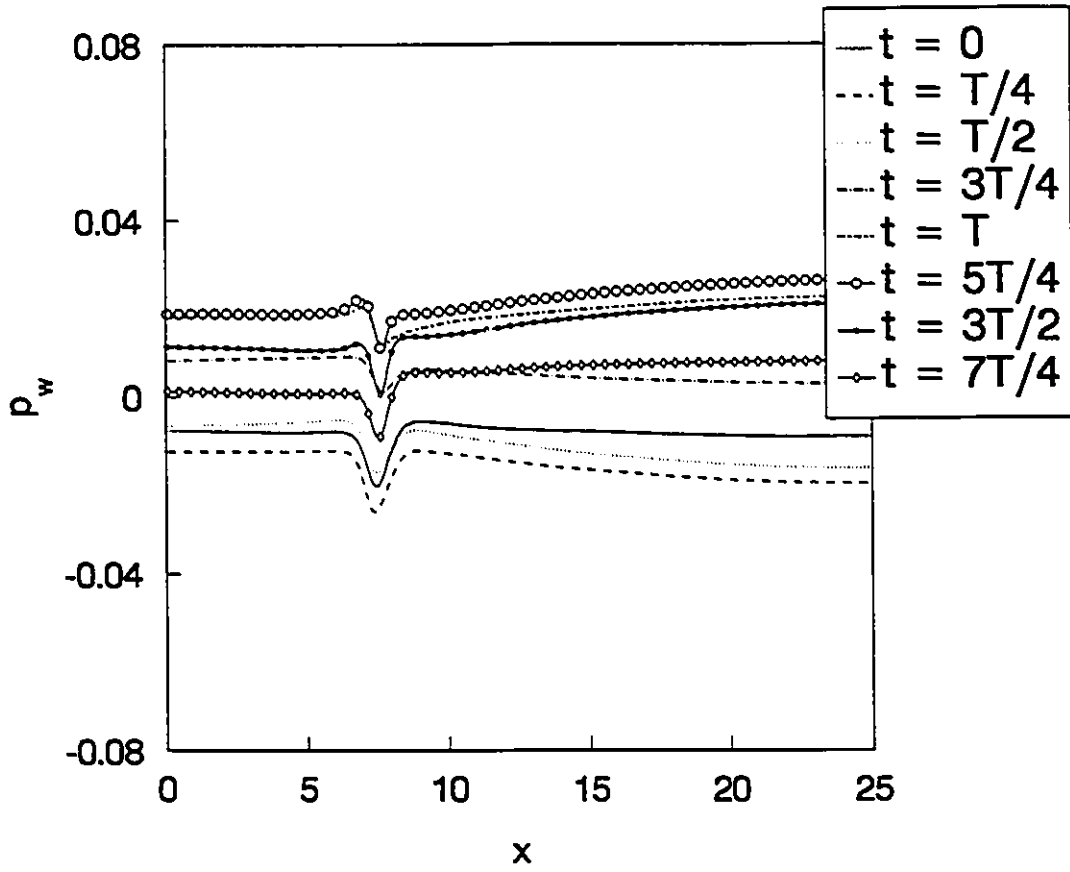
$t = 7T/4$

**Figure 5.21 Vorticity contours for one complete cycle of pulsation (Case 3) (cont'd)**



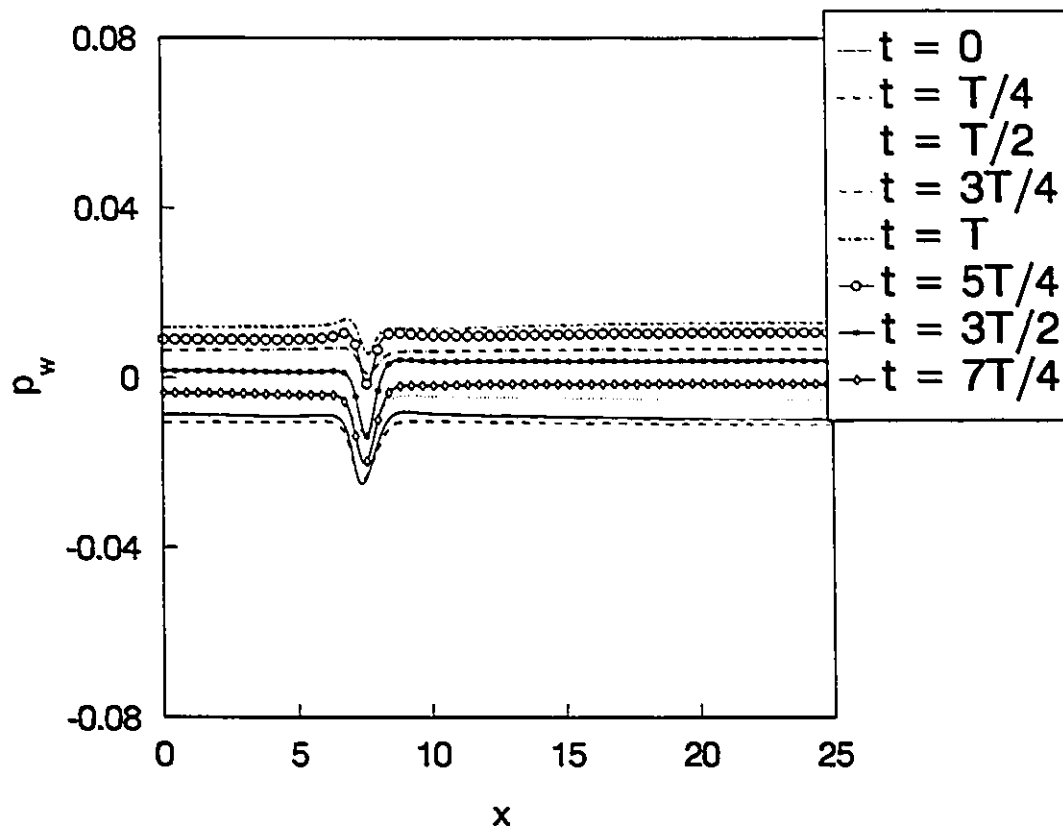
(a)  $\alpha = 10$

Figure 5.22 Non-dimensional pressure distribution along the wall (Case 3)



(b)  $\alpha = 7.5$

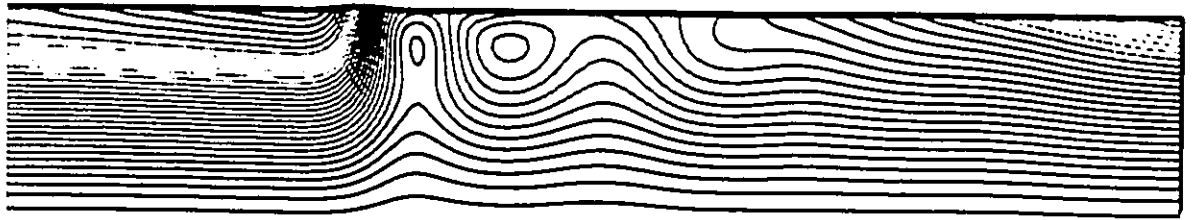
Figure 5.22 Non-dimensional pressure distribution along the wall (Case 3) (cont'd)



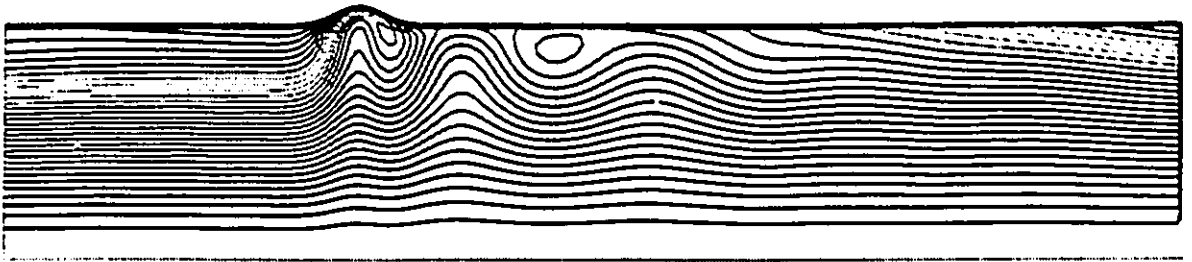
(c)  $\alpha = 5$

Figure 5.22 Non-dimensional pressure distribution along the wall (Case 3)  
(cont'd)

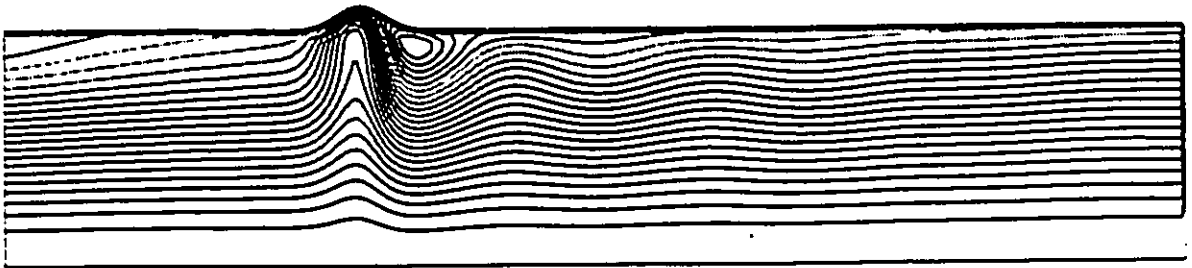




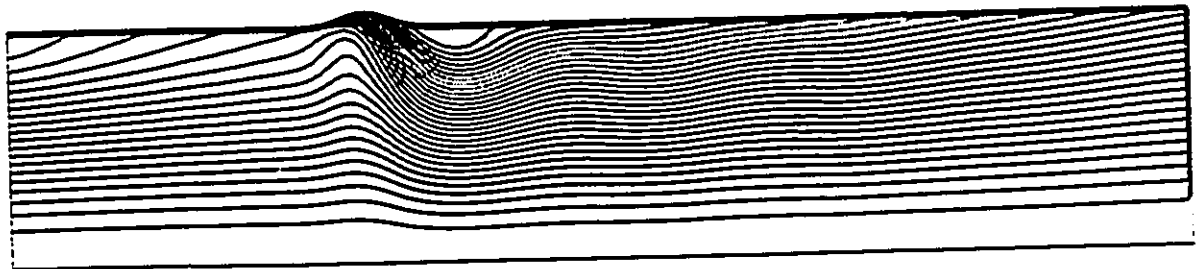
$t = 0$



$t = T/4$



$t = T/2$

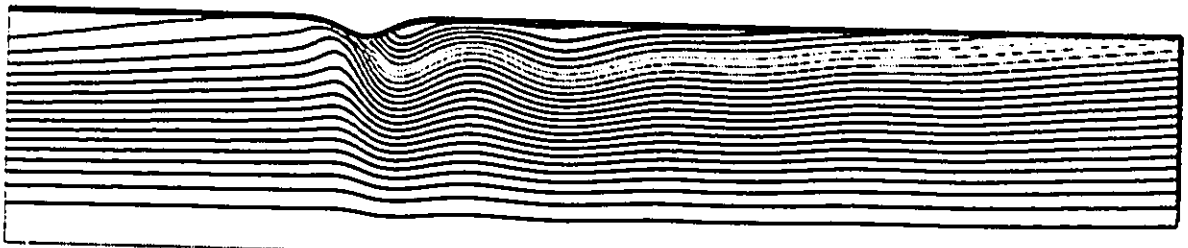


$t = 3T/4$

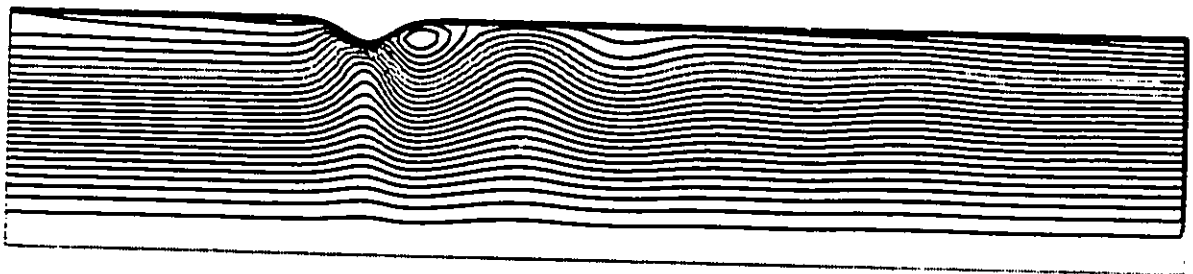
**Figure 5.23** Stream function contours for one complete cycle of pulsation (Case 4)



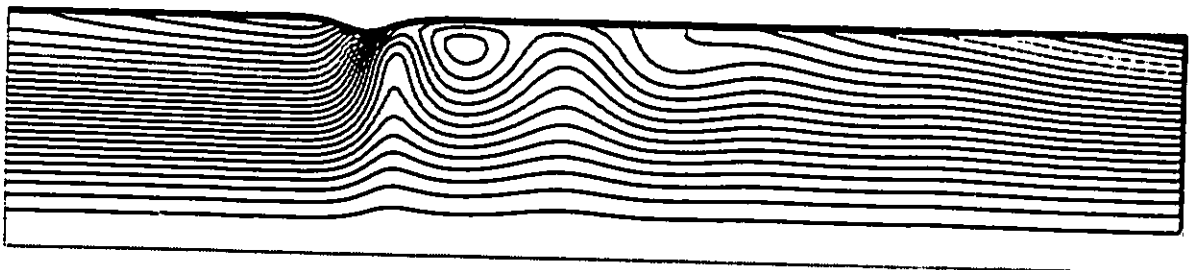
$t = T$



$t = 5T/4$

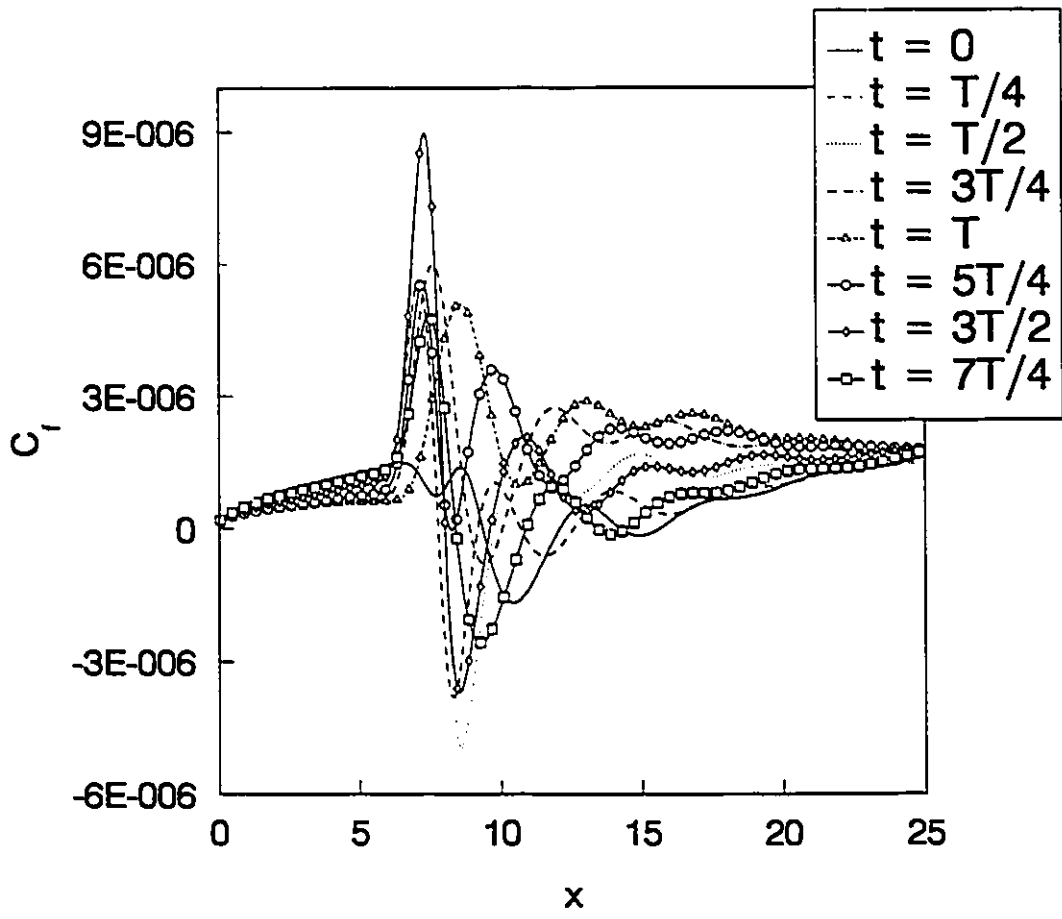


$t = 3T/2$



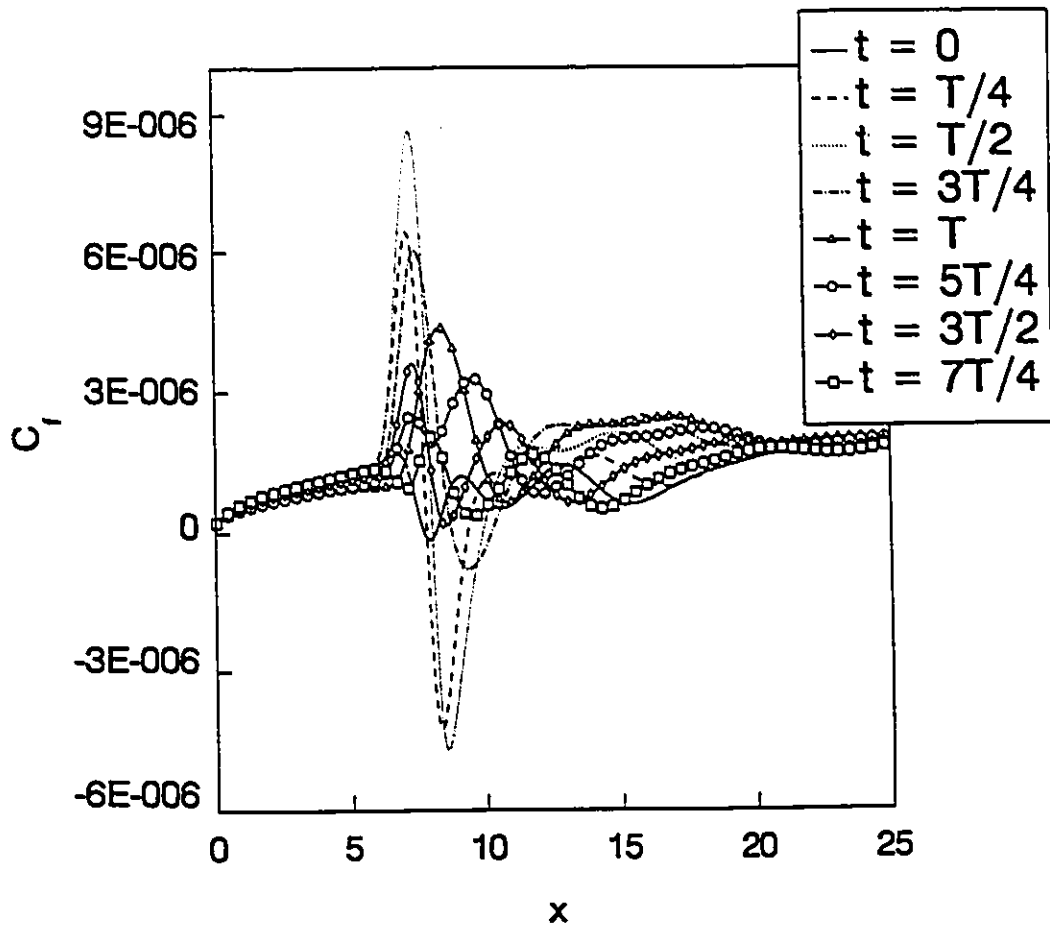
$t = 7T/4$

**Figure 5.23 Stream function contours for one complete cycle of pulsation (Case 4) (cont'd)**



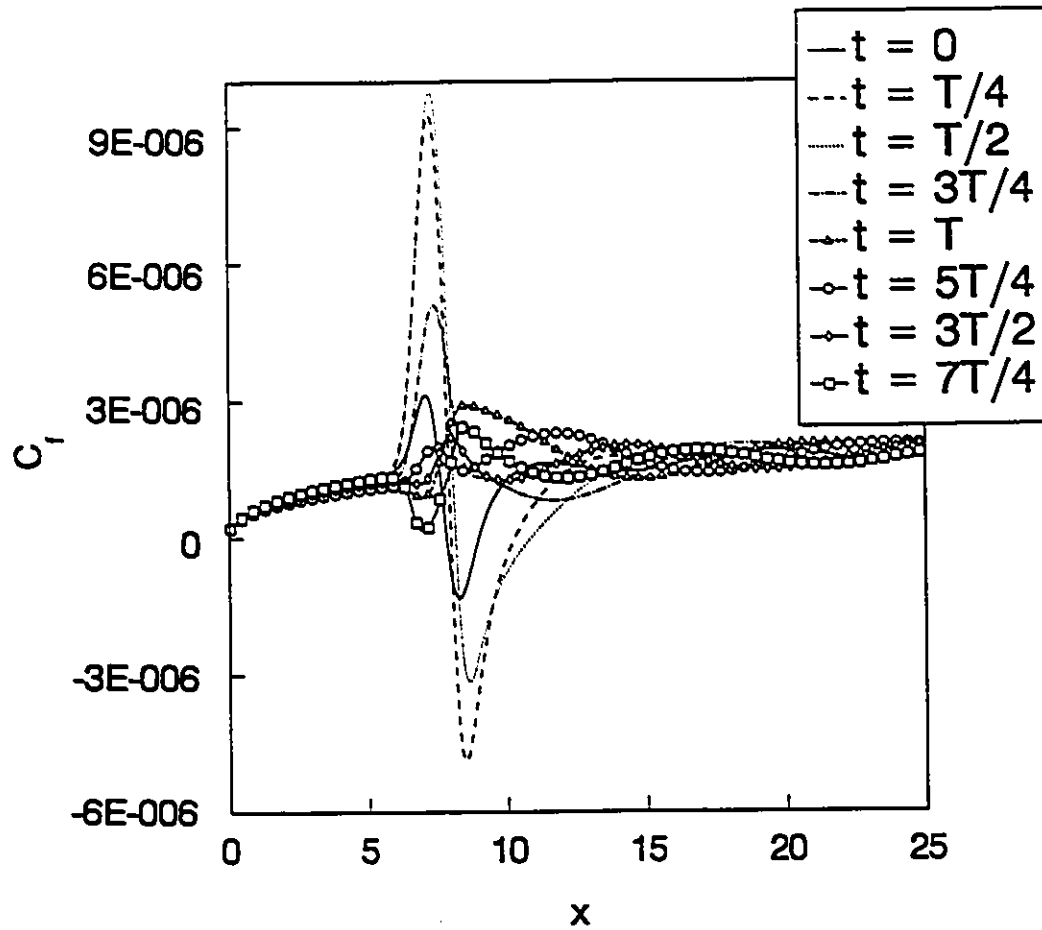
(a)  $\alpha = 10$

Figure 5.24 Skin friction coefficient distribution (Case 4)



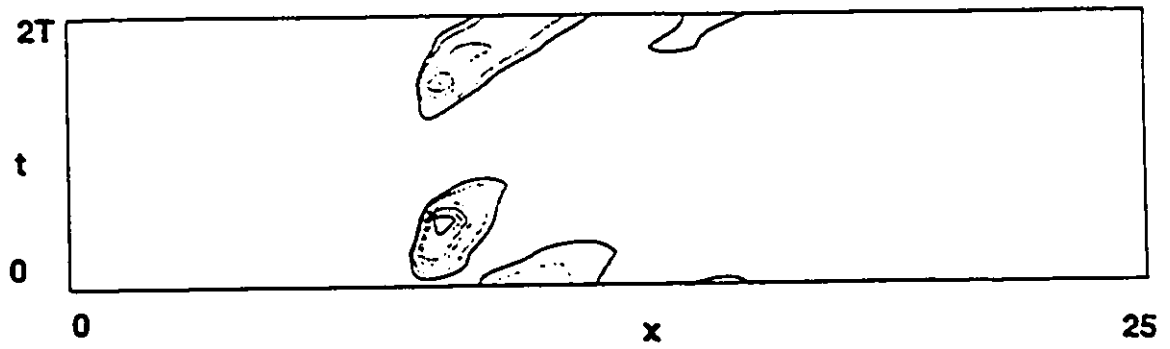
(b)  $\alpha = 7.5$

Figure 5.24 Skin friction coefficient distribution (Case 4)  
(cont'd)

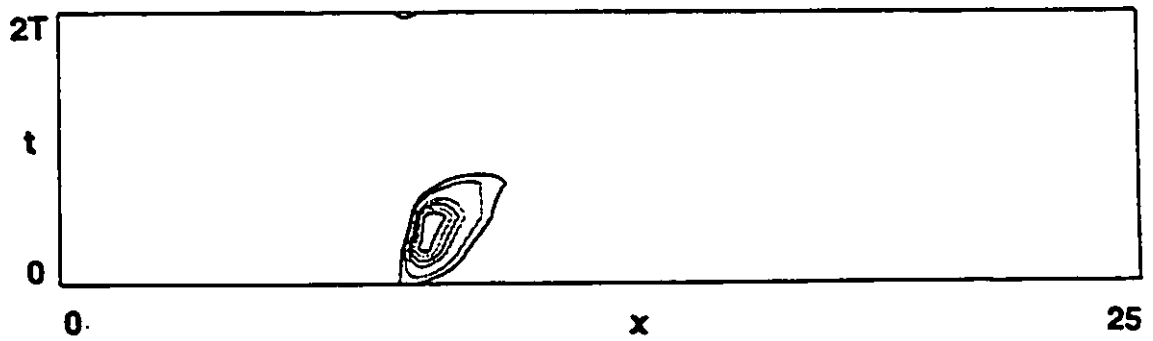


(c)  $\alpha = 5$

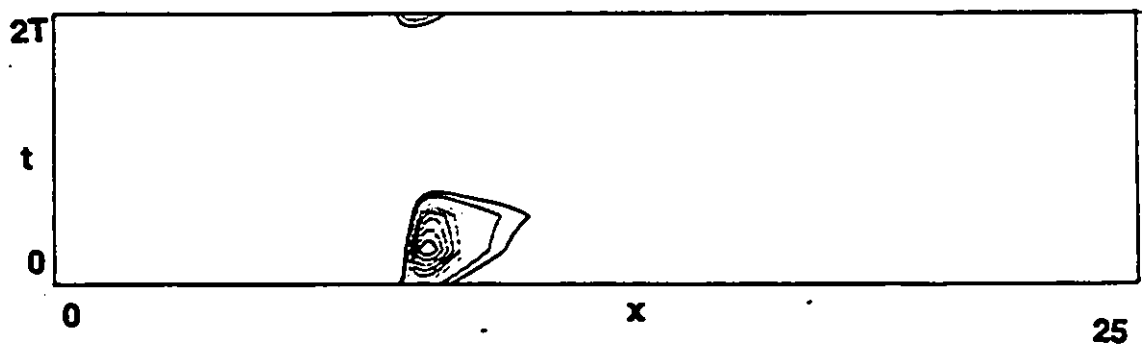
Figure 5.24 Skin friction coefficient distribution (Case 4)  
(cont'd)



(a) ( $\alpha = 10$ )

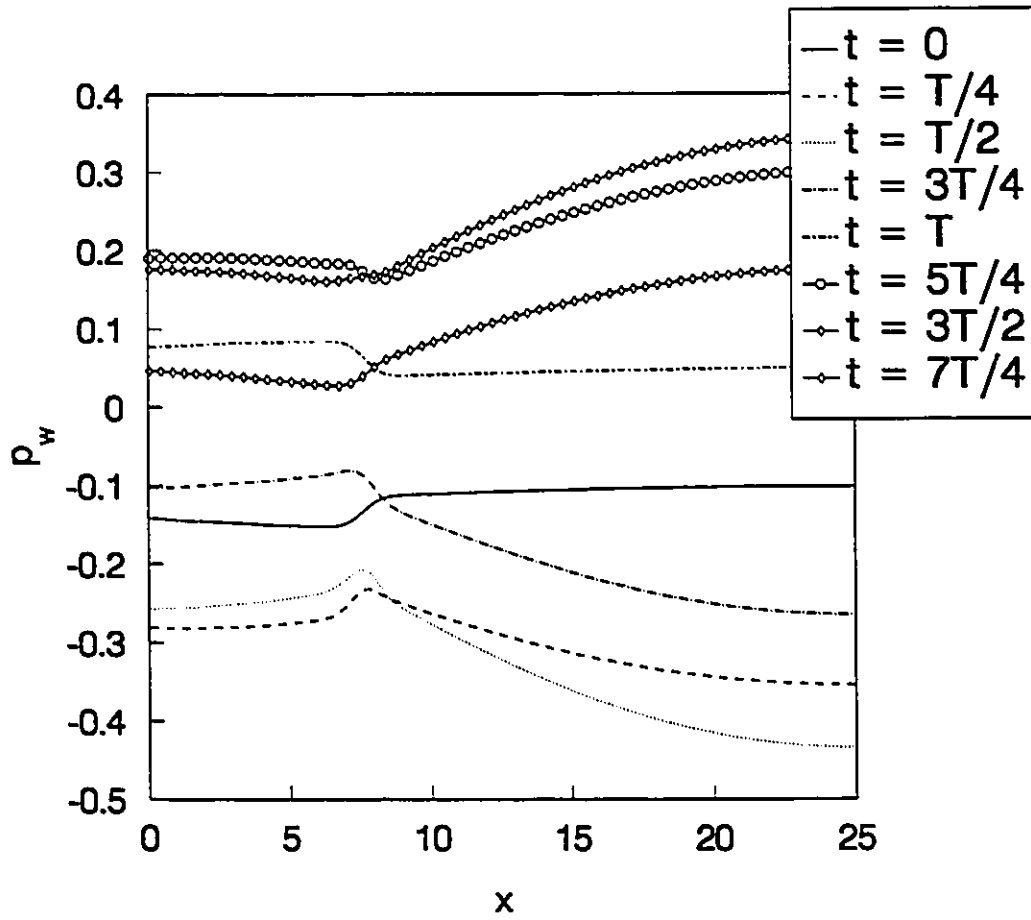


(b) ( $\alpha = 7.5$ )



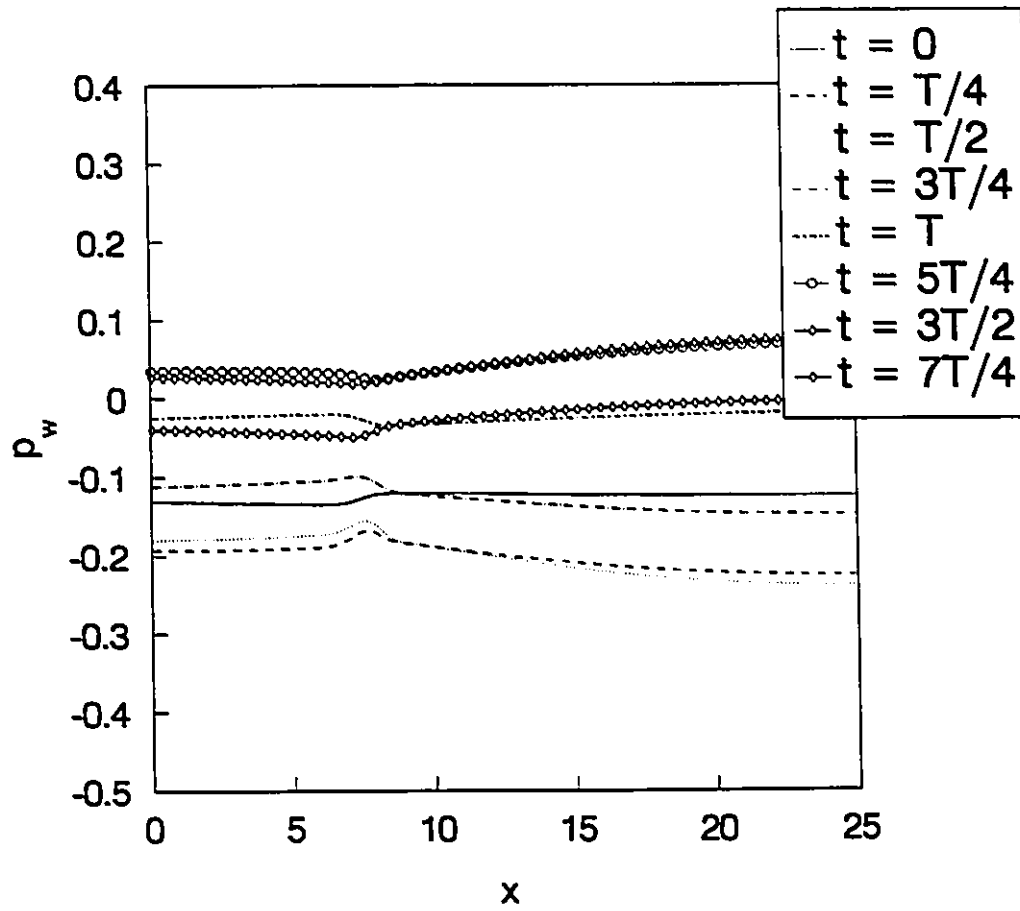
(c) ( $\alpha = 5$ )

Figure 5.25 Skin friction contours for one complete cycle of pulsation (Case 4)



(a)  $\alpha = 10$

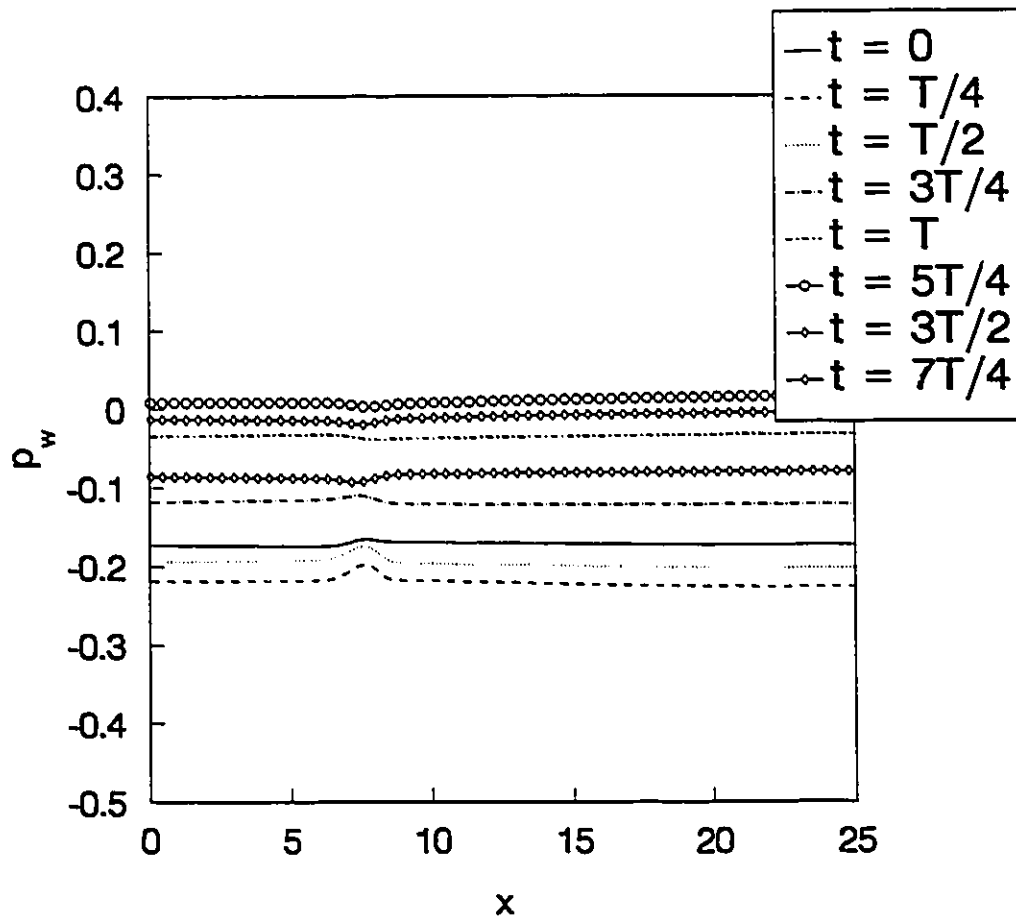
Figure 5.26 Non-dimensional pressure distribution along the wall (Case 4)



(b)  $\alpha = 7.5$

Figure 5.26 Non-dimensional pressure distribution along the wall (Case 4)  
(cont'd)





(c)  $\alpha = 5$

Figure 5.26 Non-dimensional pressure distribution along the wall (Case 4)  
(cont'd)

---

## **CHAPTER VI *Conclusions and Recommendations***

---

A numerical method has been developed to determine the fluid dynamic quantities associated with the flow through a tube with multiple constrictions and pulsatile flow through tubes with moving boundaries. The governing equations, in transformed, body fitted curvilinear coordinates, are solved using a control volume discretization procedure. The method presented here can also be used for other flow problems having arbitrary axially-symmetric domains with or without moving boundaries in the flow passage. Based on the computational investigation, a number of conclusions are drawn as listed below.

### **6.1 Conclusions**

#### **6.1.1 Flow in a tube with multiple constrictions**

The effect of the number of constrictions and the Reynolds number on flow parameters such as pressure, velocity and wall shear stress were determined and the development of periodicity characteristics were investigated.

### **a) Pressure**

1. The increase in the number of constrictions causes an increase in the non-dimensional pressure drop.
2. The non-dimensional pressure drop decreases with the increase in the Reynolds number.
3. The wall pressure shows a rapid drop as it approaches the constriction with the pressure recovery taking place over a greater length.
4. Subsequent constrictions show an increasingly similar pressure drop and recovery with the downstream profiles shifting correspondingly downwards due to the net mass flow in the positive  $x$  direction.

### **b) Velocity**

5. The maximum centreline velocity occurs slightly downstream of the constriction due to the formation of a recirculation zone near the wall as a result of flow separation.
6. As the number of constrictions increases the fluid does not have an opportunity to recover to its initial value before it encounters another constriction.

### **c) Wall shear stress**

7. The wall shear stress reaches a maximum value near the maximum constricted area. The wall shear stress takes a negative value downstream

of the constriction due to flow separation.

8. The maximum value of the wall shear stress for the first constriction is always greater than the maximum value of the wall shear generated by the second constriction as the recirculating eddies formed downstream of the first constriction has a diminishing effect on the vortices generated by the second constriction.

#### **d) Periodicity characteristics**

9. An approximate expression for the length for development of spatial periodicity on flow through a tube with constrictions and inlet conditions such as the one studied was found to be

$$n_m = \frac{l_o}{D_o} \geq 1 + \left[ \frac{Re}{100} + 1 \right].$$

10. The numerical results for a module using periodic boundary conditions, showed a reasonable comparison with the spatially periodic region of a pipe having multiple constrictions.

#### **6.1.2 Pulsatile flow with time dependent constriction**

11. At higher frequencies of pulsation two types of recirculating eddies (clockwise and anticlockwise rotation) were created in succession to each other causing an oscillating wall shear stress and creating waviness in the core flow.

12. Two regions of flow separation were predicted and they both moved downstream throughout the remainder of the cycle.
13. The size and extent of the flow separation regions decreased as the pulsation frequency decreased.
14. A decrease in the frequency of pulsation caused the unsteadiness in the flow to decrease.

### **6.1.3 Pulsatile flow with moving boundary**

15. During the downward motion of the vibrating wall, the waviness in the core flow was minimal and recirculating eddies of a counterclockwise nature were created.
16. The upward motion of the wall created eddies of both clockwise and counterclockwise rotation causing an increase in the waviness of the core flow.
17. The number of separation regions decreased from three at higher frequencies to one as the frequency was decreased.
18. A decrease in the frequency of pulsation caused the unsteadiness in the flow to decrease.

## **6.2 Recommendations**

The following suggestions are provided as possible ways of extending the scope of the present study and improving the predictions:

1. The problem of flow through a tube with multiple constrictions should be extended to the turbulent flow regime as most of the flows in real life are turbulent and such a study will also be useful in heat exchanger analysis.
2. In order to gain a better understanding of moving boundary flows, the effects of frequency, Reynolds number and phase difference between the pressure gradient and the wall motion should be examined in greater detail.
3. Accurate and faster solvers should be employed to solve the pressure correction equation.
4. The equations that describe the motion of the wall can be coupled to the equations considered in this work and solved simultaneously.

## **References**

---

- An, C.F. and Barron R.M., (1995) Transonic Euler computation in streamfunction coordinates, *International Journal for Numerical Methods in Fluids*, 20, 74-95.
- Ahmed, S.A. and Giddens, D.P., (1983) Velocity measurements in steady flow through axisymmetric stenoses at moderate Reynolds numbers, *Journal of Biomechanics*, 16(7), 505-516.
- Atabek, H.B. and Lew, H.S., (1966) Wave propagation through a viscous incompressible fluid contained in an initially stressed elastic tube, *Biophysical Journal*, 6, 481-503.
- Atabek, H.B., (1968) Wave propagation through a viscous fluid contained in a tethered, initially stressed, orthotropic elastic tube, *Biophysical Journal*, 8, 626-649.
- Bertram, C.D., (1987) The effects of wall shear thickness, axial strain and end proximity on the pressure-area relation of collapsible tubes, *Journal of Biomechanics*, 20(9), 863-876.
- Bertram, C.D., Raymond, C.J. and Pedley, T.J., (1990) Mapping of instabilities for flow through collapsed tubes of differing length, *Journal of Fluids and Structures*, 4, 125-153.
- Bertram, C.D., Raymond C.J. and Pedley, T.J., (1991) Application of nonlinear dynamics concepts to the analysis of self excited oscillations of a collapsible tube conveying a fluid, *Journal of Fluids and Structures*, 5, 391-426.
- Brower, R.W. and Scholten, C., (1975) Experimental evidence on the mechanism for the instability of flow in collapsible vessels, *Medical and Biological Engineering*, 839-844.
- Cancelli, C. and Pedley, T.J., (1985) A separated-flow model for collapsible tube oscillations, *Journal of Fluid Mechanics*, 157, 375-404.
- Clark, M.E., Robertson, J.M. and Cheng, L.C., (1983) Stenosis severity effects for unbalanced simple pulsatile bifurcation flow, *Journal of Biomechanics*, 16(11), 895-906.
- Dragon, C.A. and Grotberg, J.B., (1991) Oscillatory flow and mass transport in a flexible tube, *Journal of Fluid Mechanics*, 231, 135-155.

Demirdzic, I. and Peric, M., (1990) Finite volume method for prediction of fluid flow in arbitrarily shaped domains with moving boundaries, *International Journal for Numerical Methods in Fluids*, 10, 771-790.

Deshpande, M.D., Giddens, D.P. and Mabon, R.F., (1976) Steady laminar flow through modelled vascular stenosis, *Journal of Biomechanics*, 9, 165-174.

Durst, F. and Loy, T., (1985) Investigations of laminar flow in a pipe with sudden contraction of cross sectional area, *Computers and Fluids*, 13(1), 15-36.

Gowda, B.H.L., Prakash, B. and Singh, M., (1988) Flow through constrictions of different geometries, *First World Conference on Fluid Mechanics and Heat Transfer*, Yugoslavia.

Hamdan, M.H., Barron, R.M. and McCallum, F.M., (1993) Fluid flow through curved porous channels, *European Journal of Mechanics, B/Fluids*, 12(3), 323-336.

Jensen, O.E., (1990) Instabilities of flow in a collapsed tube, *Journal of Fluid Mechanics*, 220, 623-659.

Jensen, O.E and Pedley, T.J., (1989) The existence of steady flow in collapsed tube, *Journal of Fluid Mechanics*, 206, 339-374.

Kasivisvanathan, S.R., Kaloni, P.N. and Rajagopal, K.R., (1991) Flow of a non-Newtonian fluid through axisymmetric pipes of varying cross-sections, *International Journal of Non-Linear Mechanics*, 26(5), 772-792.

Lee, J.S. and Fung, Y.C., (1970) Flow in locally constricted tubes at low Reynolds numbers, *Journal of Applied Mechanics*, 37, 9-16.

Lee, T.S., (1990) Numerical studies of fluid flow through tubes with double constrictions, *International Journal for Numerical Methods in Fluids*, 11, 1113-1126.

Lighthill, J., (1975) *Mathematical Biofluidynamics*, No. 17 in the SIAM Regional Conference Series in Applied Mathematics, Society of Industrial and Applied Mechanics, Philadelphia, Pennsylvania.

Majumdar, S., (1988) Role of underrelaxation in momentum interpolation for calculation of flow with nonstaggered grids, *Numerical Heat Transfer*, 13, 125-132.

Mateescu, D., Mekanik, A. and Paidoussis, P., (1994) Computational solutions for unsteady annular flows with oscillating boundaries based on time dependent coordinate transformations, *Second Annual Conference of CFD Society of Canada*, 51-58.



- Misra, J.C. and Chakravarthy, S., (1986) Flow in arteries in presence of stenosis, *Journal of Biomechanics*, 19(11), 907-918.
- O'Brien, V. and Ehrlich, L.W., (1985) Simple pulsatile flow in an artery with a constriction, *Journal of Biomechanics*, 18(2), 117-127
- Ojha, M., Cobbold, R.S.C., Johnston, K.W. and Hummel, R.L., (1989) Pulsatile flow through constricted tubes; an experimental investigation using photochromatic tracer methods, *Journal of Fluid Mechanics*, 203, 173-197.
- Pedley, T.J. and Stephanoff, K.D., (1985) Flow along a channel with time dependent indentation in one wall: the generation of vorticity waves, *Journal of Fluid Mechanics*, 160, 337-367.
- Peric, M., Kessler, R. and Scheueerer, G., (1988) Comparison of finite-volume numerical methods with staggered and collocated grids, *Computers and Fluids*, 16(4), 389-403.
- Patankar, S.V and Spalding, D.B., (1972) A calculation procedure for heat, mass and momentum transfer in three dimensional parabolic flows, *International Journal of Heat and Mass Transfer*, 15, 1787-1805.
- Patankar, S.V., Liu, C.H. and Sparrow, E.M., (1977) Fully developed flow and heat transfer in ducts having streamwise periodic variation in cross sectional area, *Journal of Heat Transfer*, 99, 180-186.
- Prata, A.T. and Sparrow, E.M., (1984) Heat transfer and fluid flow characteristics for an annulus of periodically varying cross section, *Numerical Heat Transfer*, 7, 285-304.
- Ralph, M.E. and Pedley, T.J., (1988) Flow in a channel with moving indentation, *Journal of Fluid Mechanics*, 190, 87-112.
- Ralph, M.E. and Pedley, T.J., (1989) Viscous and inviscid flows in a channel with a moving indentation, *Journal of Fluid Mechanics*, 209, 543-566.
- Rhie, C.M. and Chow, W.L., (1983) Numerical study of the turbulent flow past an airfoil with trailing edge separation, *AIAA Journal*, 21(11), 1525-1532.
- Rosenfeld, M. and Kwak, D., (1991) Time dependent solutions of viscous incompressible flows in moving coordinates, *International Journal for Numerical Methods in Fluids*, 13, 1311-1328.

Shapiro, A.H., (1977b) Physiologic and medical aspects of flow in collapsed tubes. Proceedings of the 6th Canadian Congress on Applied Mechanics, 883-906.

Sparrow, E.M. and Prata, A.T., (1983) Numerical solutions of laminar flow and heat transfer in a periodically converging-diverging tube, Numerical Heat Transfer, 6, 441-461.

Talukder, N., Karayannacos, P.E., Nerem, R.M. and Vasco, J.S., (1977) An experimental study of fluid mechanics of arterial stenosis, ASME Journal of Biomechanical Engineering, 99, 74-82.

Theodorou, C. and Bellet, D., (1986) Laminar flows of a non-Newtonian fluid in mild stenosis, Computer Methods in Applied Mechanics, 54, 111-123.

Uchida, S., (1956) The pulsating viscous flow superposed on steady laminar motion of incompressible fluid in a circular pipe, ZAMP, 7, 403-422.

van Dreumel, S.C. and Kuiken, G.D.C., (1989) Steady flow through a double converging-diverging tube model for mild coronary stenosis, Journal of Biomechanical Engineering, 111, 212-221.

Venkat, N.K. and Spaulding, M., (1991) A numerical model to predict the nonlinear response of external flow over vibrating bodies (planar flow), Journal of Fluids Engineering, 113, 544-554.

Vradis, G., Zalak, V. and Bentson, J., (1992) Simultaneous variable solutions of incompressible steady Navier-Stokes equation in general curvilinear coordinate system, Journal of Fluids Engineering, 114, 299-305.

Wang, D.M and Tarbell, J.M., (1992) Nonlinear analysis of flow in an elastic tube (artery): steady streaming effects, Journal of Fluid Mechanics, 239, 341-358.

Watson, G.M., (1966) A treatise on the theory of Bessel functions, Second Edition, Cambridge University Press.

Yeung, R.W. and Vaidhyanathan, M., (1992) Non-linear interaction of water waves with submerged obstacles, International Journal for Numerical Methods in Fluids, 14, 1111-1130.

Young, D.F., (1968) Effect of time dependent stenosis on flow through a tube, Journal of Engineering for Industry, 90, 248-254.

Young, D.F. and Tsai, F.Y., (1973) Flow characteristics in models of arterial stenosis-I. Steady flow, Journal of Biomechanics. 6, 395-410.

Young, D.F., (1979) Fluid mechanics of arterial stenoses, *Journal of Biomechanical Engineering*, 101, 157-174.

## VITA AUCTORIS

- 1968 Born in Kumbakonam, Tamilnadu, India on July 30
- 1985 Completed high school at R.S. Krishnan Higher Secondary School, Tiruchirapalli, Tamilnadu, India
- 1989 Received the Degree of Bachelor of Engineering from the Birla Institute of Technology and Science, Pilani, Rajasthan, India
- 1991 Received the Degree of Master of Applied Science in Industrial Engineering from the University of Windsor, Windsor, Ontario, Canada
- 1995 Currently a candidate for the Degree of Doctor of Philosophy in Mechanical Engineering at the University of Windsor, Windsor, Ontario, Canada